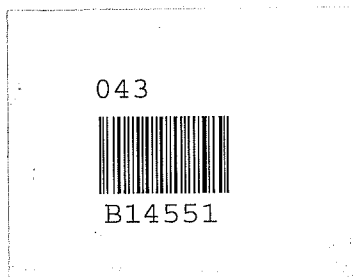# XENON PRODUCTION CROSS-SECTIONS ON BARIUM TARGETS BY ENERGETIC PROTONS FROM ACCELERATORS AND SIMULATION EXPERIMENTS ON MODEL METEOROIDS

MATHEW K.J.

Ph. D. Thesis

JULY 1991

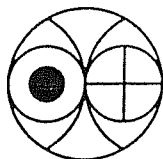PHYSICAL RESEARCH LABORATORY

AHMEDABAD 380009

INDIA

XENON PRODUCTION CROSS-SECTIONS ON BARIUM TARGETS BY ENERGETIC PROTONS FROM ACCELERATORS AND SIMULATION EXPERIMENTS ON MODEL METEOROIDS

by

Mathew K.J.

Physical Research Laboratory

Ahmedabad 380009, India

A thesis

submitted to the

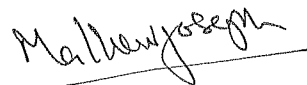Gujarat University

for the degree of

Doctor of Philosophy

JULY 1991

PHYSICAL RESEARCH LABORATORY

AHMEDABAD 380009, INDIA

CERTIFICATE

I hereby declare that the work presented in this thesis is original and has not formed the basis for the award of any degree or diploma by any University or Institution.

Mathew K.J.

(Author)

Certified by:

M.N.Rao

(Thesis Supervisor)

July 1991

ABSTRACT

The primary objective of the work presented here is to experimentally determine the production cross-sections of xenon isotopes in proton induced reactions on barium targets by irradiation experiments using the low and high energy accelerators in Europe. For this purpose, both the "thin" and thick" target irradiation techniques have been employed. The proton energies used for these irradiations fall into two categories: (a) low (12 to 45 MeV) and (b) high (600 to 2600 MeV).

Based on the cross-section data covering a wide range of proton energies, obtained as a direct result of the present studies, excitation functions for the production of xenon isotopes in all energy regions are constructed. The excitation functions, thus obtained, can be used to calculate the SCR and GCR cosmogenic xenon production rates in moon and meteorite samples with the help of existing theoretical models. Here, SCR production rates of xenon isotopes on the lunar surface material are calculated and the production rate estimates are discussed together with the cross-section measurements.

The outline of the thesis is as follows.

Chapter I. Description of the energetic particles (GCR and SCR) in the interplanetary space and their interaction with extraterrestrial matter. Relevance of the simulation experiments in determining the cosmogenic production rates is emphasized and the various processes contributing to xenon in an extraterrestrial sample are briefed.

Chapter II. The mass spectrometric techniques are discussed in this Chapter, and the lunar rock samples studied here are described. Also discussed are the cosmic ray simulation irradiation experiments.

Chapter III. The results obtained in the low energy cross-section measurements are discussed. SCR xenon production rates in lunar surface material are elaborated. The results of the lunar rock xenon measurements are also discussed in the later parts of this Chapter.

Chapter IV. Here the results obtained in the high energy thin target proton irradiation experiments are discussed. The production rates of xenon isotopes measured in the diorite (R =5 cm) and gabbro (R =26 cm) spheres (thick target experiments) are also discussed in this Chapter.

ChapterV. Conclusions. In this concluding Chapter the results obtained during the course of the present work are summarised and the cosmochemical applications of the present results are discussed.

The results obtained in this study can be summarised as follows.

Our xenon production cross-section measurements on Ba targets in the proton energy range of 12 MeV <E <45 MeV show that in this low-energy range there is a significant production of Xenon isotopes. The isotopes ^{129}Xe, ^{131}Xe and ^{132}Xe are produced with larger abundance compared to the other xenon isotopes. For

example at ~24 MeV the production cross-sections of ^{129}Xe, ^{131}Xe and ^{132}Xe are, respectively, 2.53 ±0.38 mb, 3.62 ±0.54 mb and 1.01 ±0.15 mb, compared to the cross-section values of 0.25 ±0.04 mb for ^{130}Xe and 0.03 ±0.004 mb for ^{128}Xe. The relatively higher production cross-sections of these isotopes at proton energies of ~24 MeV indicate that pre-equilibrium α-emission reaction channels involving barium targets are operational and these reactions favourably produce isotopes ^{129}Xe, ^{131}Xe, and ^{132}Xe.

The SCR production rates of xenon isotopes in lunar surface material are estimated using the cross-sections measured by us as input parameters in an existing model. These calculations show that the SCR xenon production rates estimated by us are ~ a factor 2 higher than the estimates available in literature. The surface production rates of ^{132}Xe estimated in the present calculations are 0.55 x10^{-15} ccSTP.g^{-1}.Ma^{-1}.ppmBa^{-1} compared to the Hohenberg et al.,(1978) values of 0.283 x10^{-15} ccSTP.g^{-1}.Ma^{-1}.ppmBa^{-1}. This discrepancy is due to neglect of Xe production by low energy protons (E <60 MeV) in the earlier calculations. In an effort to deduce the solar cosmic ray produced Xe spectra in documented samples from oriented lunar rocks 61016, 64435 and 79215 the Xe concentrations measured in these rocks are deconvoluted into its constituent components. Our results show that in these rocks there are qualitative indications for the production of xenon isotopes ^{129}Xe, ^{131}Xe and ^{132}Xe by SCR protons. The SCR xenon spallation spectra deduced from these rocks is (large errors are associated with these numbers).

$$^{129}\text{Xe} : ^{131}\text{Xe} : ^{132}\text{Xe} = 0.94 : 2.30 : 1.00$$

In the high energy region, the production cross-sections for xenon isotopes on Ba targets (thin target irradiations) at proton energies of 600 MeV, 800 MeV, 1200 MeV and 2600 MeV are determined. In the energy range 600 MeV to 1200 MeV the production cross-sections of xenon isotopes remains more or less constant but at energies higher than 1200 MeV the production cross-sections decrease substantially. The ^{126}Xe production cross-sections at 600, 800, and 1200MeV are, respectively, 54.5 ±3.8 mb, 85.4 ±6.0 mb and 65.5 ±5.0 mb which are higher in comparison to the cross-section value of 31.2 ±2.3 mb at 2600 MeV. More significantly, the relative yields (spallation spectra) for the production of xenon isotopes change considerably in the proton energy region of 600 MeV <E <2600 MeV and this change is in such a way that the heavier isotope productions are enhanced with respect to the lighter xenon isotopes. The ^{129}Xe/^{126}Xe and ^{131}Xe/^{126}Xe isotopic ratios at 2600 MeV are, 1.420 and 1.901 as compared to 1.131 and 1.229 at 600 MeV.

In the "thick-target" experiments, we here found that xenon isotopes produced from barium glasses irradiated inside small sized bodies (i.e. diorite sphere, R =5 cm) do not show any variation as a function of depth. Based on these measurement, we conclude that the depth profiles for the production of cosmogenic xenon isotopes in small meteoroids (size ~5 cm) in space are essentially flat.

Our results (thick target) from the measurement of Ba glasses irradiated inside gabbro sphere (R ~25 cm) shows that there is a significant production of xenon isotopes from the secondary particles in the thick target bodies having radii, R ~25

cm. The size effects are most pronounced in the case of isotope ^{131}Xe. The production rates of ^{131}Xe measured in Ba glass samples kept near the surface and near the center of the gabbro (R =26 cm) mock-up meteoroid are, 7.65 ±1.15 and 4.6 ±0.70 (both quantities in units of x10^{-10}ccSTP.g^{-1}.Ma^{-1}). The corresponding values for isotope ^{126}Xe are 1.68 ±0.26 and 2.32 ±0.35 (in units x10^{-10}ccSTP.g^{-1}.Ma^{-1}). The enhanced production of this isotope is attributed to (n,α) reactions on ^{134}Ba and (n,2n) reactions on ^{132}Ba target nuclide.

The production of xenon isotopes in proton induced reactions in extraterrestrial objects like moon and meteorites can be evaluated fairly accurately using the cross-section measurements obtained from the present study. For the first time we have a consistent set of xenon production cross-section measurements covering a wide range of energies 12 MeV <E <2600 MeV. However, it may be noted that, in the intermediate range (i.e. ~60 to 200 MeV), we had to use theoretically estimated cross-sections as there are no experimental xenon cross-sections available. In quantifying the cosmogenic production of xenon in moon and meteorite samples as well as deducing the other xenon components in these samples, this data base provided in this work is an important contribution.

(v)

ACKNOWLEDGEMENTS

I thank Sivasankaran and M.P.K. Kurup for excellent and skillful glass blowing work on the Mass Spectrometer.

I am extremely fortunate to have enjoyed the company of a very large number of friends, inside and outside PRL. I sincerely thank them all for being very nice to me and for encouraging me in all my endeavours. I should have made an attempt to mention them here by name but I am afraid that words are too few to describe my feeling to them.

Thanks are due to the staff of PRL library for being extremely co-operative, Mr.S.C. Bhavsar for drafting work, Mr.D.R. Ranpura for photographic work and to the staff of the computer section, workshop and maintenance sections for their kind co-operation throughout the period of this work.

Finally I express my deep sense of gratitude to my parents and all my teachers and to them, I dedicate this dissertation.

LIST OF TABLES

LIST OF FIGURES

CHAPTER I
INTRODUCTION

The products of nuclear interactions of the Galactic and Solar Cosmic ray (GCR and SCR) particles with matter, commonly referred to as cosmogenic nuclides, provide information on the flux, energy spectra and temporal and spatial variations of these radiations as well as about the history of the irradiated objects themselves [Reedy et al.,(1983), Nishiizumi et al.,(1980), Bhandari et al.,(1980), Schultz and Signer (1976), Lal (1972), Begemann and Wanke (1969), Fireman (1967) and other references therein]. The cosmogenic nuclides produced in these nuclear interactions are of two types (i)radio-active isotopes, e.g., ^{10}Be, ^{26}Al and ^{53}Mn and (ii)stable rare gas isotopes, e.g., ^{3}He,^{21}Ne, ^{38}Ar and ^{126}Xe. The radioactive cosmogenic nuclides and the lighter rare gas nuclide (^{3}He, ^{21}Ne) production in extraterrestrial matter is studied rather extensively and has led to a reasonable consensus among the scientific community regarding the production rates of these nuclides in extraterrestrial samples [Aylmer et al., (1988), Honda (1988), Graf et al., (1987), Masarik et al., (1986), Michel et al., (1982), Englert and Herr (1980), Begemann et al., (1976), Herzog and Cressy (1974) and Cressy (1971)]. However, in the case of xenon (though it is an important element used to understand the various processes that took place in the early solar system) the cosmogenic aspects remain relatively ambiguous. Quantifying the cosmogenic production of this element assumes special significance since the cosmogenic xenon concentrations will have to be subtracted from the measured xenon concentrations in a meteorite or lunar sample in order to

1

arrive at accurate estimates of other components, such as fission xenon and radiogenic xenon, from the measured xenon concentrations (after accounting for the trapped xenon amounts). Several attempts have been made to estimate the xenon production rates in extraterrestrial samples in the past, [Eugster(1988); Hohenberg et al., (1978), Marti et al., (1966) and other references therein] by GCR (and SCR) protons, using the experimental cross-sections measured by Kaiser (1977) and Funk and Rowe (1967). Estimates of the xenon production rates using ^{126}Xe cosmogenic excess, ^{21}Ne age and the barium content in the case of some meteorites have also been attempted [Marti et al., (1966)]. However, there are inadequacies in these methods.

The prime interest of the present study is to understand the cosmic ray induced production of xenon isotopes at different depths in extraterrestrial objects like moon and meteorites. In this introductory chapter the mechanism of the cosmic ray (galactic and solar) interaction with extraterrestrial matter is briefly described. The methods employed for determining the depth production profiles of cosmogenic nuclides are also outlined.

1.1 Nature of the Interacting Particles in the Interplanetary Space

In the following sections, 1.1a and 1.1b, the characteristics of the nuclear particles interacting with matter in space are discussed. The galactic and solar cosmic radiations having two distinct origins are described separately.

Considering the production of nuclides in our solar system matter two kinds of energetic radiations having distinct

2

origin and characteristics are generally taken into account. These are galactic cosmic ray (GCR) particles, which consist mostly of protons in the energy range of a few hundred million electron volts (MeV) to energies well above 10^{20} electron Volts (eV). On the other hand are the solar cosmic ray (SCR) particles, consisting of mostly protons in the energy range of a few MeV up to about 200 MeV [Mc Guire et al.,(1986)]. Fig. 1.1 shows the energy ranges and penetrating depths of the energetic radiations in the interplanetary space.

1.1a Galactic Cosmic Ray Particles

The major differences between the SCR and GCR particles are their energies and fluxes. The average energy of GCR particles is about few GeV and the energies of these particles fall into a wide range of a few hundred MeV to ~10^{20} eV. The spectra and fluxes of the GCR particles get modulated by the solar wind and its expanding magnetic field from the sun. The solar cycle averaged GCR flux is ~2 to 3 protons.cm^{-2}.s^{-1}. Fig. 1.2 shows the GCR spectra during solar minimum and during solar maximum.

The composition of the GCR particles is ~87% protons ~12% alpha particles and ~1% heavier nuclei [Simpson (1983)].

The energy spectrum of the GCR particles, originating from outside our solar system gets modulated by the solar magnetic field and this spectra can be considered to have a maximum at around 1 GeV. Above 10 GeV the number of particles is proportional to $E^{-2.65}$ [Reedy and Marti (1990) and Reedy and Arnold (1972)]

3

ENERGETIC CHARGED PARTICLES IN
INTERPLANETARY SPACE AND THEIR
EFFECTS

SW   ~KEV/ NUCLEON
IMPLANTATION, RADIATION DAMAGE

SEP   ~1-100 MEV / NUCLEON
IMPLANTATION, LATTICE STRUCTURE
AND ELECTRONIC DAMAGE (TRACKS AND TL)

SCR   ~1-100 MEV / NUCLEON
STABLE AND RADIOACTIVE NUCLIDES

GCR   ~ GEV / NUCLEON
STABLE AND RADIOACTIVE NUCLIDES
LATTICE DAMAGE (TRACKS)

10^{-6} 10^{-1} 1   10 10^{2}

APPROXIMATE EFFECTIVE RANGE (CM)

Fig.1.1   Energy ranges and penetrating depths of the energetic
radiations in the interplanetary space.
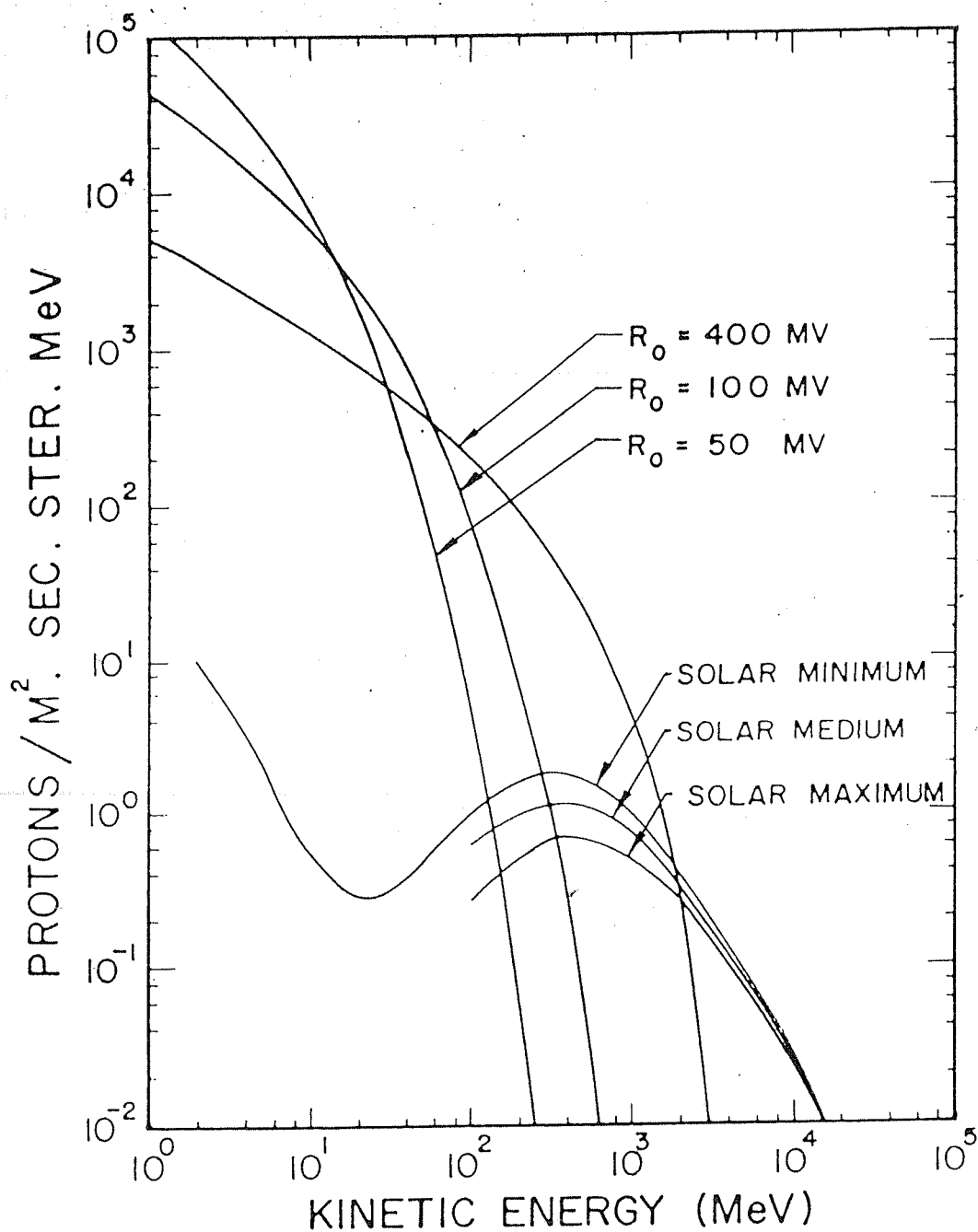
Fig.1.2   GCR proton energy spectra during periods of solar maxima

and solar minima.   Figure is reproduced from Lal (1972)

1.1b Solar Cosmic Ray Particles

The energy spectra of the solar cosmic ray particles, which are emitted from the sun in sporadic events known as solar flares, can be represented in terms of an exponential of the parameter "rigidity" (momentum per unit charge) by the expression [Mc Guire and Rosenvinge (1984)]

$$dN/dR = Kxe^{(-R/R_o)}$$

R_o represents the characteristic rigidity which, in turn, defines the spectral characteristics and has typical values in the range 35 MV to 150 MV [Reedy (1977)]. Smaller values of R_o implies lower energies of the solar cosmic ray protons and also a repidly falling proton energy spectrum.

The time averaged fluxes of these particles at a distance of 1 A.U. from the sun is determined to be ~70 particles.cm^{-2}.s^{-1} [Kohl et al.,(1978)], based on ^{26}Al an ^{53}Mn measurements in lunar samples. By direct proton measurements on several satellites the fluxes that are deduced are 92 protons.cm^{-2}.s^{-1} [Reedy (1977). The values of the spectral parameter R_o lies in between 40 MV and 100 MV [Nishiizumi et al.,(1988), Reedy (1980 and 1977) and Kohl et al.,(1978)].

1.2. Cosmogenic Nuclides: Scope of the study

Beginning with the discovery of cosmic ray produced (cosmogenic) ^{3}He in iron meteorite Grant by Paneth et al., (1952 and 1953) several cosmogenic isotopes have been extensively used in studying cosmic ray related phenomena like cosmic ray intensity variations in the past and irradiation history of the parent body as part of which the sample got exposed to energetic particles in

space [Eugster et al., (1984), Michel et al., (1982), Reedy (1980), Nishiizumi et al.,(1980), Rao et al.,(1979), Kohl et al., (1978), Bhandari et al., (1976), Begemann and Wanke (1969), Signer and Neir (1960) and other references therein]. ^{3}H, ^{3}He, ^{10}Be, ^{22}Na, ^{22}Ne, ^{26}Al, ^{53}Mn ^{81}Kr, ^{83}Kr and ^{126}Xe are some of the nuclides often studied in meteorites and moon samples. For example, exposure ages of meteorites are determined by measuring the activity of a cosmogenic radio isotope and the absolute concentrations of a stable cosmogenic nuclide (the isotope pairs often employed for this purpose are ^{3}H-^{3}He, ^{26}Al-^{21}Ne, ^{22}Na-^{22}Ne, ^{36}Cl-^{36}Ar and ^{81}Kr-^{83}Kr) [Eugster et al., (1988), Cressy and Bogard (1976), Begemann et al., (1976), Lugmair and Marti (1971), Lipshultz et al., (1965) and Marti (1967)]. The stable isotope concentrations provide the accumulated effect of all the exposures of the sample to cosmic radiation and it monitors the total flux 'seen' by the sample where as the radio nuclide concentration indicates the flux of energetic particles over time periods short or long according to whether or not the nuclide under study is short lived or long lived. Herpers et al.,(1983) have developed techniques to deduce the exposure ages of meteorites based on the ^{53}Mn and ^{26}Al depth profiles.

1.2a. Cosmogenic Nuclide Production Rates

In the past several years, different models have been developed for the prediction of cosmogenic nuclide production rates in extra terrestrial matter and they have been used with varying degrees of success [Graf et al.,(1988), Eugster (1988), Schultz and Freundel (1985), Michel et al.,(1986) and Michel and

Brinkmann(1980), Bhandari and Potdar (1982), Bhandari et al., (1976), Reedy and Arnold (1972), Amstrong and Alsmiller (1971), Fisher (1972), Begemann and Vilesek (1969) and Signer and Nier (1962)].

The energetic particles in space interact with matter in a number of ways depending on the mass and energy of the interacting particles. The low energy particles, the solar wind particles and heavy nuclei in solar cosmic rays, for example, get directly implanted on the meteoroid surfaces (under pre-atmospheric conditions) and the surface samples of the lunar regolith. The galactic cosmic ray protons and the α's as well, on the other hand, penetrate deeply and produce a variety of nuclear reaction products in terrestrial (under special circumstances) and extraterrestrial material.

The incident particles on traversing through extraterrestrial matter lose their energy due to (i)ionization of the medium, which can be calculated by models of Reedy et al.,(1983) and C.F.Willaimson et al.,(1966) and (ii) due to nuclear interactions with the target nucleus. These nuclear interactions, in general, lead to the production of the secondary particles, the neutrons and protons, in addition to producing residual nuclei having a mass less than that of the target, formed from the taget nucleus by loss of few nucleons by processes such as knock-on collision, fragmentation of the excited nucleus left in an excited state after the knock on phase or due to evaporation of nucleons from the residual nucleus after its collision with the incoming particle. The secondary neutrons and protons produced in this manner lead to further production of cosmogenic nuclides,

thus leading to the generation of the cascade. The accurate prediction of cosmogenic nuclide production rates at different shielding depths inside an extraterrestrial body (for example the Moon) will have to take into consideration all the complex processes mentioned above. The above scenario is further complicated by the fact that the incoming particles (mostly protons) are not mono-energetic as shown in Fig 1.2. Further, the fluxes and other spectral parameters, such as energy, are observed to vary with time and also with orbital distance form the sun. Techniques have been developed .in the past to understand these changes in the cosmic ray spectra through the study of comic ray produced (cosmogenic) nuclides in extraterrestrial matter [Eugster et al., (1988), Reedy (1980), Rao et al., (1979), Kohl et al., (1978), Bhandari et al., (1976) and other references therein].

In this context it may be pointed out that the study of cosmogenic rare gas isotopes is of special importance in cosmochemistry. This is because the rare gas isotopes have relatively small solar system abundances and hence even small variations in their concentrations by a physical or nuclear process can be accurately quantified. Because of their chemical inertness noble gases do not participate in chemical reactions and hence fractionation does not occur. Another advantage of noble gas isotopes is that they can be separated from each other and analysed in ultra high vacuum easily.

1.2b. Depth Profiles of Cosmogenic Nuclide Production: Thin and Thick Target Methods:

Two different approaches are generally employed to obtain the production rates of cosmogenic nuclides as a function of depth in an extraterrestrial object. These are 'thin target' and 'thick target' approaches [Reedy and Marti (1990), Michel et al.,(1986), Kirsten and Schaeffer (1971) and other references therein].

In the thin target approach the cross-sections for the production of the nuclide of interest are determined from all its cosmochemical target elements. Such data can be procured from laboratory irradiation experiments using accelerators. The particle flux and energy spectra at different depths inside the extraterrestrial body are calculated from parameters such as density of the interacting medium, interaction length of the incoming particles, rate of energy loss of the incoming radiations due to ionization of the medium, the average multiplicity of the incoming radiations etc. The production rate at depth d inside an object can then be expressed by the relation

$$P_j = \sum_{i=1}^{n} N_i \sum_{k=1}^{m} \int_0^{\infty} \sigma_{ijk}(E) \, J_k(E,d) \, dE$$

N_i is the number of target atoms of the kind i per Kg of the interacting material

k represents the individual reacting particle

σ_{ijk} is the cross-section for the production of nuclide j from target i by particle type k having energy E

On the other hand, in thick target experiments, meteoroid mock-ups of appropriate size and material are irradiated with high energy protons from an accelerator and the targets of

10

interest are kept at various shielding depth positions inside the "thick target" body. The thick target is used as a medium to generate secondary particles and the production observed at any given depth is the combined effect of the primary and the secondary particles.

1.2c Simulation Experiments.

Recently the thick target irradiation experiments have diverged into two directions. The first one of these in which Englert and co-workers [Englert et al., (1987)] have made significant contributions is to irradiate bigger and bigger thick target bodies. The other in which Michel and co-workers have made important contributions is to simulate the cosmic-ray irradiation conditions of meteorites as closely as possible. In the experiments carried out by Michel et al.,(1986 and 1989) at CERN accelerators, three stony meteorite models were irradiated with 600 MeV protons and the mock-up model meteoroids were provided movements (with respect to the proton beam) in such a way that they received isotropic irradiation. These experiments have been discussed in detail in Chapter II of this thesis.

Ever since the first thick target irradiation experiments by Firemann and Zahringer (1957), the irradiation experiments have advanced a great deal with the irradiation of larger thick target bodies and different kinds of thick target objects. A large number of cosmogenic nuclide targets have been irradiated and the nuclear reaction products studied. [Kohmann and Bender (1967) has given a summary of the irradiation experiments prior to 1967]. Ginnekan and Turkevich (1970)

measured the production of ^{54}Mn from Cu in Fe targets irradiated with 1GeV and 3 GeV protons. Lavrukhina et al., (1973), and Arakita et al., (1979) reported production of cosmogenic nuclides from various targets in Fe thick target bodies. Only few experiments involving stony meteorites as thick targets are reported. Experiments with stony meteorite bodies are reported by Trivedi and Goel (1973), Michel et al., (1974), Kaiser et al., (1975), Bar and Herr (1974) and Thiel et al., (1974).

1.3 SCR Production Rate Model used here : basic approach

SCR particles (protons) have comparatively lower energies (E <200 MeV) and are stopped in the first few centimeters of an extraterrestrial body with which these particles are interacting as discussed earlier. The nuclear interaction products of SCR are also confined to these surface layers. Meteorites lose their surface layers (due to ablation) which contain the SCR irradiation records during their passage through the earths atmosphere and hence there are only few meteorites in which SCR irradiation records are observable. Meteorites which are proved to contain SCR irradiation records are Salem [Goswami et al.,(1988), Evans et al., (1987)], Gujargaon meteorite [Bhandari et al., (1988)], ALHA 77005 [Nishiizumi et al.,(1986)] and Lal and Marti (1977) detected SCR irradiation effects in St. Severin meteorite.

Considering the production of nuclides by solar cosmic ray particles the fluxes at different depths inside the extraterrestrial body can be calculated by taking into consideration the energy loss of the incident particles due to

ionization of the medium. The fluxes and energies of the particles at each shielding depth inside the body can be estimated accurately as secondary particle production is negligible. Fig. 1.3 shows the differential fluxes of the particles at different shielding depths inside the extraterrestrial body (in the present context, Moon) with which the SCR particles are interacting.

Following the procedure of Lal and Venkatavardhan (1967), Reedy and Arnold (1972) and Bhandari et al., (1975) the cosmogenic production at the surface of a lunar rock is estimated by the following expression

$$P = \frac{1}{x} \int_0^x \int_0^t P_{[x(t)]} \, dt \, dx$$

P is the production rate of the nuclide

x is the effective depth of the sample

x and t are related by the linear relation

$x(t) = x + \varepsilon.t$ where ε is the erosion rate which has values in the range 5-10 $A^\circ.yr^{-1}$ [Burnett and Woolum (1977), Hörz et al., (1975), Bhandari et al., (1975) and Bhattacharya and Bhandari (1975)]. The adopted value for ε is $\varepsilon = 5 \ A^\circ.yr^{-1}$.

The SCR rigidity spectra is assumed to be time independent following Bhandari et al., (1975).

$$dN = K.E^{-R1/R0} dR$$

with values of R0 ranging from 50 to 200 MV and the omnidirectional flux

$$J(E > 10 \ MeV) = 50 \text{ to } 200 \text{ protons.cm}^{-2}.s^{-1}$$

In the present calculations the integral flux of protons above

13
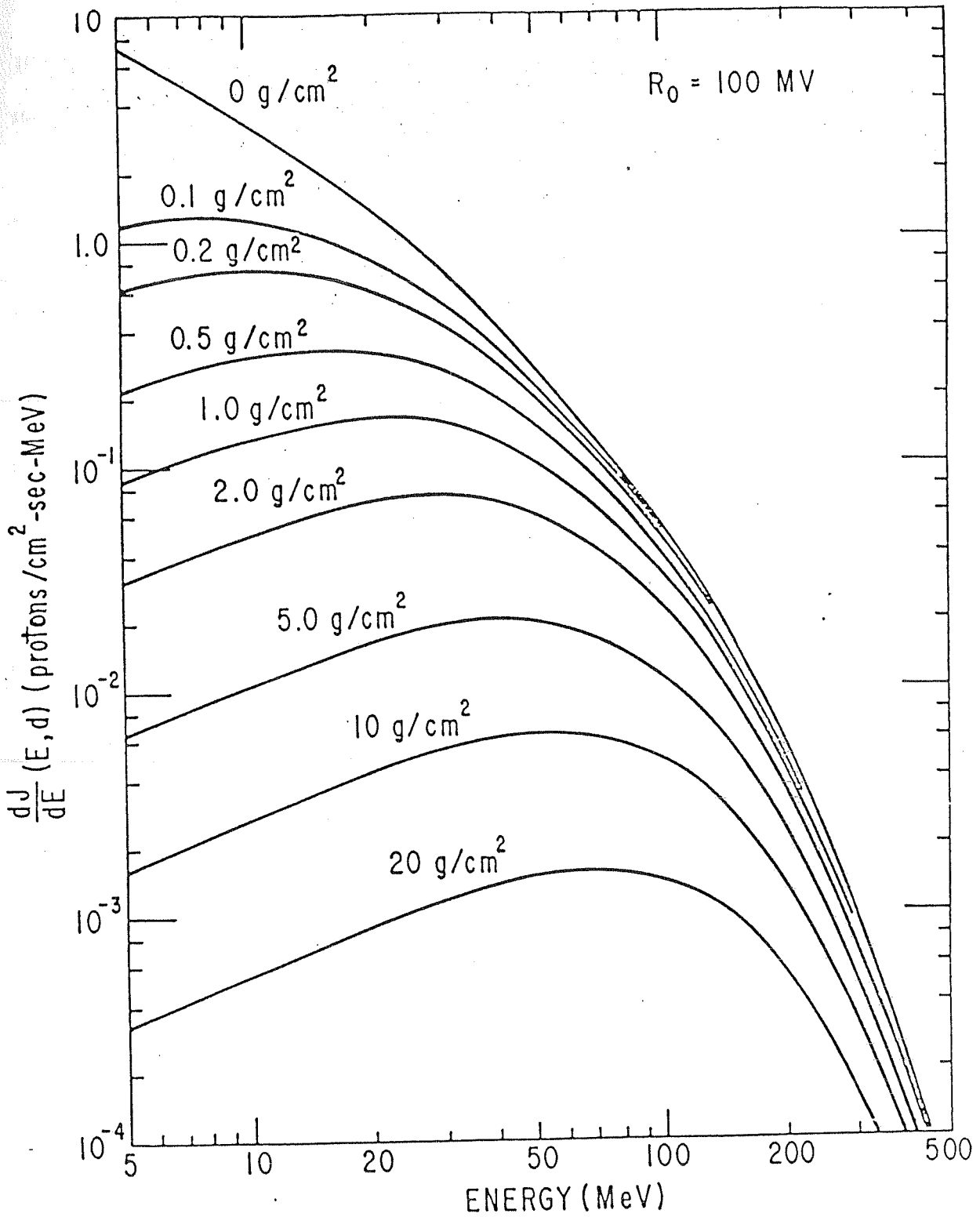
Fig.1.3 SCR particle spectra as a function of shielding depth in lunar surface material. Figure reproduced from Reedy (1990).

10MeV is taken to be 100 protons $cm^{-2}.s^{-1}$. A range energy relation of the type

$$R = CE^{\beta}$$ is used to deduce the slowing down of the SCR particles.

1.4 Xenon Components and its General Systematics

The present thesis considers only the noble gas element xenon for the discussion. xenon the has proton number 54 and has nine stable isotopes with neutron numbers of 70, 72, 74, 75, 76, 77, 78, 80 and 82. Fig. 1.4 shows the isotopic abundances of xenon and its neighbouring elements.

Fig. 1.5 shows the relative abundance of xenon compared to other rare gas elements in solar system material. It may be noted that the 'cosmic' abundances of xenon are smaller compared to other noble gas elements. Fig 1.6 shows the isotopic composition of xenon in various reservoirs of the solar system.

The processes that might have contributed to the general anomalies of meteoritic xenon are (i) mass fractionation due to gravitational, electrostatic or electromagnetic forces [Krummenacher et al., (1962)]; (ii) spallation and (n,γ) reactions induced by the exposure of the meteorite to cosmic radiation during its recent exposure; (iii) in-situ production in meteoritic constituents by particle irradiation or spontaneous fission during the early history of the solar system [Rowe and Kuroda (1965)] and Goles and Anders (1961)]; and (iv) addition of products from particle irradiation or fission to the "primordial" xenon before it became trapped in the meteorite. The terrestrial xenon also may have been altered by some of these processes [Cameron (1962)

Isotopes of Xe and neighboring elements.
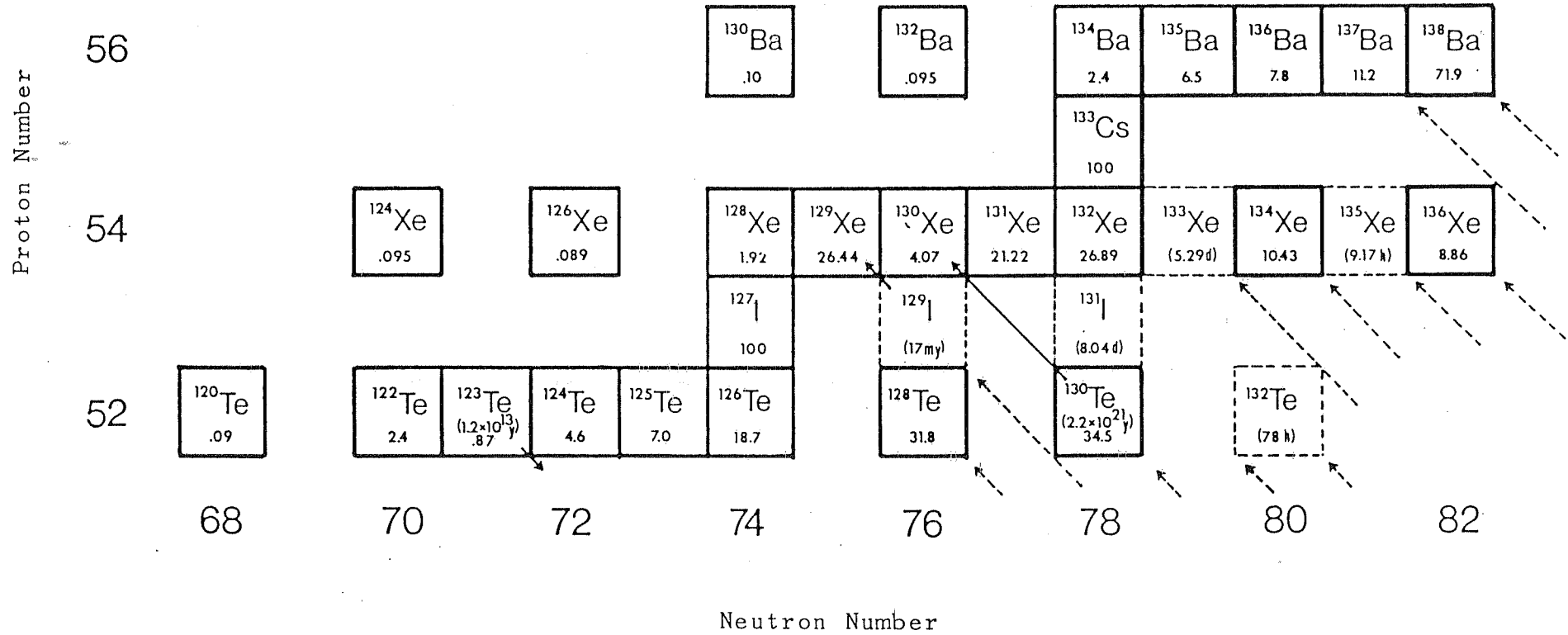
Fig.1.4   Xenon,   its   neighbouring   elements   and   their   isotopic

abundances.
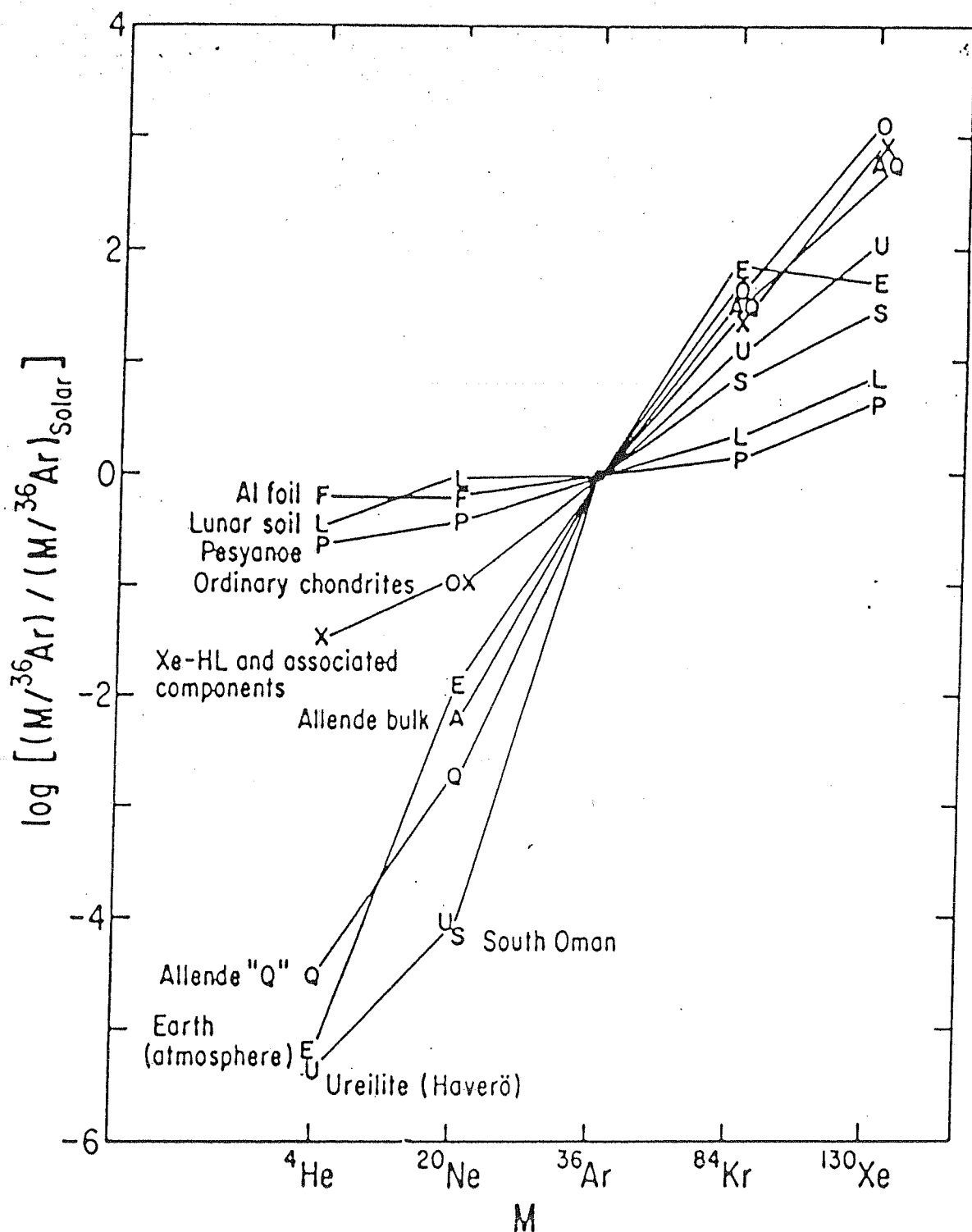
Fig.1.5   Relative abundance of xenon in solar system material,
compared to other noble gas elements.   Figure reproduced
from Swindle (1988).
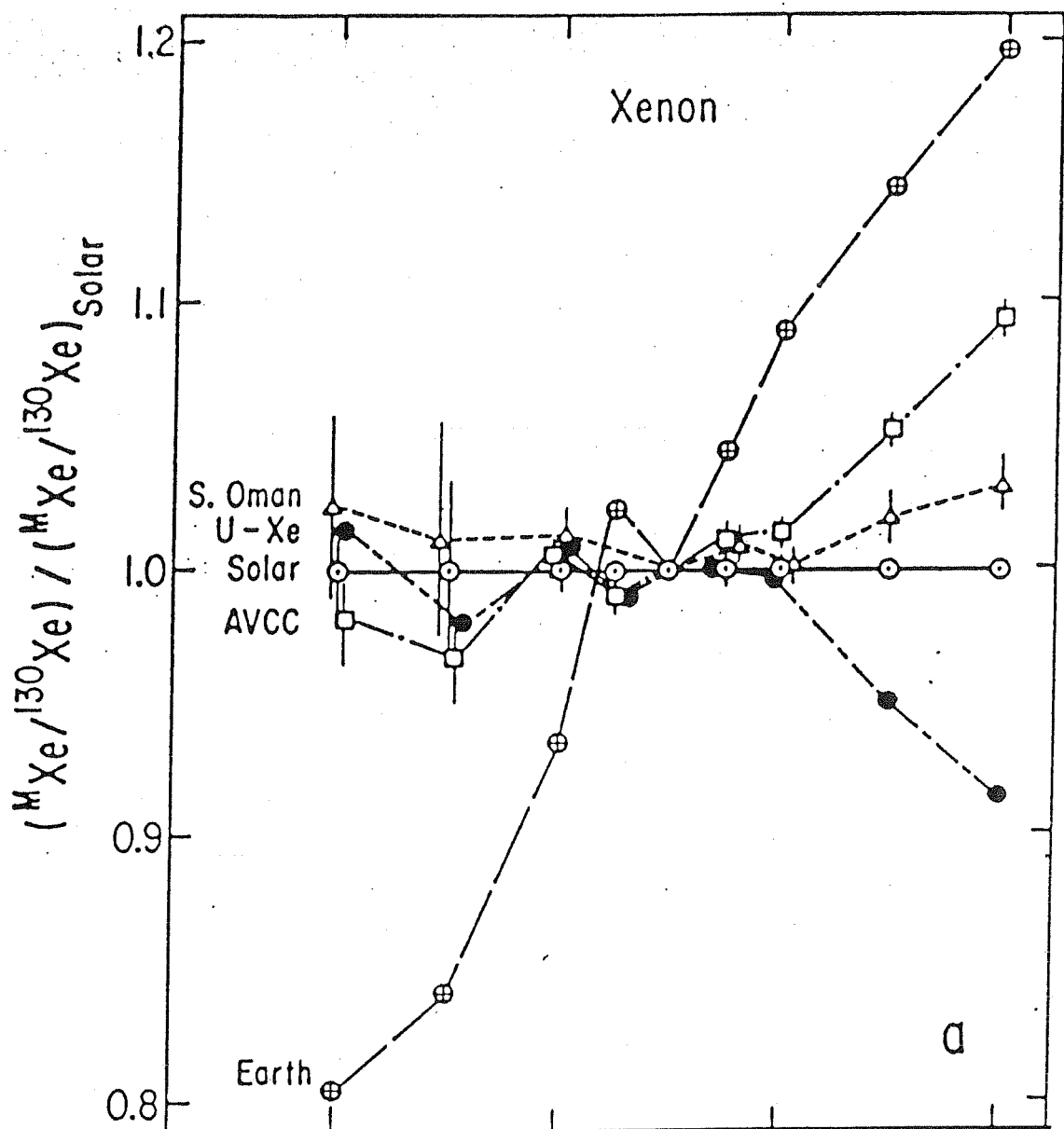
Fig.1.6   Isotopic   composition   of   xenon   in   various   solar   system
reservoirs.   Figure reproduced from Swindle (1988).

18

and Kuroda (1960)]. The processes (iii) and (iv) listed above includes the following possibilities: (a) spallation reactions on Ba, Te, La and Ce; (b) (n,γ) reactions, specially on ^{130}Ba and ^{127}I; (c) spontaneous fission of ^{238}U or transuranium elements and (d) neutron induced fission. The method of step wise heating have been successfully applied in establishing relations between the general isotopic anomalies of xenon.

The major contributions to xenon isotopes in an extraterrestrial sample are from the following components. Here the term component is used to represent a reservoir with a specific isotopic signature (or composition), or a specific mode or process of formation. The components contributing to xenon in a solid object of the solar system are:

(i) trapped component (which contributes to all xenon isotopes);

(ii) radiogenic xenon (contributes to isotope ^{129}Xe)

(iii) spallation xenon (contributes to isotopes ^{124}Xe, ^{126}Xe, ^{128}Xe, ^{129}Xe, ^{130}Xe, ^{131}Xe, ^{132}Xe and ^{134}Xe)

(iv) fission xenon (contributes to isotopes ^{131}Xe, ^{132}Xe, ^{134}Xe and ^{136}Xe)

1.4a Trapped Xenon

When considering noble gases the trapped (or primordial, in case of a meteorite) gas in an extraterrestrial sample can originate from two sources. These are the "solar" and "planetary" types. For major xenon isotopes (129 to 136) the abundances in trapped gases are large and the isotopic composition can be determined comparatively easily. It is rather difficult (relatively) to determine the trapped amounts of lightest xenon

19

isotopes ^{124}Xe and ^{126}Xe in an extraterrestrial sample owing to their low abundances in both solar and planetary components, because they yield very low signals in the mass spectrometer. The trapped gas are incorporated into the sample at the time of the grain formation in the solar nebula by trapping the planetary noble gases.

In the specific case of lunar noble gases, the trapped noble gases are referred to as solar, as these gases are acquired by direct implantation of solar wind. To a small extent some fractionation may occur during the process of implantation. The elemental ratios (normalized to ^{36}Ar) observed in Pesyanoe and lunar soils are found to resemble that of bulk solar system abundances [Anders and Ebihara (1982) and Marti (1969)]. Again, in the case of moon samples, the trapped solar xenon is surface correlated as is evident from the following results: (i) the amount of xenon released from different grain size separates decreases with increasing grain size; (ii) after removing the top surface layers by nominal etching the released neon/xenon amounts decrease rapidly. Both the above facts established by Eberhardt et al., (1972 and 1965) are in confirmation with the predictions by Suess et al., (1964).

1.4b Radiogenic Xenon

Historically, Brown (1947) suggested that it might be possible to find evidence for extinct radioactivities originating from nucleosynthetic sources in meteorites. ^{129}I was thought to be the ideal candidate for varifying the validity of such a hypothesis since this nuclide has a 17 my half life and also since

20

xenon is rare in meteorites and even small changes in ^{129}Xe could be detected by sensitive mass spectrometers. Suess (1948) discussed the cosmochemical significance of long lived ^{129}I. Following these suggestions Wasserberg and Hayden (1955) reported negative results on Beardsley chondrite. The first positive result of significant ^{129}Xe excess (due to the decay of extinct ^{129}I was reported by Reynolds (1960) in Richardton chondrite. Following this pioneering work, Jeffry and Reynolds (1961) irradiated the meteorite Abee with neutrons there by producing isotopic excesses at ^{128}Xe in ^{127}I(n,γ)^{128}Xe reactions. In these experiments, it was found that ^{128}Xe and ^{129}Xe have the same release patterns establishing that the excesses in ^{129}Xe correlats with the I sites in this meteorite. Another observation that the release patterns of ^{131}Xe are not similar to those of ^{128}Xe and ^{129}Xe, strengthened the above inference. Since then many laboratories have reported ^{129}Xe excesses due to in-situ decay of ^{129}I [Rison and Zaikowski (1980), Hohenberg and Kennedy (1981), Podosek (1970) and Hohenberg et al., (1967)].

It is generally assumed that ^{129}I is produced in r-process nucleosythesis in galactic sources [Reynolds (1963)]. It may have been produced continuously [Wasserberg et al., (1960)],or in a late supernova explosion [Cameron and Truran (1977)] or in a combination of the above two processes [Cameron (1962)]. The ^{129}I/^{127}I ratio at the time of formation of the solar system can be used to constrain models of the history of nucleosynthesis in solar system material. ^{129}I which decays to ^{129}Xe correspond to the time at which the sample started quantitatively retaining xenon. From the above information it is

possible to estimate the time interval between the last nucleosynthetic event which added live ^{129}I into solar system matter and the formation of solid objects (planetesimals) in the solar system.

1.4c Spallation Xenon

The spallation xenon contributes mainly to isotopes ^{124}Xe, ^{126}Xe, ^{128}Xe, ^{129}Xe, ^{130}Xe, ^{131}Xe, and ^{132}Xe. The most neutron rich isotope ^{136}Xe is not produced in both low energy and high energy spallation reactions on Ba [Mathew et al., (1989a, 1989b)]. Spallation xenon, in extraterrestrial objects like meteorites and lunar samples, is produced by solar and galactic cosmic ray proton induced reactions on target elements like barium (Ba) and rare-earth-elements (La, Ce etc.).

Rowe and co-workers [Rowe and Kuroda (1965) and Rowe et al., (1965)] showed that xenon extractions from Ca-rich achondrites are enriched in the lighter isotopes ^{124}Xe, ^{126}Xe and ^{128}Xe. They attributed these enrichments as due to spallation reactions induced by GCR protons on Ba targets. From the known exposure ages of the achondrites, Stannern, Pasamonte, Juvinas, Petersberg, Moore County and Pena Blanca Spring and known concentrations of Ba in these meteorites these authors calculated the 'effective' production cross-sections of the isotopes ^{124}Xe ^{126}Xe and ^{128}Xe as 0.07±0.02: 0.12±0.03: 0.13±0.06 barns.

In continued efforts to understand the cosmogenic production systematics of xenon in stony meteorites, Lafayette and Nakhla were studied by Rowe and co-workers [Rowe et al.,(1966)] and the spectrum of cosmic ray produced xenon was deduced to be

0.57: 1.00: 1.53: 0.86: 2.50: 0.60 = ^{124}Xe: ^{126}Xe: ^{128}Xe: ^{129}Xe: ^{130}Xe: ^{131}Xe: ^{132}Xe (these two stones contained only small amounts of fission produced isotopes at masses 132 to 136).

Marti et al., (1966) attempted to resolve the xenon components in meteorites based on the measurement of five meteorites, viz., Stannern, Mezo-Madaras, H-Ausson, Bruderheim and Abee, making some assumptions about the xenon components contributing to the measured xenon amounts in each one of these meteorites. These authors deduced the spallation xenon spectrum to be ^{124}Xe : ^{126}Xe : ^{128}Xe : ^{129}Xe : ^{130}Xe : ^{131}Xe : ^{132}Xe = 0.59 : 1.00 : 1.45 : 0.97 : 3.90 : 0.90.

In the first cross-section measurements of xenon isotopes by Funk and Rowe (1967) $BaCl_2$ target was employed. However the measurement was confined to only one energy as it was thought that, based on nuclear reaction systematics, the cross-sections at energies higher than few hundred MeV remain essentially the same. So only one or two cross-section measurement were considered sufficient to deduce the cross-sections at other high energies. It may be noted, prior to our experiments, the excitation functions for xenon production at low energies (E <200 MeV) were determined only in one experiment by Kaiser (1977).

The systematic determination of the cross-section measurements in the low energy region was taken up by Kaiser (1977). In a series of irradiation experiments at ORSAY and CERN accelerators, Kaiser tried to cover both the low and high energy range adequately. This was the first systematic attempt made to provide a set of reliable cross-sections for xenon isotopes

covering a wide range of energies. Unfortunately these irradiations had problems both at the time of proton-beam exposure and also during mass spectrometric measurement. The Ba targets used in the irradiation got excessively heated by the large proton flux from the accelerator during irradiation and some amount of xenon was lost in this manner. It was not possible to quantify the losses. At a later stage, during measurement, some of these targets absorbed moisture and in an attempt to drive out the absorbed water vapour from these irradiated targets they were pre-heated to ~200 °C. Considerable amounts of xenon were lost in this process. Unfortunately, these irradiation experiments did not yield the desired results and the aim with which the above experiments have been initiated remained unfulfilled.

It took another full decade to plan such irradiation experiments. The flaws and setbacks in the previous experiments have been corrected and precautionary measures taken in the experiments planned in this study. The xenon production cross-section values, obtained in this study at both high and lower energies will be discussed in detail in the following chapters.

1.4d Fission Xenon

Kuroda (1960) proposed that processes such as: (i) spallation and (n, γ) reactions induced by cosmic rays; (ii) spontaneous fission of nuclides; (iii) addition of products from particle irradiation or fission to the "primordial" xenon before it was trapped might have altered the terrestrial xenon. Following this many meteorite and terrestrial samples have been

analysed to see if they contain isotopic signatures of any of the processes mentioned above.

^{244}Pu is a radioisotope which decays primarily by α-emission. This nuclide (half life = 82 My) also decays by spontaneous fission having a branching ratio of 1.25 X 10^{-3} [Fields et al., (1966)]. The spontaneous fission of ^{244}Pu can be detected either by excesses at the heavy xenon isotopes ^{136}Xe which has an yield of ~6%, Hyde, (1971) and ^{134}Xe. The spontaneous fission of ^{244}Pu can also be detected through the study of fission tracks which are caused by lattice damage in dielectric grains produced during the passage of fission fragments. These tracks can be revealed by selective dissolution in laboratory etching. The other spontaneous fissioning heavy nuclide which can interfere with identification of ^{244}Pu is ^{238}U. However, the spontaneous fissioning ratio for ^{238}U is sufficiently low to allow the ^{244}Pu fission dominant to the fission xenon amounts measured in primitive meteorites.

Rowe and Kuroda (1965) first reported excesses in the heavy xenon sotopes of the Pasamonte achondrite. A combination of heavy isotope xenon measurement and fission track measurement in chondritic phosphates was used by Wasserberg et al., (1969) where the fissioning nuclide producing the above effects was confirmed to be ^{244}Pu. The fissioning spectrum of ^{244}Pu is measured by Alexander et al., (1971) and this is found to agree with the spectra deduced from meteorite studies.

1.5 Lunar rocks

Owing to their low energies SCR particles penetrate only into the surface layers of the extraterrestrial body and produce cosmogenic nuclides at shallow depths of the meteorite or lunar surface. The conditions under which these records are resolvable are (i) the sample should have sufficiently small total GCR exposure ages (including exposure to GCR particles at shallow depths) compared to the SCR exposure age (ii) it should have a higher concentration of target elements and (iii) the zero shielding exposure should be maximum. In meteorites the surface layers are lost by ablation during their flight through the atmosphere. Hence, the SCR irradiation records are in general not available for examination and there are only few meteorites in which SCR records has been clearly established. These are Salem [Evans et al.,(1987) and Goswami et al.,(1988)] and ALHA 77005 [Nishiizumi et al.,(1986), Lal and Marti (1977) found signatures of SCR exposure in St. Severin meteorite and Bhandari et al., (1988) found isotopic signatures of SCR irradiation in meteorite Gujargaon. The situation is quite different in the case of lunar samples. Among the lunar samples, lunar soils are not very suitable for study of SCR irradiation effects due to the facts that (i) they are exposed to GCR particles for very long periods of time; (ii) micro meteorite impact on the lunar surface continually churn the lunar soil surface and the SCR irradiation effects get mixed up, in this manner. Lunar rocks have the advantage that documented samples can be made available for study of SCR produced isotopic effects. Yaniv and Marti (1981) showed that some of these rocks like 68815 may even have stopped solar

26

flare helium. The irradiation history of these samples can be obtained from other techniques like nuclear track studies.

By a combination of nuclear track studies, ^{26}Al measurements and Ne isotope studies it was shown earlier that the rocks 61016, 64435 and 79215 were irradiated by SCR particles at the lunar surface [Venkatesan et al., (1980), Rao et al., (1979) and Bhandari et al., (1976)].

In an attempt to verify if SCR effects could be seen in the xenon isotopic concentrations measured in these rock samples, three samples from each one of the above rocks have been analysed. The topmost samples of all the three rocks came from shielding depths which are ~1.00 mm from the rock surface. The deeper samples analysed here came from depths of ~4 to 5 mm below the surface and the deepest sample analysed was from a shielding depth of about 17 mm (in case of 61016) and ~8 mm in case of lunar rocks 64435 and 79215. More details regarding the samples, the depth positions from which they are obtained etc. can be found in Section 2.2 of Chapter II.

CHAPTER II

EXPERIMENTAL TECHNIQUES

The first part of this chapter consists of a brief description of the Mass Spectrometer (MS) along with its functional elements. Also, a brief sketch of the characteristics of the MS used, the sample preparation methods, the various corrections and errors that may be introduced in during the measurement, how they are dealt with and how the behavior of the MS is monitored during the period of analysis of the samples is given. Moreover, the mass spectrometric conditions required for the measurement of the sample and details of the lunar rock samples used in this study are described. The second part of this chapter outlines the details of the irradiation experiments. Both the thin target and thick target experiments are discussed at some length, with an emphasis on the production of xenon isotopes from Ba.

2.1 Mass Spectrometric Techniques

The Mass Spectrometer(MS) consists of (i) an ion source, which produces a beam of monoenergetic ions; (ii) a magnetic analyser which separates ions having different mass/charge ratio and (iii) a collection and measuring system for the separated ion beam currents.

The system used in the study, schematically shown in Fig.2.1, is an all glass MS of the Reynolds type [Reynolds (1956)] with some modifications and is fabricated indegeneously at Physical Research Laboratory/TIFR(Bombay). It is of the single

GENERAL VIEW OF THE MASS SPECTROMETER
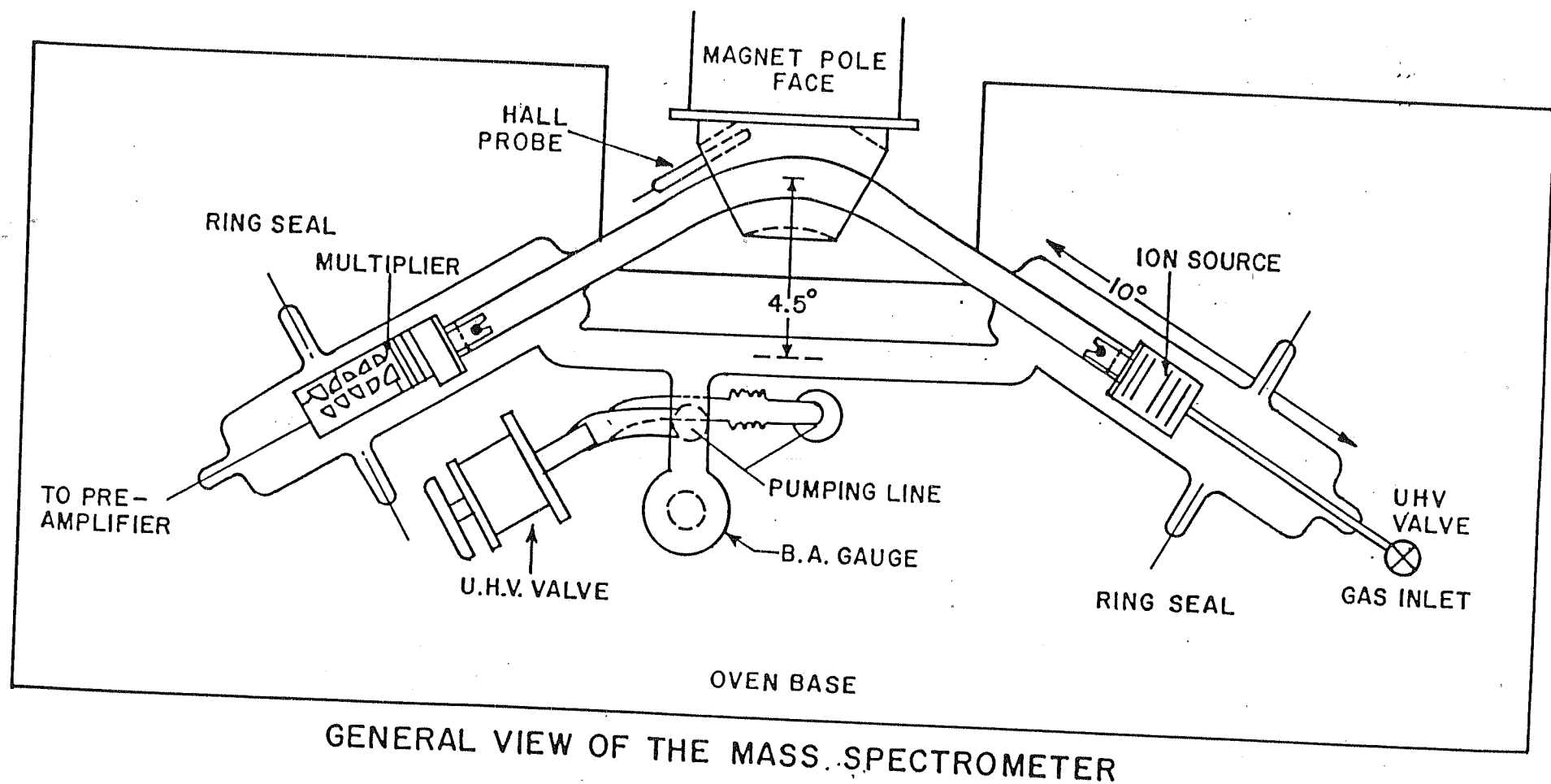
Fig.2.1   Schematic diagram of the Reynolds type Mass Spectrometer used in the present study.

focussing type with a 60° magnetic analyser with a radius of curvature 4.5" and is a dedicated instrument for noble gas studies. Metal parts have been kept to a minimum to minimise outgassing problem.

2.1a The Ion Source

A Nier type [Nier (1947)] electron impact ionization source is used since the elements studied here are all noble gases. The electron beam, produced by a tungsten filament, is accelerated by a potential of about 75 V (the neutrals are ionized at this energy), accelerating them to 75 eV at and around which the ionization probabilities are maximum for the noble gases. The ion beam, produced in this manner by electron bombardment, are acclerated by passing them through an electric potential of about 2.5 KV. A pair of half plates help to deflect the ion beam in the horizontal direction. The final slit which allows the gases out, has a width of 0.009" and 0.315" height. The efficiency of transmission of the ion source is increased by collimating the ionizing electron beam with a small permanent magnet (source magnet) placed externally. More details are given in Gopalan et al., (1973).

2.1b Sector Magnetic Analyser

The magnetic analyser has a 60° sector angle. The pole faces are shaped in such a way as to provide a concentration of flux lines in the region through which the ion beam passes and to minimize the fringe effects. The poles are separated by an air gap of 0.44". The coil used has a resistance of 1,000 Ω and the

field is linear with energising current upto 250 mA corresponding to a magnetic field strength of 8,000 gauss.

2.1c Ion Detection and Measurement

The collector slit has a width of 0.018" and a height of 0.315". The split half plates following the collector slit are used to deflect the ion beam so that good peak shapes are obtained. The ion beam is pre-accelerated by a third plate and detected by a 10 stage electron multiplier with Cu-Be dynodes. The anode of the multiplier is connected to the low leakage feed through along the axis by a coaxially shielded cable to carry the signals to the electrometer head amplifier. The schematic diagram of the mass spectrometer with the source and analyser assemblies are shown in Fig.2.1. A sputter ion pump has been introduced in the extraction side to provide better vacuum conditions. Except for the above change, the system·used in this study has remained the same as that described by Gopalan et al.,(1973) and Nautiyal (1980).

Fig.2.2 shows the xenon peaks obtained during a sample run. The peaks have a flat top indicating that the collector slit width is much wider than the beam width of the ions analysed. More details on this topic are given in a technical report by Gopalan et al., (1973).

2.2 Mass Spectrometer Characteristics

The electron emission current used for the ionization of the gases is ~ 0.1 mA. The electron multipliers have been provided with a voltage that can be raised upto 5,000 Volts. For
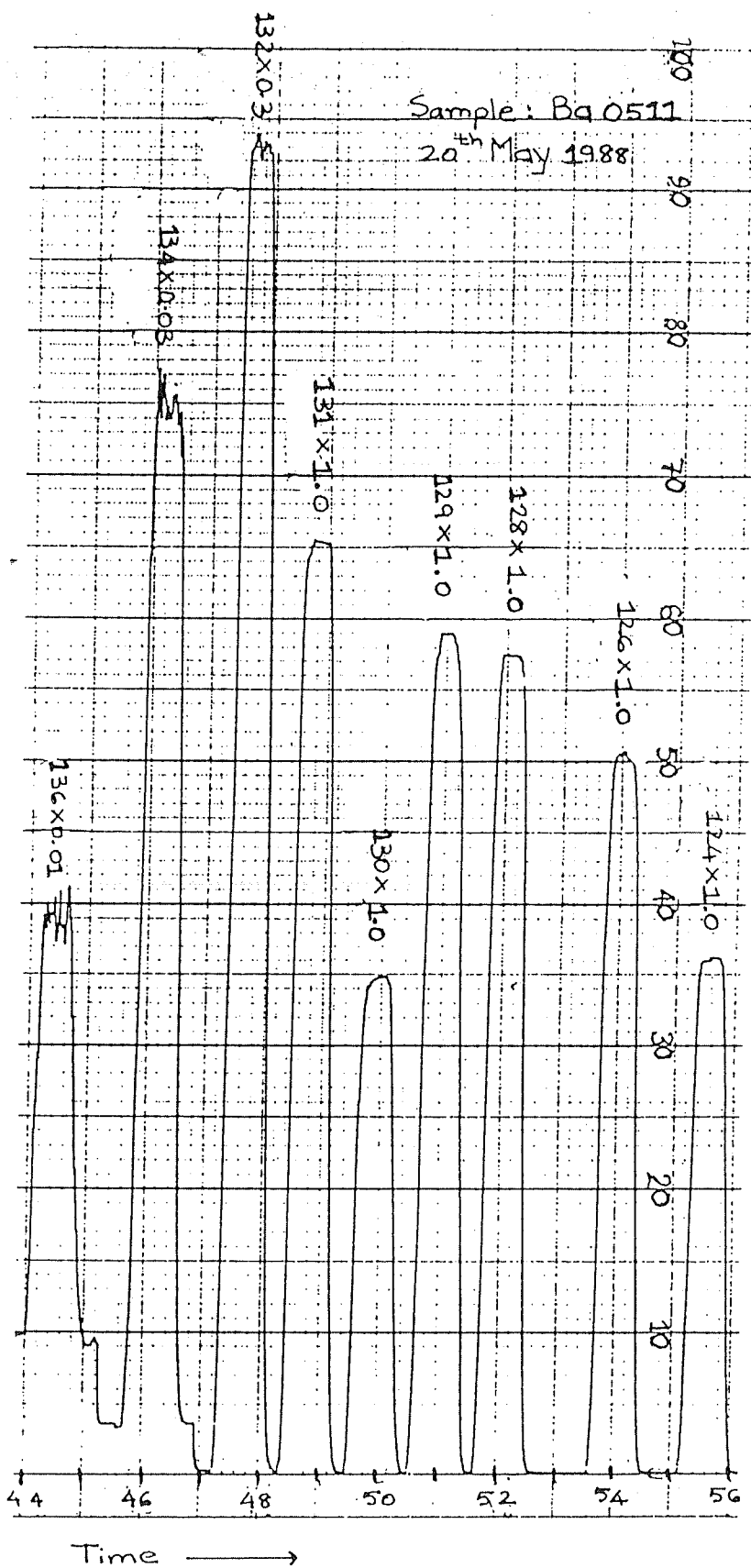
Fig.2.2   Xenon peaks measured during a sample (irradiated Ba
glass) run.

general operations during xenon analysis, the voltage used is only 1,600 Volts. The overall gain of the multiplier system at this voltage is about 10^5.

The resolving power of the instrument is 150, i.e. the peaks corresponding to the two atomic masses 150 and 151 amu are well resolved by the machine.

The energy of the ionizing beam, the electron emission current used for ionizing the gases and the voltage applied to the electron multiplier are all kept constant throughout the period of analysis of one set of samples, so that the mass spectrometer characteristics remain the same for all MS runs including hot blanks, air standards and samples.

2.2a. Sensitivity

The sensitivity of the MS is monitored by intermittent analysis of 0.0958 cc of standard air delivered through a Dorflinger-type metal pipette and further standardised by measurement of Bruderheim meteorite samples (kindly provided by Prof.J.H.Reynolds, University of California, Berkeley). Fig. 2.3 shows a typical xenon air spectrum obtained from the instrument, and Fig.2.4 shows the mass discrimination of the various xenon isotopes. The xenon sensitivity of the instrument typically is 8 x 10^{-14}ccSTP.mV^{-1}. The variation in sensitivity for xenon over the period of analysis of one set of samples is $\pm 9\%$, as obtained from the ^{132}Xe concentrations in the Air Standard. As the filament of the MS burned off during the tenure of the measurement, it was replaced. The set of 15 air standards analysed after this showed only $\pm 6\%$ variations between the ^{132}Xe
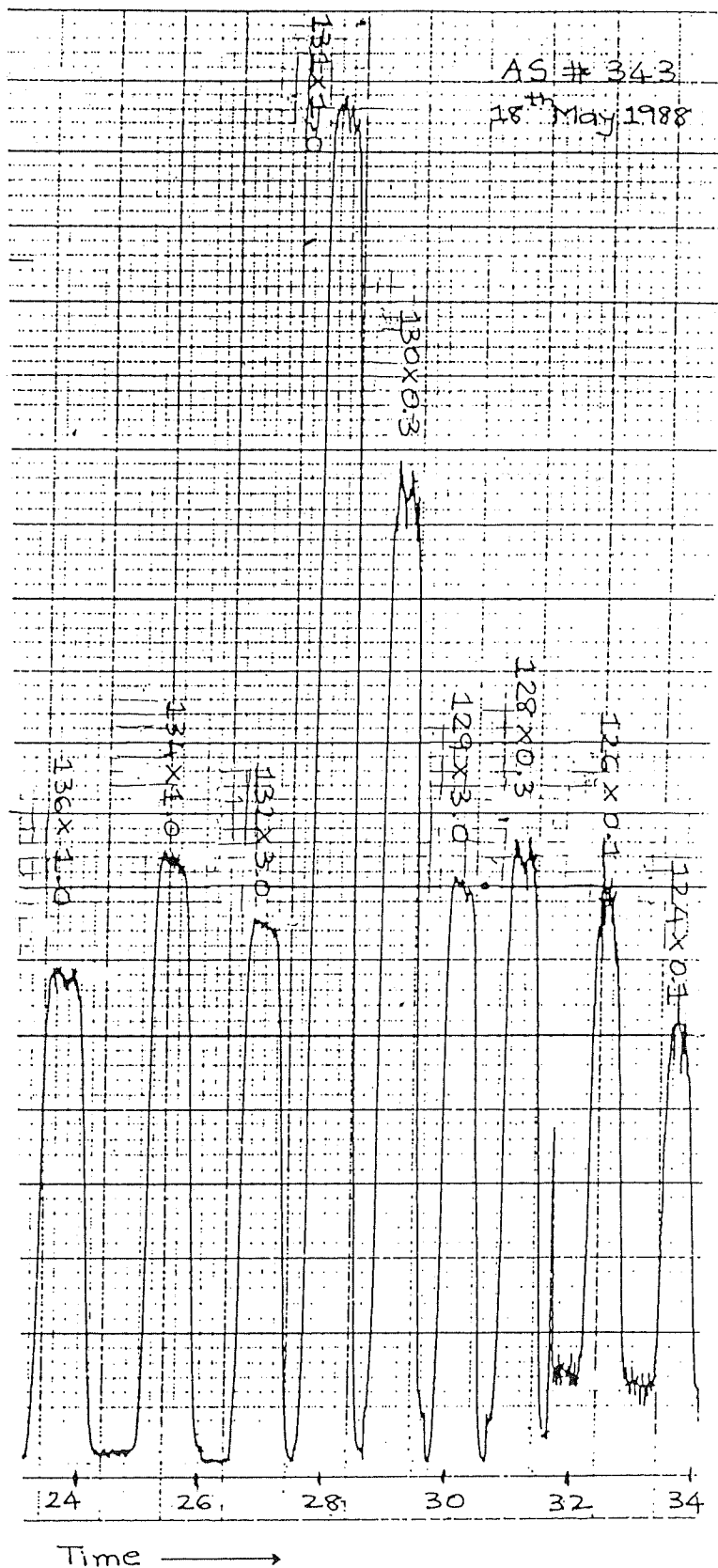
Fig.2.3   Typical xenon air spectrum measured by the MS.

34
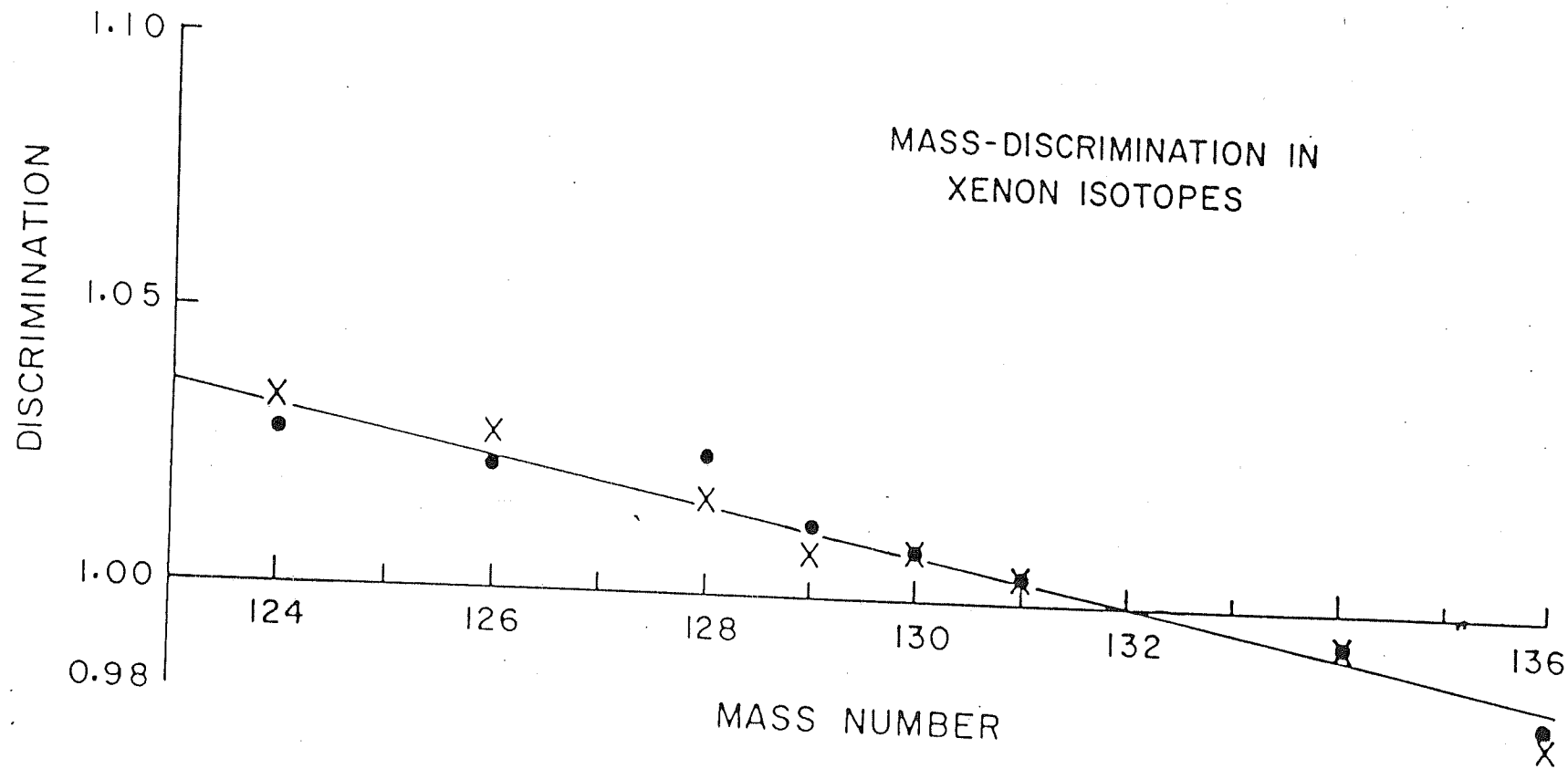
Fig.2.4   Mass discrimination of the various xenon isotopes.

signals which means that the the xenon analysis carried out with the new filament operational have less errors. The measured ^{132}Xe signals (after blank and m.d. corrections) are multiplied by the sensitivity and divided by the sample weight to obtain ^{132}Xe concentrations in ccSTP.g^{-1} of sample.

2.2b. Blank Corrections

When a sample is heated in the Mo crucible, gases are released from the crucible and also some residual gases are always present in the analyser. Hence, the measured gas concentrations are also corrected for the crucible contribution and for the background due to residual gases. For this, the crucible is heated to the same temperature as the samples and the released gases are measured. The analysis of the irradiated Ba glass samples are done in a single melting step and the extraction blanks are also determined at the same temperature. In case of the lunar rock samples discussed here a pre-heating step at 600°C is done for some of the rock samples. Also the blanks at this temperature are determined and correspondingly subtracted from the measured xenon concentrations.

The blanks measured throughout the period of analysis of the samples are small. The xenon blanks are about 2.0 x 10^{-13}ccSTP for isotope ^{132}Xe.

2.2c Mass Discrimination

The measured abundance of an isotope determined by the MS differs from the true abundance of the same isotope. This deviation arises from the differential response of the mass

spectrometer to different isotopes of a given element and is known as mass discrimination (m.d.). Among the various factors contributing to the m.d. the dominating ones are the differential response of the multiplier to the different masses and fractionation in the ion source chamber. If $R_{(t)}$ and $R_{(obs)}$ are the true and observed isotopic abundance ratios then m.d. is defined here as m.d.=$R_{(t)}/R_{(obs)}$

The m.d's in the xenon atomic mass region (124 to 136) are found to be 2% per amu (at the maximum) and is even less in several cases. Fig.2.4 shows the mass discrimination for various xenon isotopes. For the lighter isotopes, Ne for eg, the m.d.'s are still lower i.e. about 1.2% to 1.5% per a.m.u.

2.3 Sample Analysing Procedure

One of the basic requirements for the accurate measurement of a sample in a mass spectrometer is to obtain ultra high vacuum (UHV) to make the system as clean as possible, and to avoid the collision of the ionized beam with the residual air molecules in the analyser tube, otherwise this causes the beam to lose its energy and undergo varying deflections in the magnetic field producing tailing and other distortion problems in the measured peaks.

In the following sections the sample preparation and analysis procedures are described in detail. The analytical procedure has essentially remained the same as that described by Bhai et al.,(1978). The irradiated Ba glass targets are cleaned in ethanol and acetone with ultrasonic vibrators for about 3 minutes each, dried under IR lamps weighed, and wrapped in pure

Al foils and then introduced in the sample finger of the MS. Blank Al foils are also measured for blank corrections. The extraction side, schematically shown in Fig.2.5, is heated at $200^{\circ}C$ for 48 to 60 hours and the evolved gases are pumped out using a mercury diffusion pump which is backed by a two stage rotary pump. A vacuum of about 10^{-7} torr is obtained in this process. At this stage the diffusion pump is switched off and isolated and further pumping is done solely by a sputter ion pump. The samples are measured only after both the extraction and mass spectrometer sides are extremely clean i.e., a level of vacuum of the order of 10^{-9} to 10^{-10} torr is obtained. For this purpose the molybednum crucible is degassed several times at $1600^{\circ}C$ for 1 hour time-periods. By this process the system blanks are reduced to the desired levels, generally less than 1% of the ^{132}Xe signals measured in our samples. Appropriate corrections then are made.

2.3a. Gas extraction and Purification :

During the sample analysis, the temperature is increased in slow steps of in about 5 minutes each to a maximum of $1,600^{\circ}C$ and the sample is heated at this temperature for about 30 minutes. The gases evolved are collected on activated charcoal fingers maintained at liquid nitrogen temperature. The charcoal finger is heated at $100^{\circ}C$ and the released gases are cleaned using a Ti-Zr gettering furnace heated to $800^{\circ}C$ which is cooled down to room temperature in about 30 minutes. The xenon gas is absorbed on a second charcoal finger kept at $-80^{\circ}C$ for 30 minutes and the remaining gases are pumped away. The absorbed xenon is released at $110^{\circ}C$ and this fraction is further cleaned, (i.e. the active

AIR SPIKE

TO
DIFFUSION PUMP

V6B

V6F

IG

V2

V1

V4

V5

TO
MASS SPECTROMETER

VAC1

VAC2

V3

TITANIUM
FURNACE

CH1

TO
ION PUMP

CH2

V1, V2, V3, V4, V5, UHV METAL
VALVES (BAKEABLE)

V6F, V6B – UHV PIPETTE VALVE

CH1, CH2 – CHARCOAL FINGERS

IG – ION GAUGE

VAC1, VAC2 – VAC SORBS
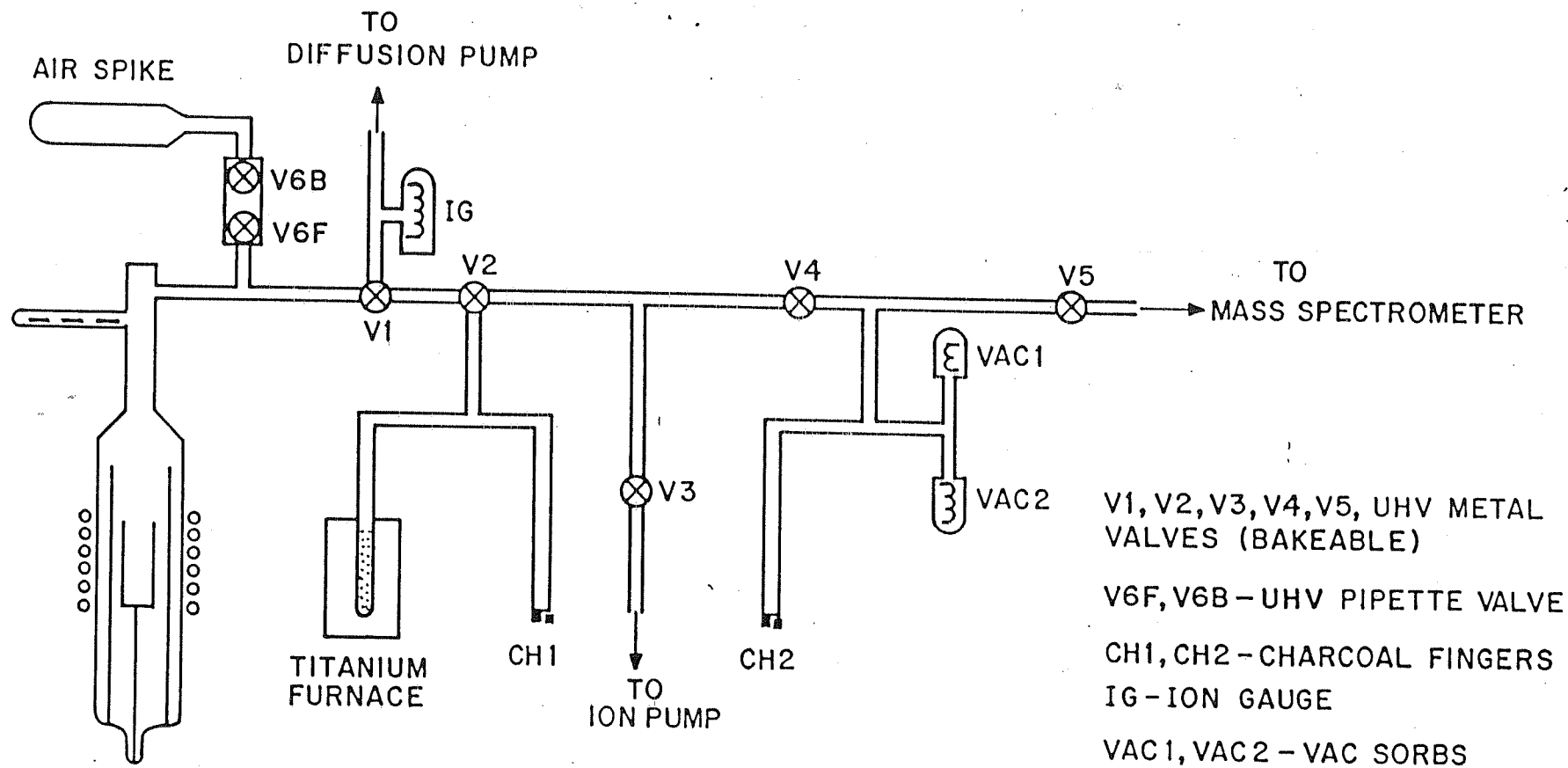
NOBLE GAS EXTRACTION AND PURIFICATION SYSTEM

Fig.2.5   Schematic   diagram   of   the   noble   gas   extraction   and
purification system.

gases H, N_2, O_2 and Hydrocarbons are removed) by using two SAES getters. The pure xenon fraction is admitted into the MS as a single fraction, while the MS is operating in the static mode. The high voltage supply of the ion guage is kept floating at the time of letting the gas into the MS and the xenon isotope peak heights are recorded using a Variable Reed Electrometer (VRE). The VRE provides a choice of input resistances, 10^9 ohms, 10^{10} ohms or 10^{12} ohms and also allows the use of a large number of ranges for each one of these resistances. This combination is very useful for the measurement of the gas concentrations usually encountered in extraterrestial samples. The xenon isotopes (M =124-136) are scanned and recorded 10 times by continuously sweeping the magnetic field. By using a computer program the isotopic peak heights are extrapolated to the 'Zero time' corresponding to the letting in time of the gases into the MS.

The repeat runs of the samples analysed in the same fashion show only slightly higher gas amounts than the hot blanks indicating that the extraction efficiency of xenon is better than 99%. As mentioned earlier, the gas release time, equilibration time, absorption time etc. are constant so that all the measurements of the samples and standards using the MS are carried out under identical conditions.

2.4 Performance of the MS

During the analysis of the Air Standards (AS), after a few irradiated Ba glass targets were measured, the less abundant isotopes of xenon, ie. ^{124}Xe, ^{126}Xe and ^{128}Xe, stated showing an increasing trend in the peak heights from scan to scan due to

memory effects. The spallation xenon spectra is quite different from the xenon spectra encountered in the AS (air standard) and that usually seen in meteorite or lunar samples. The measurement of these 'unusual' samples gave rise to a memory build up in the MS. The xenon amount released in this manner from the memory of the earlier measurements was observed to increase with the gas pressure inside the mass spectrometer. The Ar fraction of the air standard was seperated and let into the MS at a comparatively higher pressure and this fraction was allowed to remain in the MS for about 30 minutes. During this process, the Ar ions displace the xenon atoms from the metallic plates on the source and analyser side and thus remove the memory effect. The xenon isotope peak heights were monitored throughout this period and when the xenon peak heights ceased to increase any further the MS volume was pumped out by opening it to the sputter ion pump. The xenon fraction of the AS analysed after this 'Ar sputtering' demonstrated no increase in peak heights for the lighter xenon isotopes which showed an increase earlier. By this process the xenon memory from the earlier measurements was 'erased' in our glass mass spectrometer.

2.5 Description of the Lunar Rock samples

It has been pointed out in the previous chapter that the xenon concentrations measured in an extraterrestrial sample is contributed from various processes such as trapping of noble gases at the time of formation and implantation of solar wind in the surface samples; the SCR and GCR spallation at the time of cosmic ray interaction in space and fission of transuranium elements. To

resolve these components, various appropriate samples need to be chosen. From earlier investigations the rocks 61016, 64435 and 79215 are found to contain SCR irrdiation effects. SCR produced ^{26}Al, Ne isotopes and nuclear tracks were observed in these rocks [Bhandari et al., (1976), Rao et al., (1979) and Venkatesan et al., (1980)]. Details of samples studied here are given below:

Table 2.1 describe the rock samples analysed in the present work.

Table 2.1

Rock	Location (Crater)	Type	Size of the main rock piece from which spot samples were taken	Weight (Kg)
61016	Flag	Anorth	28X18X16	11.7
64435	South ray	Breccia	12X19X11	1.079
79215	Van Surge	Breccia	9X8X7.5	0.554

Three well documented lunar rocks analysed here for SCR xenon effects are anorthositic breccias from lunar highland. Two of these, 61016 and 64435 were collected during the Apollo-16 mission whereas the third rock, 79215, was collected during the Apollo-17 mission.

Rock 61016 was collected from a location near Flag Crater. An upper limit of 7 My was given for the GCR exposure age of this rock, which was dated by Stettler et al., (1973) by ^{38}Ar-^{37}Ar method.

Rock 64435 was collected from stone mountain which was covered by South Ray crater ejecta (Apollo-16 Priliminary Science Report, 1972). Its chemical compositions were determined by Laul et al., (1974) and Hubbard et al., (1974).

Rock 79215 has higher Mg content as determined by Blanchard et al., (1977) and Mc Gee et al., (1978) and is a brecciated troclolite. The plagioclase from this rock has very low Mg content (~0.06%) but the bulk sample may contain as much as 5.7% Mg [Bhandari et al., (1976)].

All the three rocks are well documented with known exposure geometries and they have recognisable top surfaces, as determined by particle track measurements. Three samples each from all the three rocks were studied during the course of the present analysis. The depth positions from which these samples are taken are indicated below (Table 2.2). Sketch is given in Figs. 2.6 and 2.7.

Table 2.2

Rock	Sample	Shielding depth depth (mm)
61016	R1	0.5 - 3.0
	R2	4.0 - 7.5
	R3	16.0 - 18.0
64435	R1	0.0 - 1.0
	R2	4.5 - 7.5
	R3	7.5 - 9.0
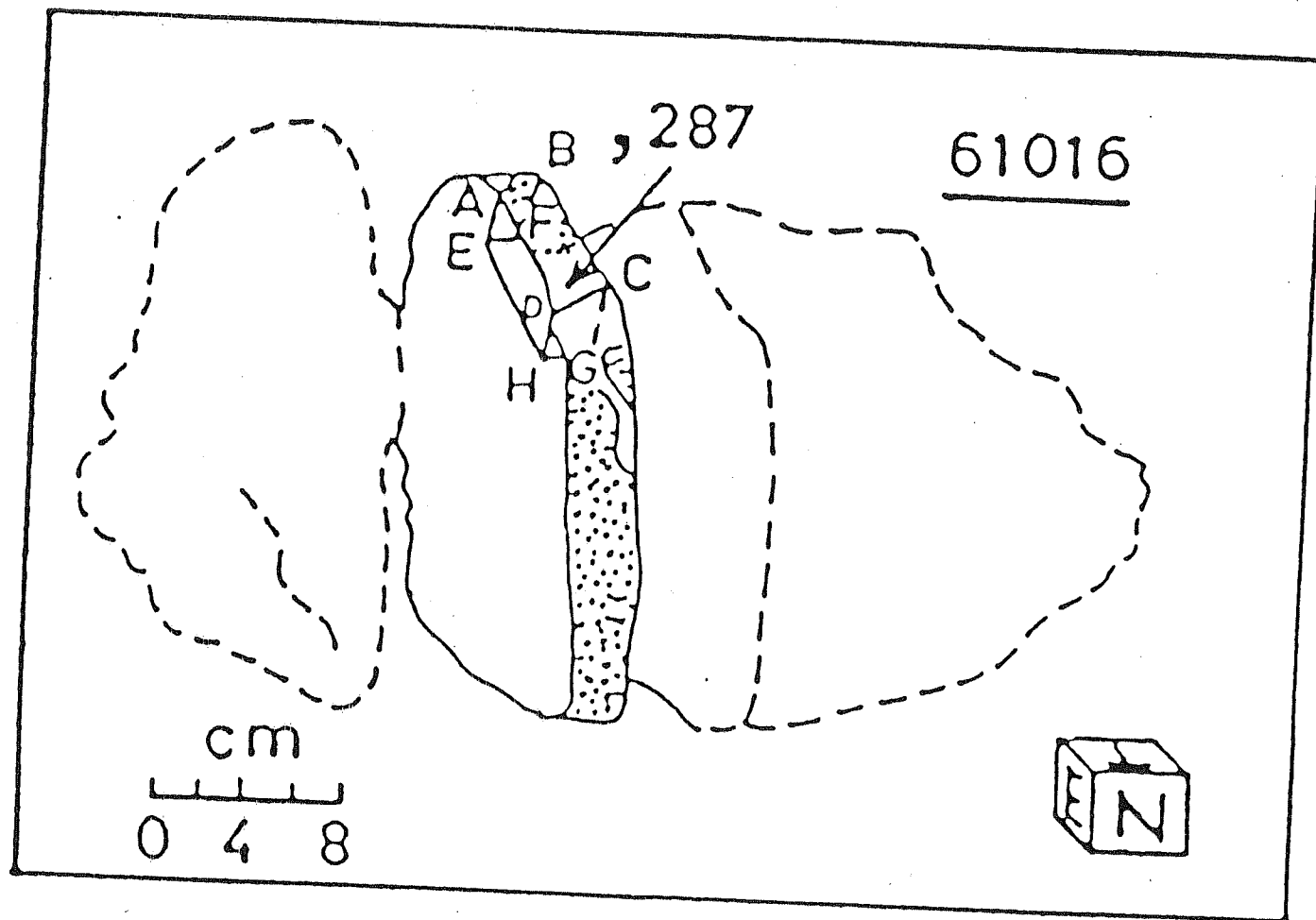
Fig.2.6   Sketch of lunar rock 61016 describing the positions of
the analysed samples.

61016-287
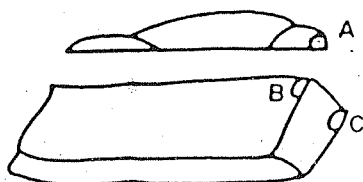
6cm X 2cm

61016-300
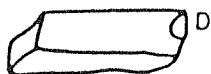
2cm X 1.5cm

A,B,C,D⟶10mg. each
TOTAL=40mg.

64435,95

1·5cm
TOP
3cm
BOTTOM
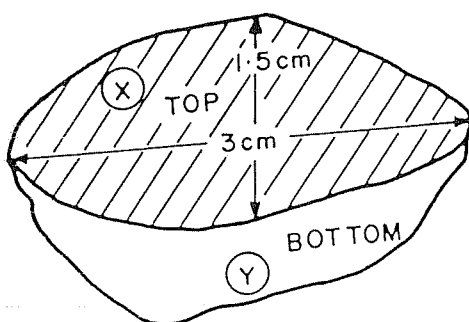
X,Y ⟶ 8mg. each
TOTAL = 16mg.

79215,78

1 cm

2·5 cm
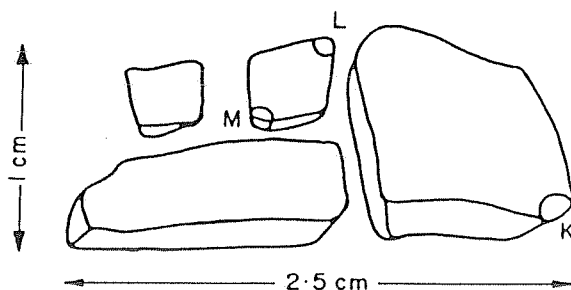
K,L,M ⟶ 10 mg. each
TOTAL=30mg.

Fig.2.7   Sketch of lunar rocks 61016 and 64435 describing the

positions of the analysed samples.

79215	R1	0.0 - 1.5
	R2	2.0 - 5.0
	R3	5.0 - 8.0

Figure 2.6 and 2.7 shows a sketch of the rock 61016, indicating the sample positions inside the rock.

2.6 Irradiation Experiments

In this section, an emphasis on the measurement of production cross-sections for the xenon isotopes from Ba targets during irradiation experiments is made. The target preparation, experimental set up used for irradiation, methods employed in monitoring the proton-flux (p-flux) etc are discussed briefly.

The Ba glass samples measured in the course of this study were irradiated with proton beams from accelerators using the standard techniques, the thin target and thick target irradiation methods. For the energies below 45 MeV (low energies) the Ba glass targets were irradiated using the stacked foil technique at JULIC cyclotron. The 600 MeV irradiations, carried out at CERN, were a combination of the thin and thick target irradiations and the 800 MeV, 1200 MeV and 2600 MeV irradiations were done in the thin target geometry (some details are given in Appendix I).

2.6a Low Energy Irradiations

For proton energies upto 45 MeV the stacked foil technique was employed to measure the excitation functions for

46

p-induced reactions on Ba. Stacks consisting of a combination of Ba glass targets (obtained from Schott Glasswerke, GmbH, Mainz) and of Al and V foils (obtained from Goodfellow Metals Ltd., UK) were irradiated on different occasions at the external beam of the isochronous cyclotron JULIC of the IKP/KFA Juelich.

The Ba glass used for irradiation contained 40.13% Ba by weight [Peiffer (1986)]. Ba was the only heavy element in this glass and all impurities which possibly could interfere with the production of the xenon isotopes during p-irradiation were found to be negligible. The Ba glass was obtained as a plate, from which circular discs of 15.7 mm dia were drilled by a hollow drill. Each disc had a thickness of 0.1 mm to 0.2 mm and was polished with a diamond grinding wheel. The cleaned glass discs were degassed for an hour at $250^{O}C$ at 10^{-6}Torr. The chemical composition of the Ba glass target used in the present experiments is given in Appendix I.

A typical stack is shown in Fig.2.8. Each stack arrangement consisted of a number of 0.1 mm to 0.2 mm Al Catcher foils and commercial grade Al degrader foils in addition to the Ba glass targets. Three different stacks were used so that the uncertainities of the proton energy due to energy straggling was minimized. The proton energy was degraded in three steps: from 44 MeV to 34 MeV, from 34 MeV to 22 MeV and from 22 MeV to 12 MeV respectively, in the three stacks. In order to supplement the flux measurement by a Faraday cup a 0.025 mm thick V foil, was used as a flux monitor. V foils were included in each stack at intermediate positions also, in order to check the determination of the proton beam current, energy determination throughout the

PROTON
BEAM

■ Au FOIL

▤ TARGET FOIL

▯ Al FOIL

I Al PIECE TO KEEP
STACKS IN POSITION

2 STACK HOLDER
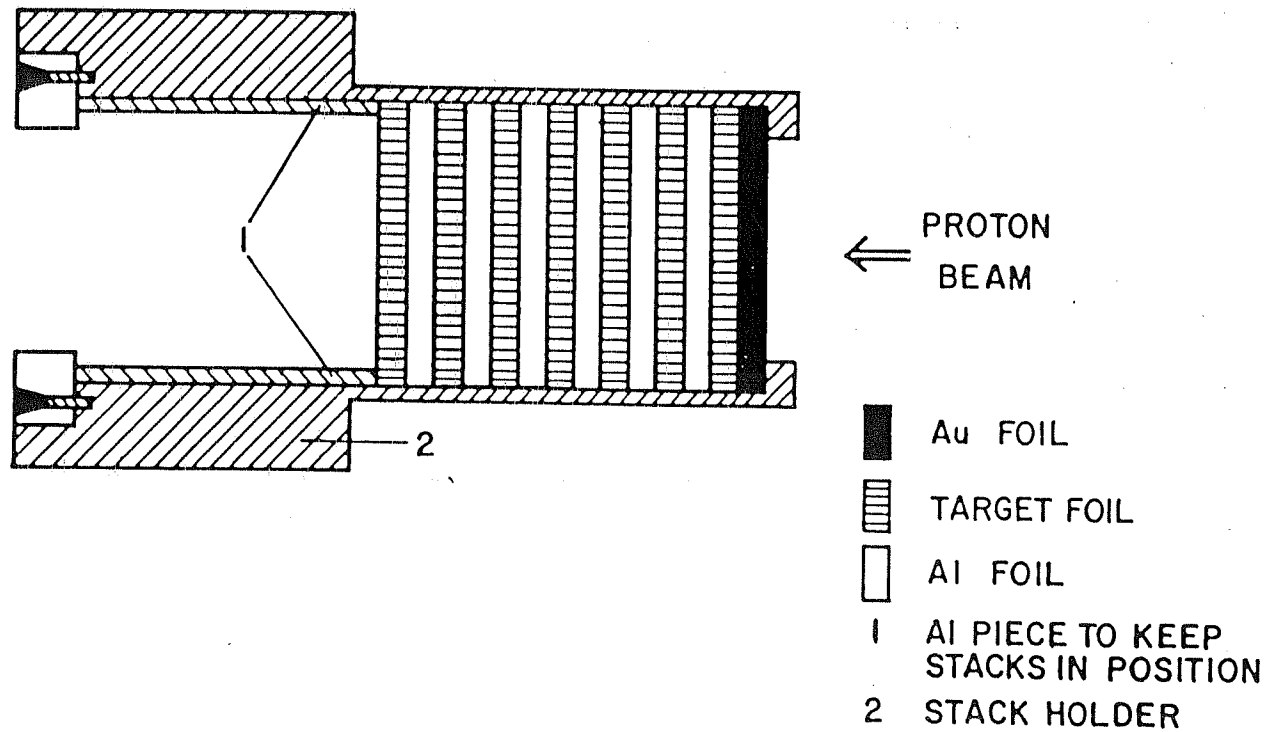
Fig.2.8   Schematic diagram of the stack arrangement for thin target

irradiations.

stack and overall accuracy of the cross section measurements. The excitation functions for the production of ^{51}Cr and ^{47}Sc from V were used for the flux determinations. More details may be found in Prescher et al.,(1980).

The irradiations were performed at the JULIC accelerator, in the irradiation chamber BK1, which allows for measuring the beam current by a Faraday cup. The three stacks were irradiated with proton currents of 3.29 x 10^{11} S^{-1}, 4.33 x 10^{11} S^{-1} and 5.54 x 10^{11} S^{-1} over periods of 589, 465 and 660 minutes respectively (further details are given in Appendix I). The temperature of the stacks, checked in separate irradiations by thermochrom monitors with 50 uA and 25 uA proton currents was found to be less than 100°C. More detailed discussions on the experimental procedure, the methods of flux monitoring and gamma spectroscopy could be obtained from Michel et al., (1978a, 1978b and 1979). These irradiations were done as a part of collaborative work between PRL and the Institute for Nuclear Chemistry at University of Cologne, FRG.

The irradiated foils were later transported to the University of Cologne and Gamma spectroscopic measurements of these target foils were done at Institute für Kernchemie at Cologne. When radio activity of these irradiated Ba glasses subsided to acceptable levels the samples were analysed at both PRL and Cologne.

2.6b Irradiation of the Model Meteoroid Spheres of Radii 5 cm and 25 cm.

Here the details of the irradiation experiment carried out at the CERN synchrocyclotron and the experimental arrangement used in the two thick target simulation irradiation experiments are described. In these experiments, meteoroid mockups of radii 5 cm and 25 cm, made of diorite and gabbro material respectively (Elemental composition of the diorite and gabbro spheres are shown in Appendix II), were irradiated with 600 MeV proton beam simulating the space irradiation conditions of the meteorites. The discussions are centered around the Ba glass samples which are used as targets for the production of xenon isotopes here. Complete details about these experiments are given in R.Michel et al (1986 and 1989), P.Dragovitsch (1987) and references therein.

Fig.2.9 shows the experimental arrangement that was used in the thin/thick target irradiations. The first thin target stack, consisted of metal foils of 8 mm diameter. The Ba glass sample Ba 11 analysed in this study was irradiated in this stack. The Ba glass foil had a thickness of 2 mm (Ba glass with 0.4021 $g.gBa^{-1}$, supplied by Schott Glaswerke, Mainz). The other metal foils were generally of thickness less than 1 mm. The metal foils were separated by Al catcher foils (0.05 mm thickness, Kryal R, 99.999% Al). (The second thin target was intended for the measurement of Kr production rates).

The model meteorite was made of terrestrial granodionte from Odenwald/FRG ($H_2 = 10^{-3}$ $g.g^{-1}$, density = 3.0 $g.cm^{-3}$, (for chemical composition see Appendix II). The high density and low water content of this material makes it suitable to be used as a

DIORITE SPHERE
R = 5 cm

Fe − CYLINDER
∅ = 30 cm

THIN
TARGETS

600 MeV
p−BEAM

Aℓ

←—— 39 cm ——→|←———— 104 cm ————→|←——— 35 cm ——→
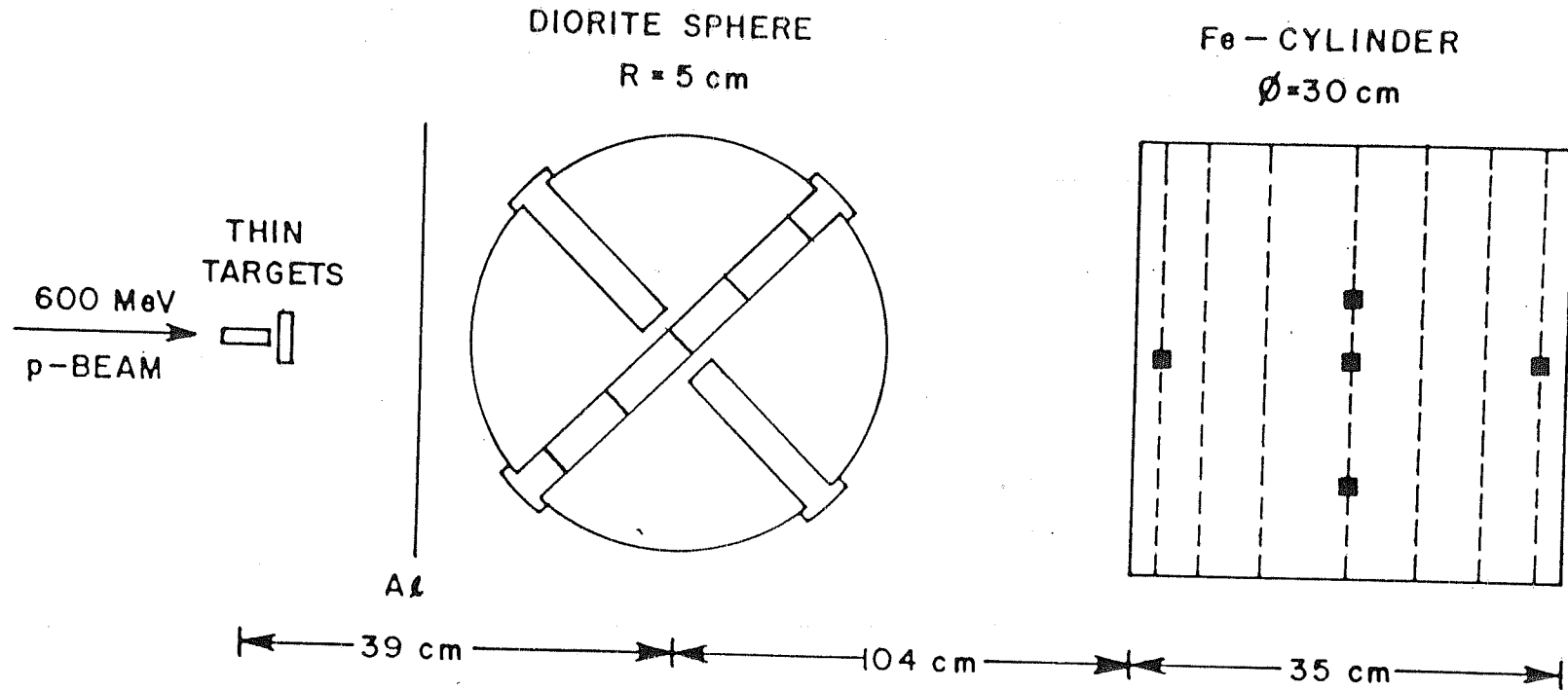
COMBINED THIN TARGET/THICK TARGET ARRANGMENT

(NOT TO SCALE)

Fig.2.9   Experimental arrangement used for the thin/thick target
irradiations at CERN synchrocyclotron.

model for stone meteorites. Two perpendicular drills, of 8 mm diameter each, were drilled in this diorite sphere and three Al tubes containing target foils were introduced inside the sphere. Fig.2.10 shows a sketch of the diorite sphere, R =5 cm, and its target cores.

Tube I contained stacks of foils similar to the first thin target stack. The Ba glass target positions and the positions of Ba 011, Ba 012, Ba 013, Ba 014 and Ba 015 samples, analysed in the course of this study are marked.

Tubes II and III contained degassed material from the L Chondrite Ladder creek and containers with pressed LiF, $K_2Cr_2O_7$, MgF_2, Pbs and CaF_2. The third part of the target arrangement consisted of a cylindrical Fe beam stop with cores filled with the same kind of target foils as used in the meteoroid model. Al monitor foils were kept in front of the sphere and the cylindrical Fe beam stop so that the p-fluxes could be monitored.

The 25 cm meteoroid mock-up that was irradiated in the second phase of these experiments was made of gabbro. Due to the considerable size of this body it could not be made as a regular sphere and was made out of slabs. The composition of the material is nearly identical with the diorite used in the previous experiment and is given in Appendix II. The effective radius of this model, calculated from its mass of 223.5 kg, was 26.1 cm. The slabs were arranged on steel tubes with an inner diameter of 19 mm and a wall thickness of 1.5 mm and were held together by two Fe clamps, threaded with nuts and bolts. Most of the fabrication was done at the Institute fur Kernchemie, University of Cologne, FRG.

I

STACKS OF FOILS:
Mg, Al, Si, Quartz, Tl, Fe, Co,
Ni, Cu, Rh, Ba, Lu, Au

$\emptyset = 10$ cm   II

Fe & Al FOILS

LADDER CREEK

III

PbS, CoF_2 PILLS

Cu, Al FOILS
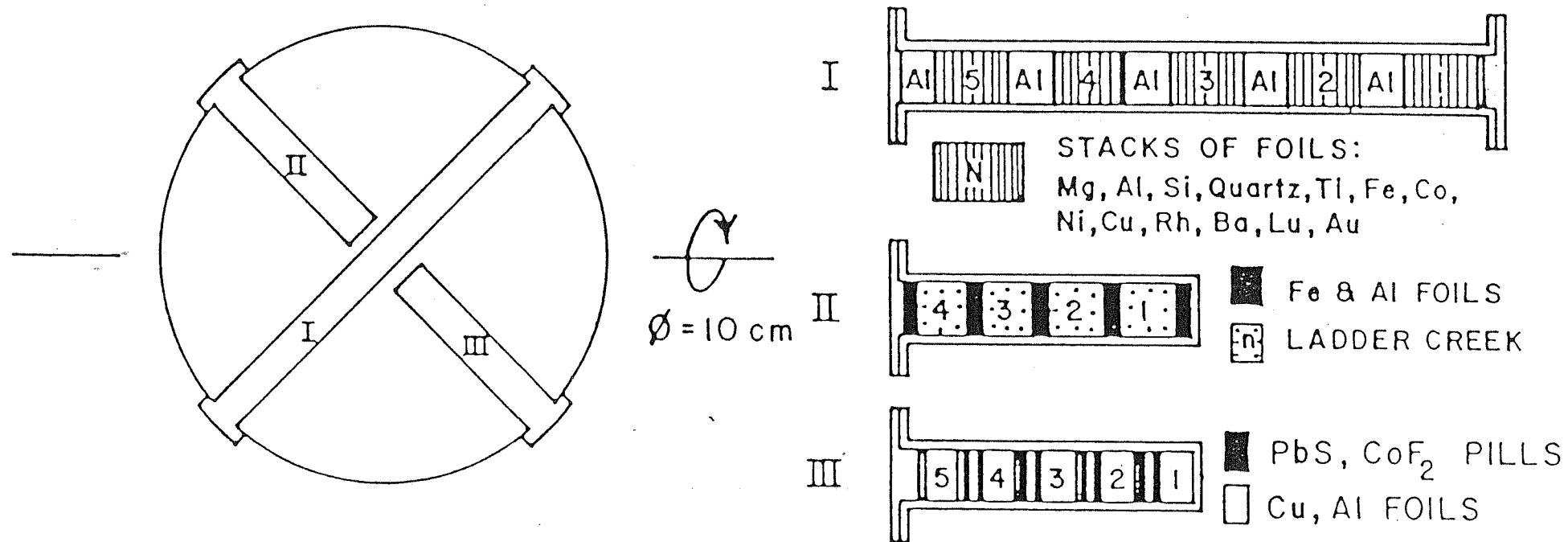
Fig.2.10 Sketch of the Diorite (R =5 cm) sphere and its target

cores.

The targets for the production of the cosmogenic nuclides were placed inside Al containers in the central steel tubes. Altogether a total of 17 Al containers probed 9 different depths inside this model. The positions of the Ba glass targets Ba 0122, Ba 0312, Ba 0412, Ba 0522, Ba 0612, Ba 0712 and Ba 0922 measured during the course of this study have been marked in Fig.3.10. As in the previous experiment, the Ba glass target foils had a thickness of 2 mm and a Ba content of 40.21% by weight.

2.6c Irradiation and Flux Monitoring

Both the spheres were irradiated at the external beam of the CERN synchrocyclotron with p-beam having an energy of 600 MeV. By a complex movement of the sphere a 4π isotropic irradiation was achieved. The 5 cm and 25 cm meteoroid models underwent translational motion about two perpendicular axes with amplitudes 5 cm and 25 cm (left/right and up/down movements) respectively. This made it possible for a homogeneous proton "rain" in vertical planes of 10 cm x 10 cm and 50 cm x 50 cm. The Al monitor foils kept in beam up position of the spheres also took part in these translational movements. Along with this translational motion the spheres were rotated about two perpendicular axis. In order to avoid the irradiation of the axis and of the drive of the first rotation, the first rotation was by 2π and the second one by π back and forth. Fig. 2.11 shows the movements of the 5 cm sphere during irradiation.

The flux of primary protons through the diorite sphere was evaluated by analysing the Al foil in front of the artificial

ROTATION

$\omega = 0.733 \ s^{-1}$

$\psi = 360°$

TRANSLATION

$V_x = 0.08 \ cm \ s^{-1}$

$|x| = 5 \ cm$

ROTATION

$\omega = 2.09 \ s^{-1}$

$\psi = 164°$

TRANSLATION

$V_y = 0.034 \ cm \ s^{-1}$

$|y| = 5 \ cm$
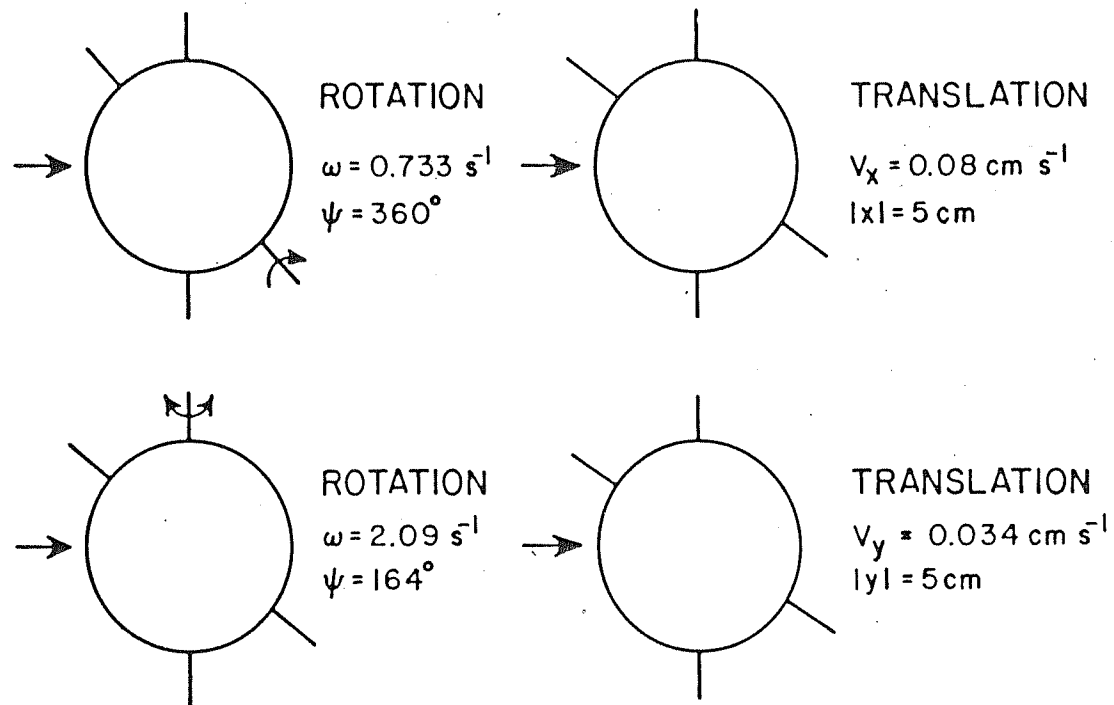
Fig.2.11 Movements of the diorite (R = 5cm) sphere during irradiation.

meteorite. The reaction ^{27}Al (p 3p3n) ^{22}Na, which has a high and constant cross section at high energies and is least affected by the secondaries is used for the flux determination. The deduced p-flux is $1.64 \pm 0.01 \times 10^{11}$ $S^{-1}cm^{-2}$ for the R = 5 cm sphere. The corresponding value for the gabbro sphere, estimated in the same manner, is $4.82 \pm 0.01 \times 10^{11}$ $S^{-1}.cm^{-2}$. Some more inputs regarding the irradiation time, p-dose etc can be found in Appendix III. In the case of the granodiorite sphere (R =5cm) the total spread in the flux values was 18% with 90% of the values within ±4% of the mean. It needs to be pointed out that this homogenity is further improved by the rotational movement of the meteoroid mockups.

The gabbro sphere (R =25 cm) is given the following movements at the time of irradiation (i) two translatory motions of 50 cm each in the horizontal and vertical directions, the velocities of the horizontal and vertical motions are respectively 5.0 cm/min and 3.3 cm/min; (ii) two rotational motions of 2π each with velocities of 5 r.p.m. and 2 r.p.m. about the horizontal and vertical axes passing through the centre of the gabbro spheres.

The secondary particle background in the irradiation chamber was determined by keeping Fe and Co monitor foils near the individual targets and in numerous places around the target assembly. The background of low energy neutrons, fast neutrons and protons estimated using the reactions ^{59}Co (n, γ)^{60}Co, ^{59}Co (n,p) ^{59}Fe and Fe (p, xn) ^{56}Co were found to be $3.4 \times 10^{8} S^{-1}.cm^{-2}$, 3.6×10^{8} $S^{-1}.cm^{-2}$ and 5×10^{8} $S^{-1}.cm^{-2}$ respectively, in both the experiments.

2.6d Irradiations at Proton Energies of 800, 1200 and 2600 MeV

The Ba glass targets irradiated at energies 800 MeV, 1200 MeV and 2600 MeV have been obtained from the irradiations at Los Alamos and Saclay accelrators. These are thin target irradiations similar to those discussed in Section 2.2. Al monitor foils have been used to evaluate the fluxes that the targets received. The reaction $^{27}Al(p,x)$, ^{22}Na is employed for the above purpose and the cross section values of 15.5 mb, 14.6 mb and 11.7 mb as calculated according to J.Tobailem, c.H.deLassus, St. Genies, Additif No.2 ala CEA-N 1466(1) (1975), CEA-N-1466(4)(1977) et CEA-N-1466(5)(1961) have been adopted for the above reaction at energies of 800 MeV, 1200 MeV and 2600 MeV respectively. These have been found to be 7.25($\pm$0.14) x $10^{10}cm^{-2}.S^{-1}$, 8.67($\pm$10) x $10^{10}cm^{-2}.S^{-1}$ and 2.47($\pm$0.05) x $10^{10}cm^{-2}.S^{-1}$. The time of irradiation for the 800, 1200 and 2600 MeV Ba targets are respectively 20400 sec, 39660 sec and 43080 sec making the total flux seen by the targets as 1.48 ($\pm$0.03) x 10^{15} protons.cm^{-2}, 3.44 ($\pm$0.04) x 10^{15} protons.cm^{-2} and 1.06 ($\pm$0.02) x 10^{15} protons.cm^{-2} (see Appendix III for more information about these irradiations).

The fluxes of the thermal neutrons and fast neutrons in the irradiation chamber have been determined by using Co foils kept at different places inside the experiment chamber. The following reactions are employed for this purpose. ^{59}Co (n_{th}, gamma), ^{60}Co and ^{59}Co (n_{fast},p) ^{59}Fe. These are determined to be respectively 2.06 x$10^{6}cm^{-2}S^{-1}$, 3.54 x$10^{6}cm^{-2}S^{-1}$ and 1.49 x$10^{6}cm^{-2}.S^{-1}$ for the thermal neutrons and 2.80 x$10^{8}cm^{-2}.S^{-1}$, 5.34 x$10^{8}cm^{-2}.S^{-1}$ and 9.34 x$10^{7}cm^{-2}.S^{-1}$for the fast neutrons in the

case of the Ba glass 800 MeV, 1200 MeV and 2600 MeV.

Appendix III gives a quick glance at the irradiation times, fluxes and p-doses received by the Ba glass targets and also the background fluxes of neutrons in the experimental chamber for the high energy irradiations.

CHAPTER III
Results and Discussions

Part I (Low Energy)

Production Cross-sections of Xenon at p-energies <50 MeV and SCR Production Rates on the Lunar Surface

In the next two chapters the results of the thin and thick target irradiation experiments carried out in this study are discussed. Further the xenon production rates in lunar surface material, calculated by using standard models and including the cross-sections measured by us at different energies are also discussed. The SCR (low energy) production rates and the corresponding cross-section measurements are discussed in this chapter whereas the high energy measurements (corresponding to GCR particle energies) are discussed in Chapter **IV**. The calculated xenon production rates are applied· in the case of documented lunar rock samples, exposed to the sun on the´ lunar surface so as to verify if the SCR production rates can explain the xenon excesses observed at some of the isotopes in these rocks.

As explained in the previous chapters, the cross-section measurements carried out during the course of this study can be classified into two categories. The first category is the low-energy cross-section measurements for the production of stable xenon isotopes from barium targets by protons having energy <45 MeV. The second category consists of high energy cross-section measurements on Ba targets at proton energies of 600 MeV, 800 MeV, 1200 MeV and 2600 MeV. In this Chapter III, only the low energy cross-sections will be discussed. The data set presented in this

chapter provides the much needed production cross-sections that are essential in models to calculate the production rates of xenon isotopes in extraterrestrial matter, by SCR particles.

3.1 Low Energy Cross-section Measurements

Here the excitation functions for the xenon isotopes up to 45 MeV are presented, followed by a discussion on the calculated xenon production rates in lunar surface material by SCR protons. The methodology used for the calculation is briefly described in Chapter II. In addition, an attempt has been made to deduce the SCR xenon spallation ratios, by studying samples from known depths inside well documented lunar rocks 61016, 64435 and 79215. The experimental results obtained from the analysis of these rocks are compared with the estimated theoretical production rates.

The Ba glass samples analysed by us in the low energy range of 12 MeV $<E<45$ MeV (which are obtained from the irradiations at the JULIC synchrocyclotron) are, BA1, BA3, BA5, BA7, BA10, BA3-6, BA4-2 and BA4-6. The p-energy received by the individual target discs are, 44.55 MeV, 40.59 MeV, 36.42 MeV, 32.22 MeV, 26.38 MeV, 24.13 MeV, 20.06 MeV and 11.9 MeV, respectively. The isotopic composition and absolute concentrations of ^{132}Xe measured in the Ba glass targets are listed in Table 3.1. The ^{132}Xe gas amounts are given in units $(X10^{-10}ccSTP.g^{-1})$. The errors quoted include the errors due to statistical variations in the peak height determination, mass discrimination, blank corrections and variation in the sensitivity of the MS between consecutive measurements. Table 3.2 lists the

Table 3.1 : ^{132}Xe concentrations and isotopic composition of Xe produced from natural Ba by protons in the energy range of 12 MeV $<$E $<$45 MeV. The ^{132}Xe amounts are in units [x10^{-10}ccSTP.g.Ba^{-1}].

SAMPLE	ENERGY	^{132}Xe	$\dfrac{^{124}Xe}{^{132}Xe}$	$\dfrac{^{126}Xe}{^{132}Xe}$	$\dfrac{^{128}Xe}{^{132}Xe}$	$\dfrac{^{129}Xe}{^{132}Xe}$	$\dfrac{^{130}Xe}{^{132}Xe}$	$\dfrac{^{131}Xe}{^{132}Xe}$	$\dfrac{^{134}Xe}{^{132}Xe}$
BA4-6	11.90 ±0.78	0.78 0.12	–	–	0.0227 0.0002	0.0123 0.0001	0.0191 0.0002	0.5990 0.0060	–
BA4-2	20.06 ±0.52	4.27 0.6	–	0.0041 0.0001	0.0103 0.0002	3.5400 0.0500	0.0583 0.0009	4.8900 0.0700	–
BA3-6	24.13 ±0.75	7.94 1.18	–	0.0280 0.0004	0.0300 0.0003	2.5140 0.0300	0.2460 0.0030	3.5940 0.0380	0.0010 0.0001
BA10	26.38 ±0.88	6.67 1.00	–	0.0290 0.0003	0.0464 0.0005	2.2200 0.0200	0.2770 0.0030	3.2500 0.0300	–
BA7	32.22 ±0.72	14.0 2.10	–	0.0284 0.0004	0.0523 0.0080	0.8190 0.0120	0.5460 0.0080	1.4000 0.0200	0.0267 0.0004
BA5	36.42 ±0.64	17.50 2.60	–	0.0134 0.0002	0.5870 0.0090	0.5507 0.0080	0.6590 0.0100	2.9300 0.0400	0.0459 0.0007
BA3	40.59 ±0.55	43.60 6.50	–	0.0046 0.0001	0.3110 0.0050	0.4630 0.0070	0.4310 0.0070	4.6400 0.0700	0.0347 0.0005
BA1	44.55 ±0.40	89.8 10.8	0.0016 0.0001	0.0036 0.0002	0.1480 0.0020	0.3495 0.0046	0.2621 0.0033	3.5540 0.0440	0.0199 0.0003

Table 3.2 : ^{132}Xe concentrations and isotopic composition of Xe produced from natural Ba targets by protons in the energy range of 12 MeV <E <45 MeV. The ^{132}Xe amounts are in units [x10^{-10}ccSTP.g.Ba^{-1}]. These measurements were done at Nuclear Chemistry Institute, Cologne, FRG.

SAMPLE ENERGY	^{132}Xe	$\dfrac{^{124}\text{Xe}}{^{132}\text{Xe}}$	$\dfrac{^{126}\text{Xe}}{^{132}\text{Xe}}$	$\dfrac{^{128}\text{Xe}}{^{132}\text{Xe}}$	$\dfrac{^{129}\text{Xe}}{^{132}\text{Xe}}$	$\dfrac{^{130}\text{Xe}}{^{132}\text{Xe}}$	$\dfrac{^{131}\text{Xe}}{^{132}\text{Xe}}$	$\dfrac{^{134}\text{Xe}}{^{132}\text{Xe}}$
18.21	4.61	–	–	–	2.950	0.0103	5.100	–
±0.58	0.92				0.350	0.0012	0.070	
22.02	7.63	–	0.0152	0.0180	3.220	0.1650	4.360	–
±0.52	1.53		0.0002	0.0008	0.040	0.0030	0.050	
27.68	8.88	–	0.0343	0.1410	1.690	0.3710	2.450	–
±0.68	1.78		0.0006	0.0020	0.020	0.0050	0.030	
31.81	12.00	–	0.0272	0.5730	0.743	0.5840	1.336	0.0220
±0.57	2.40		0.0006	0.0050	0.005	0.0040	0.007	0.0020
33.98	17.00	–	0.0193	0.6260	0.550	0.6460	1.730	0.0328
±0.50	3.40		0.0003	0.0060	0.006	0.0070	0.020	0.0020
37.72	21.00	–	0.0079	0.4620	0.504	0.5820	4.750	0.0408
±0.64	4.20		0.0004	0.0030	0.003	0.0030	0.020	0.0012
39.96	37.20	–	0.0045	0.2890	0.468	0.4050	4.430	0.0375
±0.58	7.40		0.0001	0.0020	0.005	0.0040	0.020	0.0006
44.17	79.50	0.0021	0.0038	0.1400	0.352	0.2550	3.600	0.0196
±0.45	16.00	0.0002	0.0001	0.0020	0.006	0.0040	0.060	0.0004

results of the measurements on other target discs from the same irradiation stacks measured at the Nuclear Chemistry Institute, Cologne, FRG, included for purposes of comparison (these results are also expressed in the same units as those in Table 3.1). The results obtained at PRL are plotted in Figure 3.1 and 3.2, which shows the excitation functions (cross sections as a function of energy) for the various xenon isotopes upto proton energy of 45 MeV. For proton energies up to 45 MeV (10 MeV $<$E $<$45 MeV) these are the first cross-section measurements available so far in literature.

3.1a: Analysis of the Data from the Nuclear Spallation point of view

Natural Ba is the major target for the production of xenon in extraterrestrial matter by spallation process (excluding some contribution from light rare earth elements). Barium has got seven stable isotopes, with ^{138}Ba having an abundance of 71.9% as the major isotope. The lighter isotopes of Ba are much less abundant compared to ^{138}Ba. The availability of various Ba isotopes as targets for xenon production makes the reaction scenario quite complex. A large number of reaction channels are energetically possible and there are, in fact, a number of nuclear reactions leading to the same xenon isotope as the end product. From our measurements it is not possible to distinguish between the contributions from different reaction channels unequivocally. In the present study as the analysed end product is a stable xenon nuclide it represents the cumulative yield of all the channels contributing to its production. After

63

the irradiations the samples have been cooled for a considerable period of time (years) so that the intermediate radioactive progenitors decayed into stable end-products.

Table 3.3 gives the nuclear reactions contributing to the xenon isotopes, including the radiogenic isotope ^{127}Xe (half life = 36.4 days). Also shown are the highest Q values for the production of these isotopes, taking into consideration all the Ba target isotopes.

For mass numbers between 124 and 129 and for 131 the measured xenon concentrations have contributions from nuclear reaction channels of the kind ^{M}Ba(p, xpyn)^{i}Xe, with x = 0, 1, 2 and 3 and y = 0,1 and 2. For ^{130}Xe and ^{132}Xe just the (p, 2pyn) and (p, 3pyn) reactions seem to be the major contributors. The excitation functions for the stable xenon isotopes (only PRL measurements are included in these Figures) are shown in Figs 3.1 and 3.2. The excitation functions for all xenon isotopes, in general, are found to be smooth curves in the energy range studied here and they exhibit structures in some cases. The theoretically predicted cross-sections in this investigated range of energies by ALICE LIVERMORE 87 [Blann (1987)] agrees with the measured cross-section values. ALICE LIVERMORE 87 is a modified version of ALICE LIVERMORE 82 [Blann and Vonach (1983) and Blann and Bisplinghoff (1982)]. Several aspects of Alice Livermore 87 program were discussed by Prescher et al., (1991). For the reaction ^{138}Ba (p, 3p2n) ^{134}Xe, the measured cross-sections are lower by an order of magnitude as compared to ALICE predicted values. This may be due to the pre-equilibrium emission of α-particles, ie., the occurrence of (p, αp) reaction. Also the

Table 3.3 : The reactions leading to the production of various Xe isotopes. Also shown are the maximum Q values for each isotope along with the reactions which produce them.

Nuclide	Reaction	Half life	E(KeV)	I%	Q value (MeV)
^{124}Xe	Ba(p,3pyn),y=4,12	Stable	–	–	^{130}Ba(p,p^{4}He2n):-18.4
^{126}Xe	Ba(p,3pyn),y=2,10	Stable	–	–	^{130}Ba(p,p^{4}He):-0.6
^{127}Xe	Ba(p,3pyn),y=1,9	36.4days	202.84	68.0	^{132}Xe(p,^{4}He^{3}He):-9.4
^{128}Xe	Ba(p,3pyn),y=0,8	Stable	–	–	^{132}Ba(p,p^{4}He):-1.0
^{129}Xe	Ba(p,3pyn),y=1,7	Stable	–	–	^{132}Ba(p,p^{3}He):-21.8
^{130}Xe	Ba(p,3pyn),y=0,6	Stable	–	–	^{134}Ba(p,^{4}He):+3.8
^{131}Xe	Ba(p,3pyn),y=1,5	Stable	–	–	^{134}Ba(p,p^{4}He):+4.0
^{132}Xe	Ba(p,3pyn),y=0,4	Stable	–	–	^{135}Ba(p,^{4}He):+4.2
^{134}Xe	Ba(p,3pyn),y=0,2	Stable	–	–	^{136}Ba(p,3p):-18.7
^{136}Xe	Ba(p,3pyn),y=0,2	Stable	–	–	^{138}Ba(p,3p):-22.7
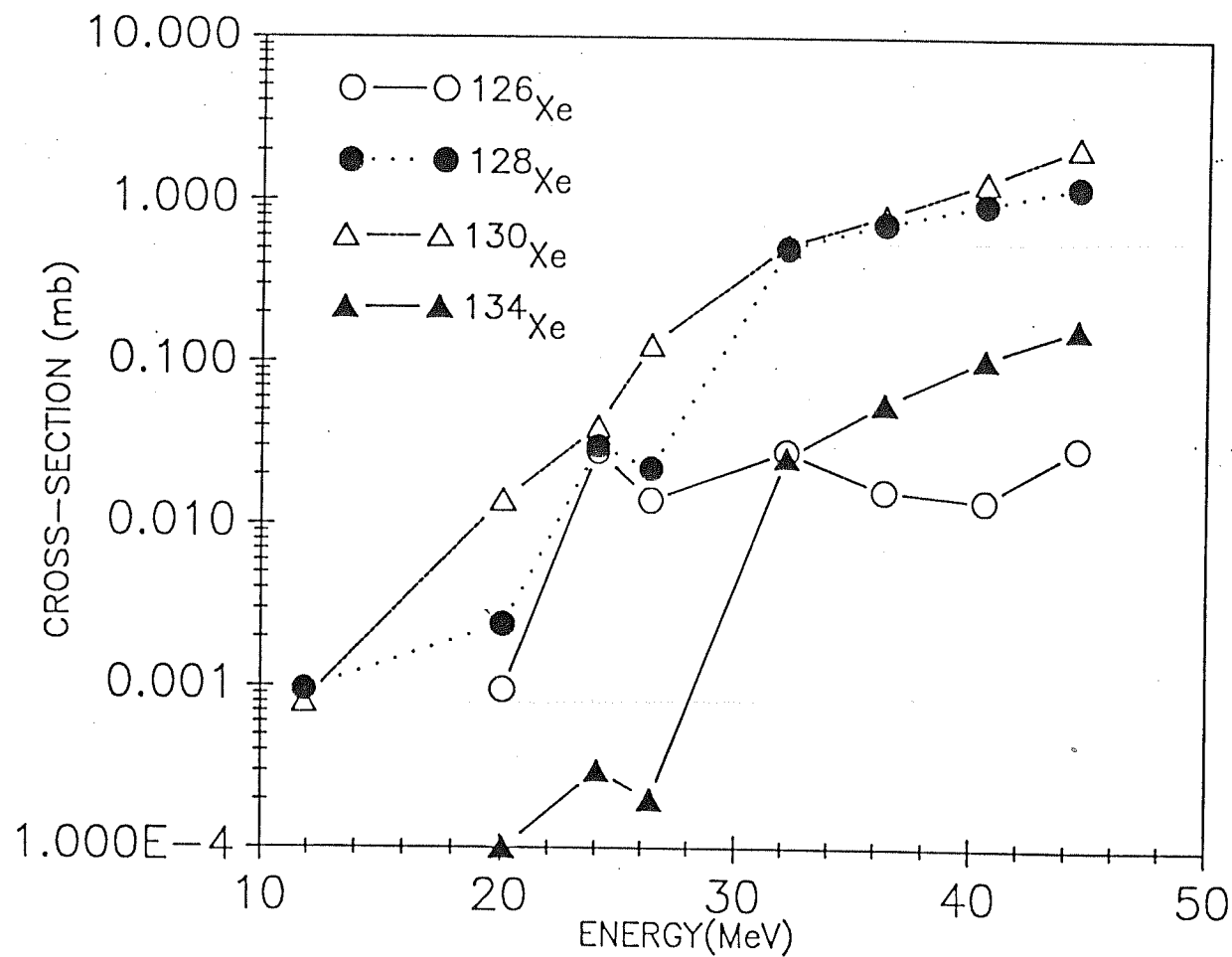
Fig.3.1 Excitation functions for production of isotopes ^{126}Xe, ^{128}Xe, ^{130}Xe and ^{134}Xe in p-induced reactions on Ba targets up to 45 MeV. Only PRL measurements are shown in this figure.
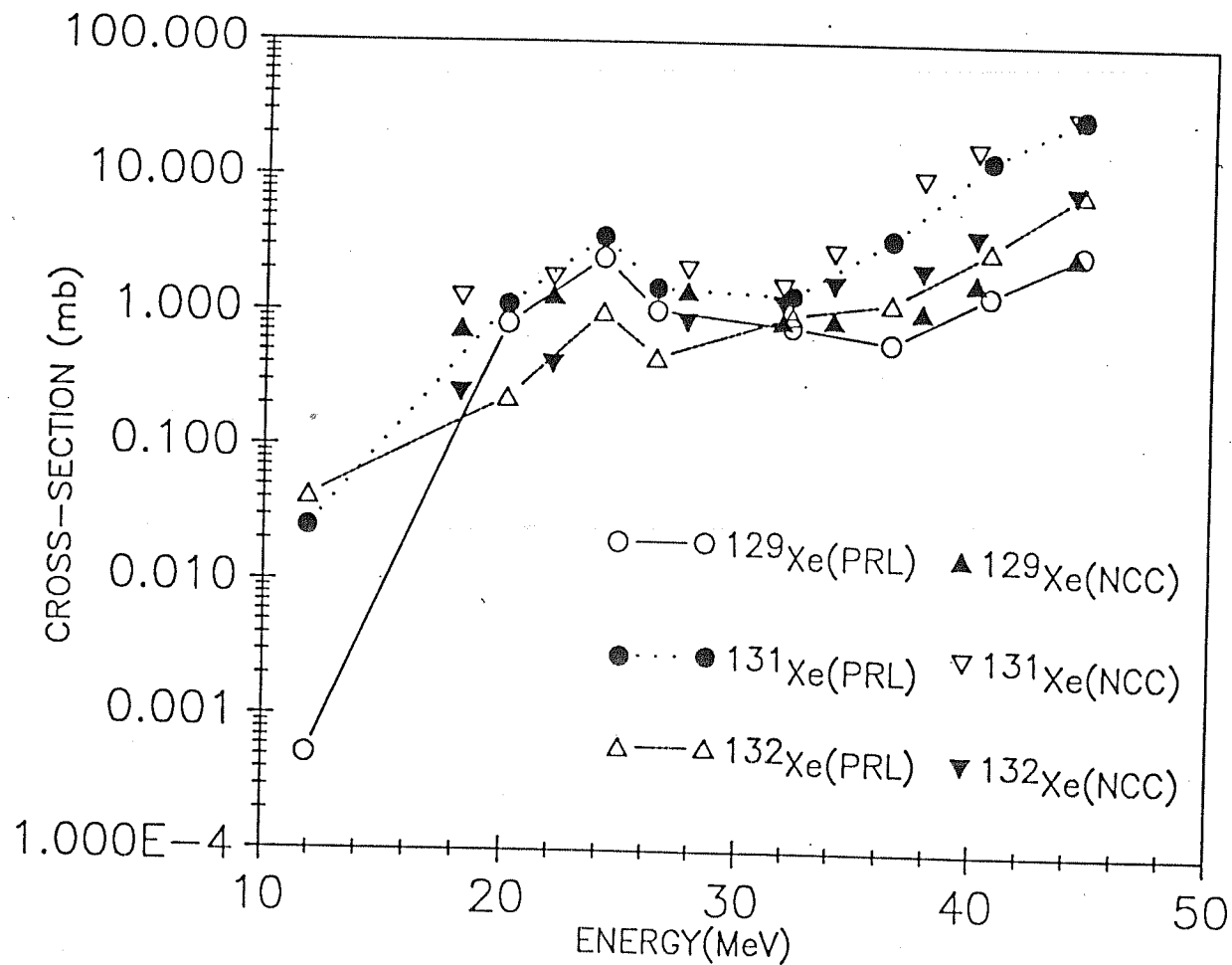
Fig.3.2 Excitation functions for production of isotopes [129]Xe, [131]Xe and [132]Xe in p-induced reactions on Ba targets up to 45 MeV. PRL measurements are indicated by symbols and joined with lines. NCC (Nuclear Chemistry Cologne) measurements are indicated by symbols alone.

magic neutron shell of ^{138}Ba makes it difficult for the nuclear parameters used in the calculations to be valid for this target isotope. The production of ^{134}Xe seem to be predominentantly from this nuclide. A similar effect is seen in the case of (p, 2p3n) reactions [ie.(p,αn) reactions, also]. ^{138}Ba (p, 2p3n) ^{134}Cs is such a case in point which is dominated by (p,αn) reaction [Prescher et al.,(1991)]. The nature of (p, yn), (p, pyn), (p, 2pyn) and (p,3pyn) reactions cannot be deduced from the results obtained in this study. But the energy shifts which are observed with radionuclides are seen in the case of stable isotopes also. In case of isotopes lighter than ^{131}Xe the calculated data are too low by up to 4 MeV, which suggests that the measured cross-sections at energy E MeV corresponds to calculated values at an energy of (E-4) MeV. For ^{131}Xe the shift is in the opposite direction and the amount by which the energy has shifted is 2 MeV. These energy shifts become less significant for energies above 24 MeV.

It has been pointed out earlier that [Mathew et al.,(1989b)], in the energy range investigated here, low energy contributions are significant in the case of isotopes ^{129}Xe, ^{131}Xe and ^{132}Xe. For the isotope ^{134}Xe which can only be produced by (p, 3p2n) reactions low yields are to be expected. ^{124}Xe and ^{126}Xe production are also relatively small at these energies since the threshold for producing this isotope is comparatively higher than that for other xenon isotopes. ^{130}Xe and ^{128}Xe have determinable production cross-sections at these energies. The ^{130}Xe production cross-section is higher than ^{128}Xe cross-sections. Table 3.4 records the measured production

Table 3.4 : Measured cross-sections for the production of xenon isotopes from Ba targets by protons having different energies.

ENERGY	^{124}Xe	^{126}Xe	^{128}Xe	^{129}Xe	^{130}Xe	^{131}Xe	^{132}Xe	^{134}Xe
11.9 ±0.8	–	–	0.00095 0.00014	0.00052 0.00008	0.00080 0.00012	0.025 0.004	0.042 0.006	–
20.1 ±0.5	–	0.00095 0.00014	0.0024 0.0004	0.82 0.12	0.0135 0.002	1.13 0.17	0.231 0.035	–
24.1 ±0.8	–	0.028 0.004	0.030 0.004	2.53 0.38	0.248 0.037	3.62 0.54	1.010 0.152	–
26.4 ±0.9	–	0.014 0.002	0.022 0.003	1.04 0.16	0.129 0.019	1.52 0.23	0.470 0.07	0.002 0.0002
32.2 ±0.7	–	0.028 0.004	0.508 0.077	0.80 0.12	0.531 0.08	1.36 0.29	0.97 0.15	0.026 0.004
36.4 ±0.6	–	0.016 0.003	0.72 0.11	0.62 0.09	0.81 0.12	3.59 0.76	1.22 0.18	0.06 0.01
40.6 ±0.6	–	0.014 0.002	0.95 0.14	1.41 0.21	1.31 0.20	14.1 2.1	3.04 0.46	0.106 0.016
44.6 ±0.4	–	0.030 0.005	1.220 0.183	2.88 0.43	2.16 0.32	29.30 4.39	8.25 1.24	0.164 0.025

69

cross-sections, for all stable xenon isotopes in p-induced reactions on Ba upto proton energy of 45 MeV. Only the measurements done at PRL are included in this table. These cross section values compare very well with the values measured at Nuclear Chemistry Institute, Cologne, F.R.G as evident from a comparison of Tables 3.1 and 3.2.

The lowest energy used in the present analysis is 11.9 MeV. The coulomb barrier for the Ba target nucleus is about 10.8 MeV and protons having energies less than 11 or 12 MeV does not induce nuclear reactions on these target nuclides. The production cross-sections for all isotopes increases from very low values as the p-energies are increased from 11.9 MeV to 45 MeV. The ^{129}Xe, ^{131}Xe and ^{132}Xe production rates are much larger compared to other xenon isotopes at these low energies. In general, all excitation functions increase with energies, the cross-section values passing through comparatively higher values at ~24 MeV. The maxima are more pronounced in the case of isotopes ^{129}Xe, ^{131}Xe and ^{132}Xe. The cross-section values of ^{129}Xe for example are 0.82 ± 0.12 mb at 20.1 MeV; 2.53 ± 0.38 mb at 24.1 MeV and 1.04 ± 0.16 mb at 26.4 MeV. The cross-section values for isotopes ^{131}Xe at the above energies are, respectively 1.13 ± 0.17 mb (at 20.1 MeV), 3.62 ± 0.54 mb (at 24.1 MeV) and 1.52 ± 0.23 mb (at 26.4 MeV). The corresponding production cross-sections in case of isotope ^{132}Xe are 0.231 ± 0.035 mb at 20.1 MeV; 1.01 ± 0.15 mb at 24.1 MeV and 0.47 ± 0.07 mb at 26.4 MeV. The other isotopes also show slightly enhanced production cross-sections at proton energy of 24 MeV, but the enhancements are much less compared to ^{129}Xe, ^{131}Xe and ^{132}Xe.

After ~24 MeV proton energy the production

70

cross-sections fall slightly followed by a steady increase beyond ~32 MeV. The increase is much sharper in case of isotopes ^{131}Xe and ^{132}Xe. The production cross-sections of these isotopes at 32.2 MeV are 1.36 ± 0.29 mb and 0.97 ± 0.15 mb, respectively. At a proton energy of 44.6 MeV the production cross-section values are 29.3 ± 4.4 mb and 8.25 ± 1.24 mb respectively.

The enhanced production of the isotopes ^{129}Xe, ^{131}Xe and ^{132}Xe at the low energies and the comparatively larger production cross-sections of these isotopes at ~ 24 MeV, owing to pre-equilibrium α emission reactions, are indicated in the isotopic ratios ^{M}Xe/^{130}Xe (M = 126 to 132). Fig. 3.3 and 3.4 show the isotopic ratios for the production of xenon isotopes in p-induced reactions on,Ba up to proton energies of 45 MeV. In Fig.3.3 the ^{126}Xe/^{130}Xe, ^{128}Xe/^{130}Xe and ^{134}Xe/^{130}Xe ratios are plotted as a function of energy whereas Fig. 3.4 shows a plot of the isotopic ratios ^{129}Xe/^{130}Xe, ^{131}Xe/^{130}Xe and ^{132}Xe/^{130}Xe in the same proton energy range. Here it may be noted that both the figures have been plotted using the same scales so that the changes in the isotopic ratios are expressed in the same scales. The isotopic ratios ^{129}Xe/^{130}Xe, ^{131}Xe/^{130}Xe and ^{132}Xe/^{130}Xe have very high values around p-energies of <24 MeV. As an illustration, these isotopic ratios at 20.1 MeV are 60, 84 and 17 and at p-energy of 24.1 MeV the ^{129}Xe/^{130}Xe, ^{131}Xe/^{130}Xe and ^{132}Xe/^{130}Xe ratios are, respectively, 10, 15 and 4. These ratios decrease to ~1.5, 2.5 and 1.8 at a p-energy of 32.2 MeV and all these ratios increases thereafter.
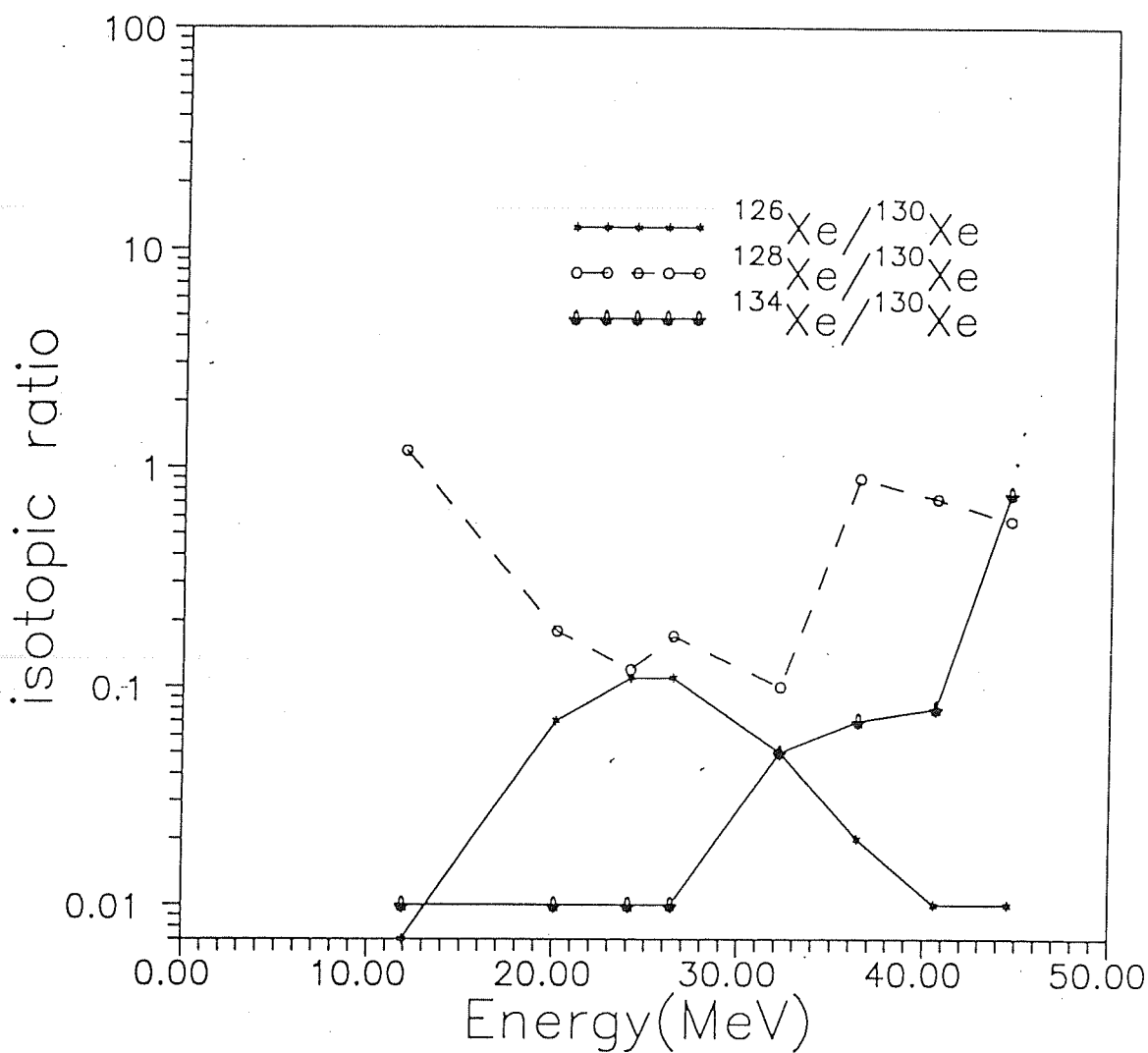
Fig.3.3 Xe isotopic ratios in p-induced reactions on Ba targets for proton energies up to 45 MeV. The ^{126}Xe/^{130}Xe, ^{128}Xe/^{130}Xe and ^{134}Xe/^{130}Xe ratios are shown.
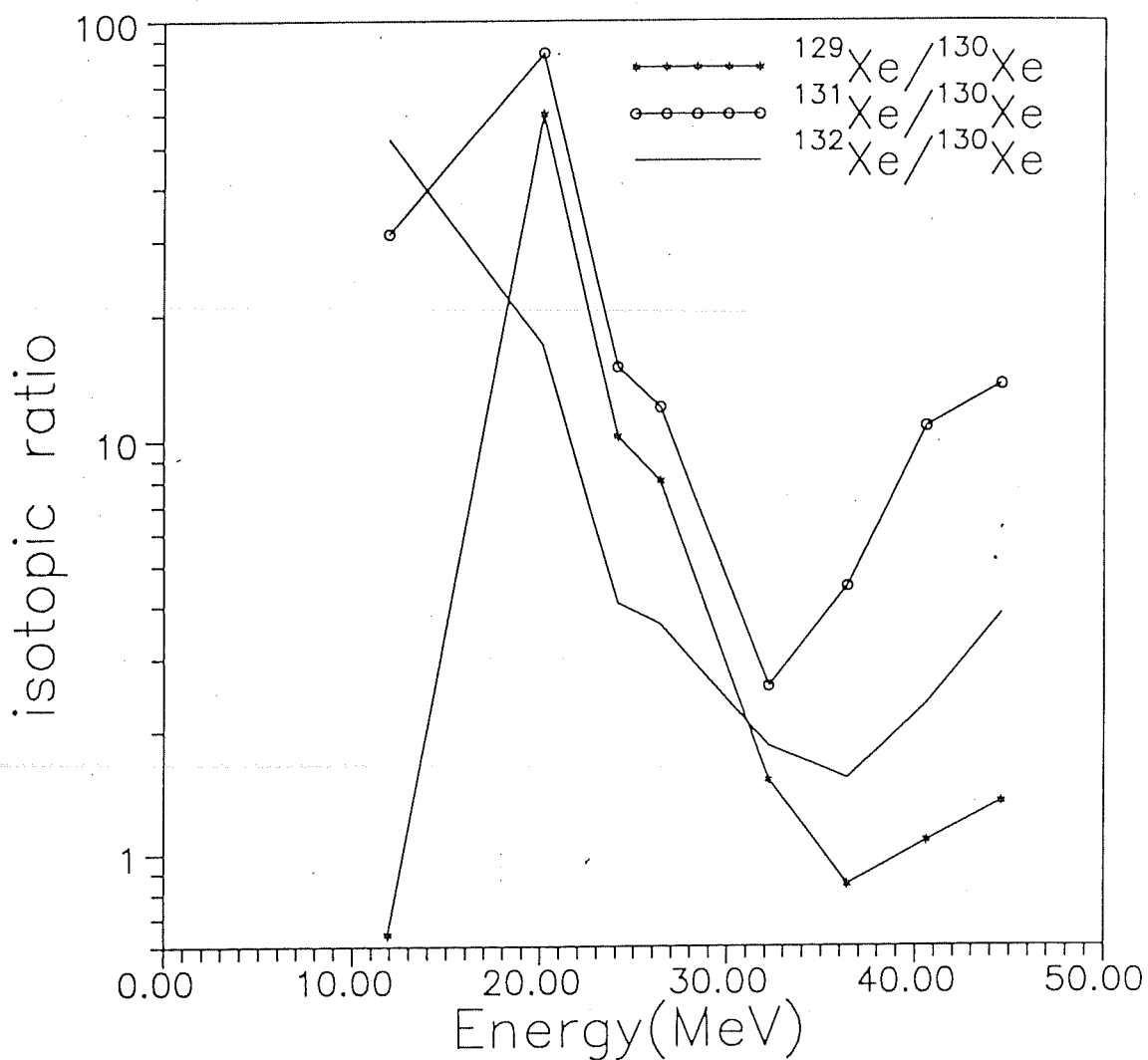
Fig.3.4 $^{129}Xe/^{130}Xe$, $^{131}Xe/^{130}Xe$ and $^{132}Xe/^{130}Xe$ isotopic ratios in p-induced reactions on Ba targets for proton energies up to 45 MeV.

3.1b. Comparison of the present Results with existing Cross-section Measurements

The present cross-section measurements shows that the production of the xenon isotopes is significant in the low proton energy range. Kaiser (1977) concluded that there is an insignificant production of xenon isotopes on Ba targets in proton induced reactions in the low energy range (E <60 MeV). But there is a general agreement between the measurements carried out at two different institutes, PRL and NCC (as can be seen from Tables 3.1 and 3.2).

In the Figure 3.5 the ^{127}Xe excitation function has been plotted, which was measured only at NCC. The results of the ^{127}Xe measurements are published in Prescher et al.,(1991). This nuclide is used for absolute normalization purposes in Kaiser's experiment. In the experiments by Kaiser (1977) ^{127}Xe is measured by gamma spectroscopy and also by mass spectrometry and the results are used for absolute calibration of the cross-section measurements for p-energies from 75 MeV to 200 MeV. The cross-sections for xenon isotopes other than ^{127}Xe are deduced from the measured ^{M}Xe/^{127}Xe ratios obtained mass spectrometrically and the absolute amounts of ^{127}Xe, obtained from counting experiments. At 38 MeV the cross-sections are deduced by assuming a production cross-section of 3 mb for the nuclide ^{131}Ba from Ba.

As compared to the cross sections measured in this experiment Kaiser's cross-sections are low by a factor of ~3 . However, at high energies the discrepancies between the measured values by Kaiser (1977) and those calculated by the hybrid model (ALICE LIVERMORE 87) decreases. Kaisers measurements for the

74
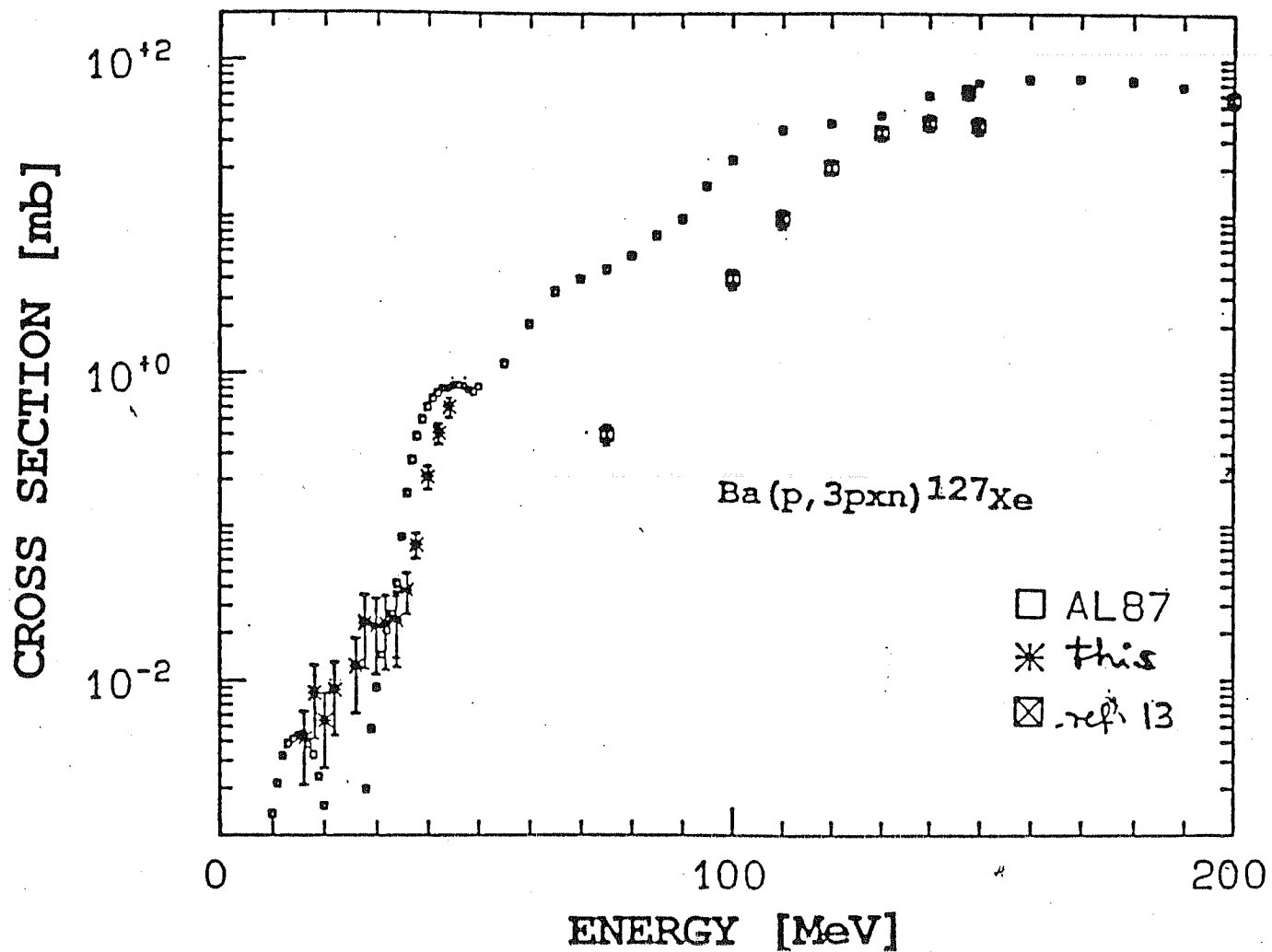
Fig.3.5 Excitation functions for production of isotope [127]Xe in p-induced reactions on Ba targets up to 45 MeV. [Figure reproduced from Prescher et al., (1991)].

energy range of 200 MeV to 600 MeV seem to be reliable. One possible reason which might have created problems in the Kaiser's (1977) experiments is that during ORSAY irradiations, Kaiser used an internal beam of the accelerator for irradiating the targets. In such a case the energy of the beam received by the targets depends on its position inside the accelerating tube and the position of the target is controlled by a mechanical adjustment. Under these circumstances it becomes difficult to maintain a control on the p-energy received by the target foils. This is in addition to the problem of thermal heating and of leaching effects discussed by Kaiser (1977). These two problems are discussed at length by the author.[Kaiser (1977)]. But Kaiser's results cannot be explained by energy shifts explained here.

In the models for the calculation of cosmogenic nuclide production rates by SCR protons the p-induced cross-section values upto 200 MeV are required as input information. For xenon isotopes in this energy range the only measurements available are those by Kaiser(1977) and by Shukolyukov and Gorin (1988) at the energies of 72 MeV and 100 MeV. The differences between both these data sets and our measured values (wherever available) and the calculated values by ALICE manifest not only in the absolute magnitudes of the production cross-sections alone but they also show up in the isotopic ratios as well. In fact the isotopic ratios (relative yields) measured by Kaiser (1977) at 38 MeV agree with those measured by us at 25 MeV. At 72 MeV Shukolyukov and Gorin (1988) the isotopic ratios which are significantly different from the values predicted by ALICE at the same energy. The $^{132}Xe/^{130}Xe$, $^{131}Xe/^{130}Xe$ and $^{129}Xe/^{130}Xe$ ratios, for example, are

respectively 0.792, 7.77 and 0.930 in comparison with the values 0.162, 2.971 and 1.509 predicted by ALICE. ALICE also predicts a relatively higher cross section of 17.3 mb for the isotope ^{130}Xe at this energy which can be measured quite accurately using the MS techniques. At 100 MeV the cross-section value measured by Shukolyukov and Gorin (1988) is 6.1 mb in comparison with the value of 13.3 mb predicted by ALICE LIVERMORE 87 [Blann (1987)]. At this energy also the xenon isotopic ratios are considerably different from the values obtained from calculations. The ^{132}Xe/^{130}Xe, ^{131}Xe/^{130}Xe and ^{129}Xe/^{130}Xe ratios are respectively 1.01, 11.5 and 3.25 as against the ALICE calculated values of 0.696, 10.075 and 4.872.

Considering the facts that (i) the agreement between the measurements carried out at PRL and at NCC are quite good (ii) the agreement between the general shapes and structures of the measured excitation functions which are reproduced well by the theoretical calculations (up to 45 MeV) and (iii) the success with which ALICE predicted the cross-section values for the production of a large number of well studied radioactive nuclides from Ti, V, Mn, Fe, Co and Ni targets all the way up to 200 MeV; we conclude that one may have to look for systematic errors in the work of Kaiser (1977) and Shukolyukov and Gorin (1988). We are all the more confident of our results since the radiogenic products, ^{133g}Ba, $^{131m+g}$Ba, ^{136}Cs, $^{134m+g}$Cs, ^{132}Cs, ^{129}Cs, $^{127m+g}$Xe from Ba targets at 147.5 MeV, obtained during the same irradiation experiments and measured at the Nuclear Chemistry, Cologne, yielded cross-sections which closely agree with the predictions from the hybrid model. (Unfortunately, this Ba glass could not be

made available for stable xenon isotope measurements). The results of the studies of the above radiogenic nuclides of Ba, Cs and xenon are discussed in Prescher et al.,(1991). For all the xenon isotopes, except ^{134}Xe, the non availability of measured cross-sections between 50 MeV and 200 MeV were met by making use of the calculated cross-section values by ALICE.

3.2. SCR Xenon Production Rates on the Lunar Surface

Using the measured cross section values up to 45 MeV and the calculated cross section values for the energy range of 50 MeV to 200 MeV [calculated with the help of ALICE LIVERMORE 87 [Blann (1987)], the SCR xenon production rates on the lunar surface have been calculated, based on the model available at PRL [Bhandari et al., (1976)]. This model has been used in predicting the production rates of SCR produced radionuclides on the lunar surface. The basic approach of this model is discussed in section 2.3 of chapter II. A point to be noted here is that in the present SCR calculations using the model [Bhandari et al.,(1976)] also the cross-sections calculated by ALICE LIVERMORE 87 [Blann (1987)] are used in the energy range of (50 MeV >E <200 MeV) because experimental production cross-section values are not available in this range of proton energies. The production rate values obtained here are compared with the earlier production rates calculated by Hohenberg et al.,(1978) using the Reedy and Arnold (1972) model and those estimated by Prescher et al.,(1991) using Michel and Brinkmann (1980) model. It may be pointed out here that the theoretical cross-section values in the energy range of 50 MeV to 200 MeV used in these calculations need to be

78

verified experimentally in future. Some steps in this direction are underway.

Table 3.5 gives the SCR production rates calculated for the various xenon isotopes at different shielding depths (expressed in g.cm^{-2}) on the lunar surface. Shielding depths >24 g.cm^{-2} are not considered here since production of isotopes by SCR particles falls off steeply and at larger shielding depths the contribution of SCR protons in the total cosmogenic nuclide production is insignificant. At these shielding depths cosmogenic nuclide production is mainly due to the more energetic GCR particles. The present calculations are carried out for Apollo 11 Lunar surface material composition (assumed Ba content is 320 ppm). However the data given in Table 3.5 are normalized to per ppmBa. The density of lunar surface material is taken to be 3.0 g.cm^{-3}. For the incident particles a rigidity dependent spectrum is assumed. The assumed spectra are represented by :

$$J(E, Ro) = Jo \ (E > 10 MeV) \ * \ exp \ (-R/Ro) \qquad .... (1)$$

where R is related to the energy of the proton by

$$R = p*c/ze = (E^2 + 2 \ mp * c^2 * E)^{1/2}/ze \qquad ....(2)$$

$$(z=1 \ for \ protons)$$

(Ro = characteristic Rigidity)

Jo(E >10 MeV) = 100 cm^{-2}.s^{-1} is the integral flux of SCR particles on the lunar surface. Also shown in the Table are the results of the Hohenberg et al.,(1978) and Prescher et al.,(1991) calculations for the same material, same incident particle spectra and flux (for a value Ro = 100 MV).

In the following discussion of the SCR production rates

Table 3.5 : Predicted production rates for xenon in lunar surface material having Apollo 11 lunar material compositions. The gas amounts are expressed in units $[\times 10^{-15} ccSTP.g^{-1}.Ma^{-1}.ppmBa^{-1}]$

Characteristic Rigidity (MV)	^{124}Xe	^{126}Xe	^{128}Xe	^{129}Xe	^{130}Xe	^{131}Xe	^{132}Xe	^{134}Xe
Shielding depth = 0 g.cm^{-2}								
50	0.005	0.027	0.101	0.310	0.117	1.301	0.167	0.008
75	0.044	0.177	0.470	1.033	0.375	3.462	0.351	0.032
85	0.079	0.287	0.702	1.441	0.508	4.457	0.430	0.045
100	0.151 (0.010)	0.500 (0.083)	1.123 (0.324)	2.131 (0.841)	0.731 (0.404)	6.049 (3.129)	0.553 (0.385)	0.067 (0.035).
100*	0.147	0.474	1.220	2.120	0.617	6.010	0.543	0.065
100**	0.053	0.211	0.631	1.070	0.316	3.510	0.285	0.008
125	0.325	0.959	1.943	3.376	1.136	8.086	0.761	0.106
Shielding depth = 0.1 g.cm^{-2}								
50	0.004	0.023	0.079	0.234	0.087	0.946	0.108	0.006
75	0.041	0.159	0.408	0.860	0.311	2.864	0.266	0.027
85	0.073	0.261	0.623	1.235	0.432	3.769	0.338	0.039
100	0.142 (0.008)	0.462 (0.071)	1.016 (0.273)	1.878 (0.690)	0.638 (0.336)	5.272 (2.560)	0.454 (0.279)	0.060 (0.003)

Table 3.5 Contd.....

100*	0.141	0.449	1.130	1.940	0.558	5.370	0.468	0.060
100**	0.051	0.200	0.597	1.000	0.297	3.240	0.266	0.006
125	0.308	0.900	1.793	3.057	1.022	7.264	0.654	0.097

Shielding depth = 0.5 $g.cm^{-2}$

50	0.003	0.015	0.048	0.128	0.047	0.513	0.047	0.004
75	0.033	0.124	0.303	0.600	0.210	1.924	0.156	0.019
85	0.061	0.211	0.480	0.904	0.307	2.666	0.213	0.029
100	0.123	0.386	0.817	1.446	0.480	3.956	0.309	0.046
	(0.006)	(0.052)	(0.189)	(0.462)	(0.225)	(1.695)	(0.177)	(0.021)
100*	0.123	0.382	0.929	1.550	0.432	4.060	0.338	0.048
100**	0.045	0.172	0.509	0.834	0.250	2.610	0.221	0.005
125	0.275	0.781	1.508	2.482	0.818	5.742	0.487	0.079

Shielding depth = 1.0 $g.cm^{-2}$

50	0.002	0.011	0.031	0.079	0.028	0.293	0.024	0.0006
75	0.028	0.100	0.232	0.443	0.150	1.350	0.102	0.014
85	0.052	0.173	0.381	0.693	0.229	1.942	0.147	0.022
100	0.107	0.327	0.670	1.153	0.375	3.020	0.227	0.037
	(0.005)	(0.039)	(0.137)	(0.331)	(0.160)	(1.200)	(0.116)	(0.016)

81

Table 3.5 Contd........

100*	0.107	0.328	0.776	1.270	0.346	3.190	0.259	0.039
100**	0.040	0.150	0.438	0.705	0.212	2.140	0.186	0.005
125	0.246	0.683	1.285	2.064	0.675	4.640	0.385	0.065

Shielding depth = 5 g.cm^{-2}

50	0.0005	0.002	0.005	0.009	0.003	0.041	0.002	0.0003
75	0.011	0.033	0.067	0.110	0.035	0.307	0.020	0.004
85	0.022	0.065	0.127	0.204	0.064	0.518	0.035	0.007
100	0.052	0.142	0.261	0.403	0.128	1.009	0.069	0.013
	(0.001)	(0.01)	(0.031)	(0.073)	(0.034)	(0.266)	(0.020)	(0.004)
100*	0.053	0.151	0.324	0.498	0.126	1.050	0.085	0.015
100**	0.020	0.072	0.202	0.307	0.094	0.820	0.080	0.002
125	0.138	0.349	0.596	0.873	0.288	1.870	0.151	0.027

Shielding depth = 10 g.cm^{-2}

50	0.0002	0.0006	0.0012	0.0025	0.0007	0.0065	0.0004	0.0001
75	0.005	0.014	0.026	0.041	0.013	0.099	0.007	0.001
85	0.011	0.030	0.055	0.083	0.026	0.179	0.014	0.003
100	0.029	0.074	0.126	0.192	0.060	0.387	0.031	0.006
	(0.004)	(0.004)	(0.011	(0.025)	(0.011)	(0.094)	(0.006)	(0.001)

Table 3.5 Contd.......

100*	0.029	0.078	0.159	0.236	0.059	0.459	0.038	0.007
100**	0.011	0.039	0.104	0.153	0.047	0.386	0.040	0.001
125	0.085	0.231	0.329	0.460	0.157	0.977	0.080	0.014

Shielding depth = 20 g cm^{-2}

50	0.00003	0.0001	0.0002	0.00035	0.0001	0.00082	0.00005	0.00001
75	0.002	0.004	0.007	0.0098	0.003	0.022	0.003	0.0003
85	0.004	0.0108	0.018	0.026	0.008	0.052	0.004	0.0008
100	0.012	0.030	0.047	0.074	0.022	0.136	0.011	0.002
	(0.0012)	0.001	(0.003)	(0.006)	(0.003)	(0.025)	(0.002)	(0.004)
100*	0.012	0.029	0.056	0.080	0.020	0.144	0.013	0.002
100**	0.003	0.015	0.038	0.055	0.017	0.128	0.014	0.0005
125	0.043	0.097	0.147	0.277	0.071	0.355	0.036	0.006

Shielding depth = 24 g cm^{-2}

50	0.00002	0.00005	0.00013	0.00018	0.00005	0.0004	0.00003	0.000
75	0.001	0.003	0.005	0.0075	0.002	0.014	0.002	0.0002
85	0.003	0.008	0.012	0.023	0.006	0.037	0.003	0.0005
100	0.009	0.022	0.035	0.066	0.017	0.106	0.008	0.001
	(0.001)	(0.006)	(0.002)	(0.004)	(0.002)	(0.017)	(0.001)	(0.003)

Table 3.5 Contd.......

100*	0.008	0.121	0.039	0.056	0.014	0.098	0.009	0.002
100**	0.003	0.011	0.027	0.038	0.012	0.088	0.010	0.0003
125	0.035	0.077	0.115	0.224	0.056	0.273	0.028	0.005

* K.Prescher et al., (1991), ** Hohenberg et al., (1978).

The values given in brackets corresponding to R_o=100 MV the contribution from protons having energies <100 MeV.

in the lunar surface, the absolute production rates for ^{130}Xe, (the normalizing isotope) will be discussed first and the other xenon isotopes will be discussed in terms of the isotopic ratios afterwards. ^{130}Xe is used as the normalizing isotope because the SCR production rate of isotope ^{126}Xe, generally used for normalization purposes in cosmochemical applications, is relatively small. This nuclide is·predominantly of GCR (or high energy) origin.

The ^{130}Xe production rate decreases with depth, from its value of 0.731×10^{-15} ccSTP.g^{-1}. Ma^{-1}.ppmBa^{-1} at the surface to a value of 0.022×10^{-15} ccSTP.g^{-1}.Ma^{-1}.ppmBa^{-1} at a shielding depth of 20 g.cm^2. At all shielding depths the SCR ^{130}Xe production rate shows a strong dependence on the characteristic rigidity of the assumed SCR proton spectrum, with the production rates decreasing with decreasing Ro. For example compared to the surface production rates of ^{130}Xe, given above, using $R_o = 100$ MV, at $R_o = 50$ MV and 125 MV the corresponding values are, 0.117×10^{-15} ccSTP.g^{-1}Ma^{-1}ppmBa^{-1} and 1.136×10^{-15} ccSTP.g^{-1}Ma^{-1}ppmBa^{-1} respectively. These production rates are, 16% and 155% respectively, of the production rate obtained using · value of $R_o = 100$ MV. At larger shielding depths also the production rates obtained using different values of R_o are different. For instance at a shielding depth of 20 g.cm^{-2} the $R_o = 50$ (and $R_o = 125$ MV) production rates are less than 1% (and a factor of ~3 higher than) the production rate at the same shielding depth with $R_o = 100$ MV.

The surface as well as the 20 g.cm^{-2} depth production rates of ^{130}Xe are higher, respectively, by a factor of ~2 and by 20-30% than the values estimated by Hohenberg et al.,(1978) for
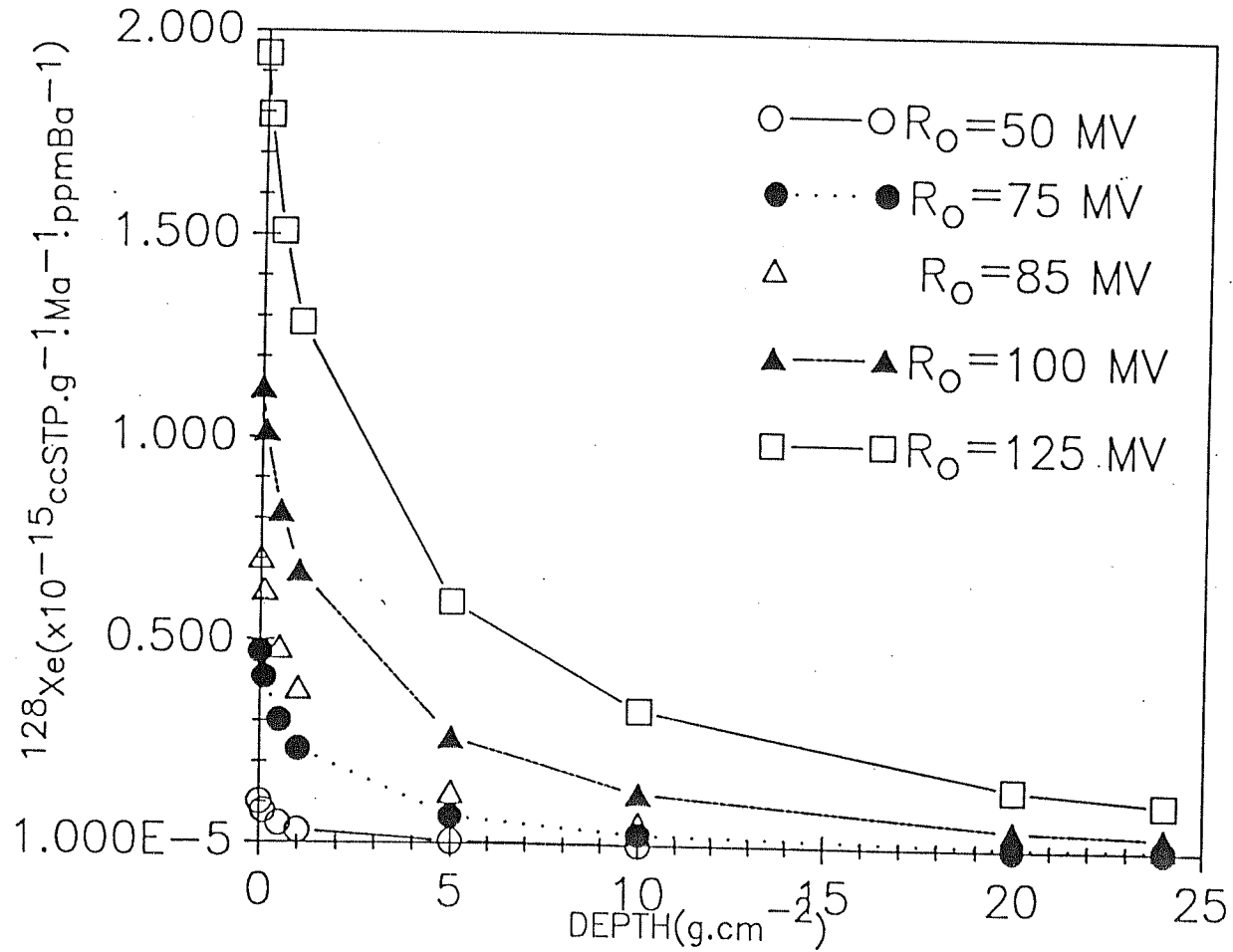
Fig.3.6 Production rates of ^{128}Xe in lunar surface material as a function of shielding depth. Production rates calculated with R_o = 50 MV, 75 MV, 85 MV, 100 MV and 125 MV are shown.
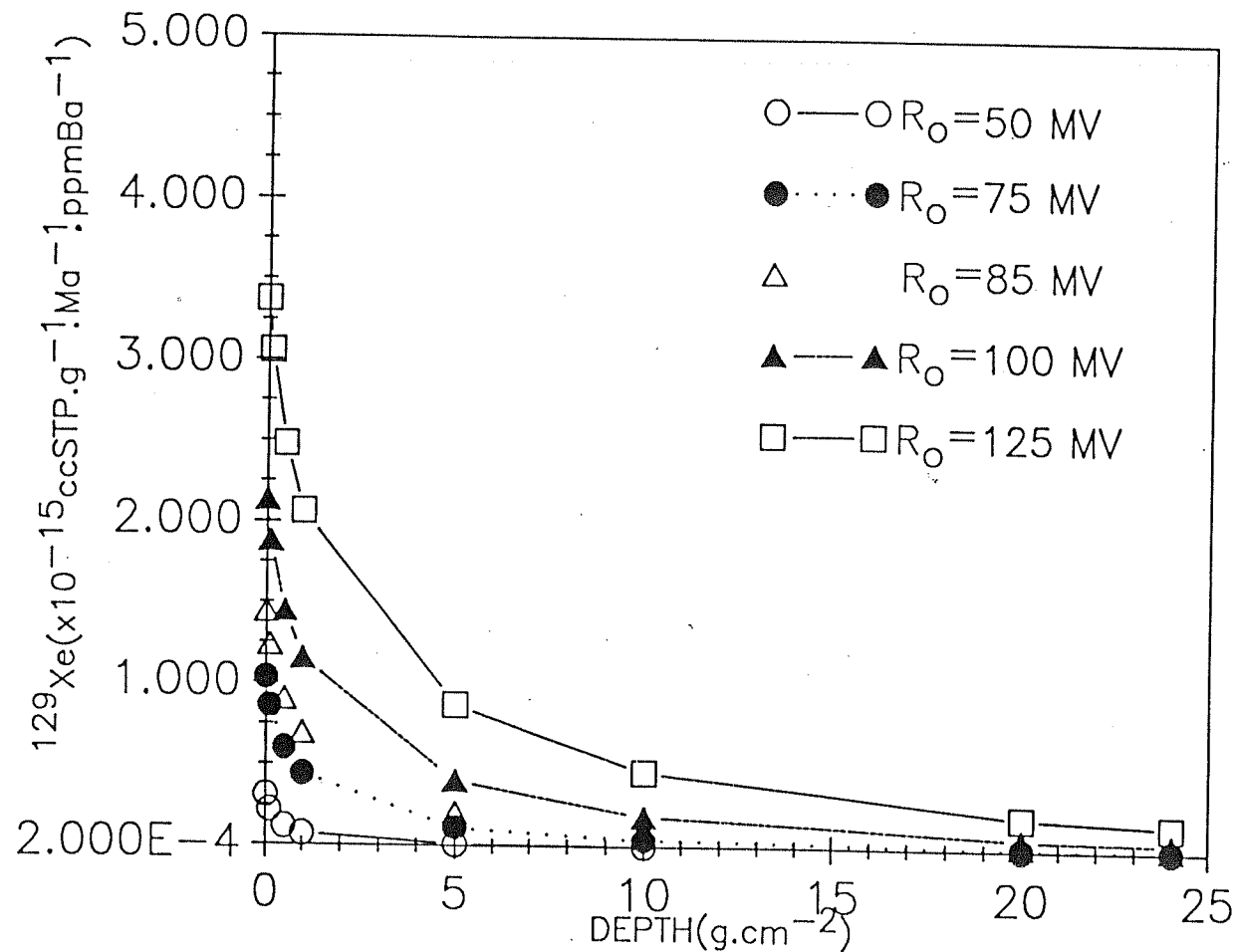
Fig.3.7 Production rates of ^{129}Xe in lunar surface material as a function of shielding depth. Production rates calculated with R_o = 50 MV, 75 MV, 85 MV, 100 MV and 125 MV are shown.
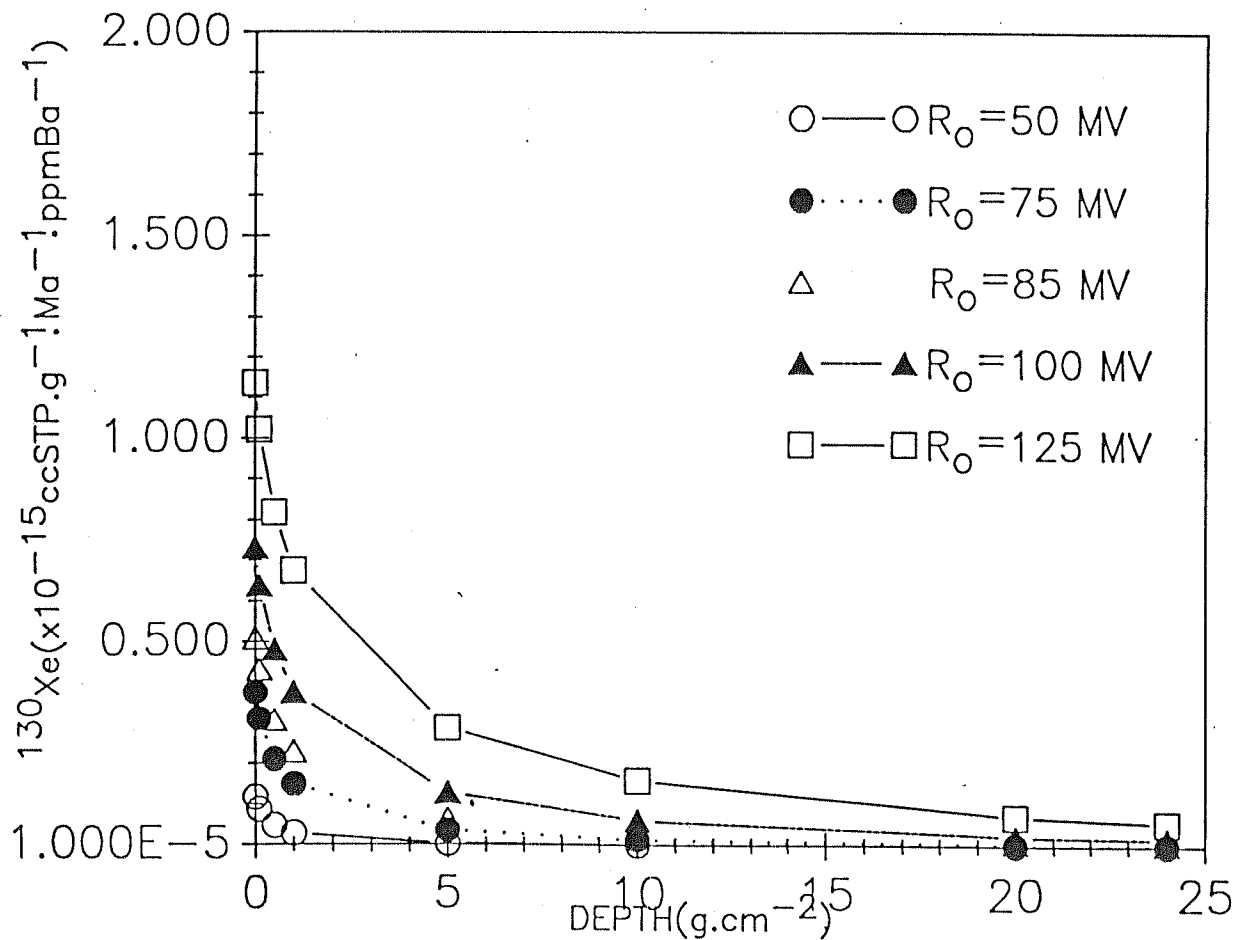
Fig.3.8 Production rates of ^{130}Xe in lunar surface material as a function of shielding depth. Production rates calculated with R_o = 50 MV, 75 MV, 85 MV, 100 MV and 125 MV are shown.
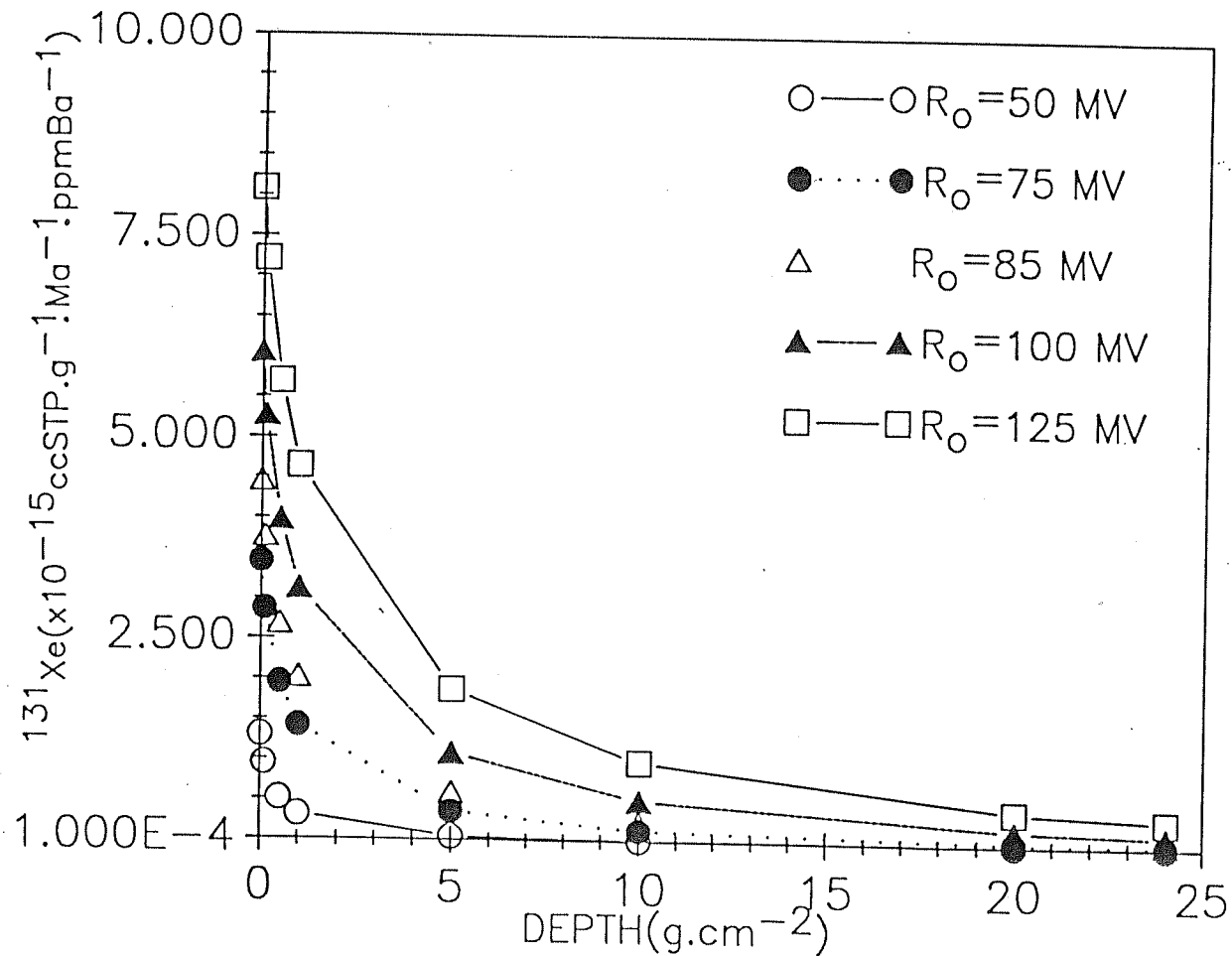
Fig.3.9 Production rates of ^{131}Xe in lunar surface material as a function of shielding depth. Production rates calculated with R_o = 50 MV, 75 MV, 85 MV, 100 MV and 125 MV are shown.
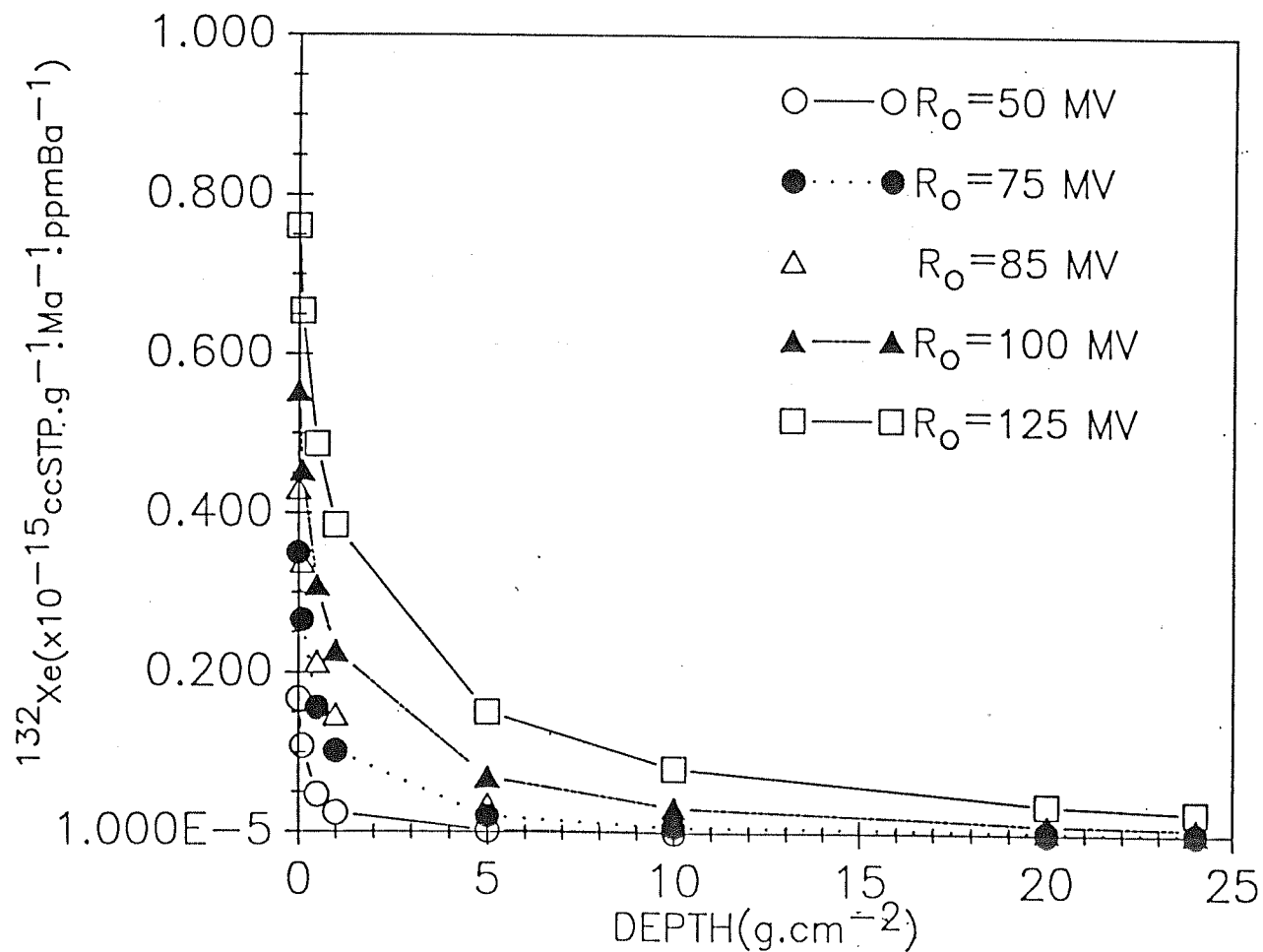
Fig.3.10   Production rates of [132]Xe in lunar surface material as a function
of shielding depth.   Production rates calculated with R_o = 50 MV, 75 MV, 85
MV, 100 MV and 125 MV are shown.

the same shielding depths. The deviation of our production rates from those calculated by Hohenberg et al.,(1978) further shows a rigidity dependence. At low rigidities (for eg. at 50 MV), the discrepancies become more pronounced and the discrepancies tend to decrease as the rigidity approaches a value of Ro =125 MV. This observation is along expected lines of thinking since a spectrum with lower rigidity, means that the number of low energy particles are higher and in the calculations by Hohenberg et al.,(1978) the production by these low energy particles are not taken into consideration. The production by low energy (E <60 MeV) are neglected in Hohenberg et al.,(1978) calculations because based on his cross-section measurements, Kaiser (1977) concluded that the cosmogenic xenon production by protons having energies below about 60 MeV is insignificant. At higher values of rigidity, R_o=125 MV for example, the SCR spectrum is much flatter and the number of particles with low energies decreases. At high energies Kaiser's (1977) production cross-sections deviate less from the theoretical cross-section values used in the present calculations.

Figures 3.6, 3.7, 3.8, 3.9 and 3.10 shows the production rates of isotopes ^{128}Xe, ^{129}Xe, ^{130}Xe, ^{131}Xe and ^{132}Xe as a function of shielding depth on the lunar surface. The production rates estimated using values of 50 MV, 75 MV, 85 MV, 100 MV and 125 MV for the SCR characteristic rigidity are plotted as a function of shielding depth on the lunar surface, in these Figures. From these plots it becomes clear that the SCR production is confined to the top layers of the lunar surface only.

The calculations at PRL are carried out with an energy

cut off at 100 MeV to separately estimate the contributions from protons having energy less than 100 MeV to the total production. This calculation has been carried out to enable us to estimate the relative importance of protons belonging to different energy ranges in the total production of xenon isotopes. The results of these calculations for the $R_o = 100$ MV are given in Table 3.5. The following features emerge from this analysis. The lighter isotopes (^{124}Xe and ^{126}Xe) being high energy products are least affected by protons having energies less than 100 MeV. As one approaches the heavier isotopes (^{131}Xe and ^{132}Xe) the scenario changes substantially and protons in this low energy region start playing a significant role in the isotope production. In the case of ^{132}Xe these protons alone (protons having E <100 MeV) account for as much as 70% of the total production of this isotope, on the lunar surface. Considering the isotopes ^{131}Xe, ^{130}Xe and ^{129}Xe these low energy protons alone contribute as much as 51%, 55% and 40% of the total production of these isotopes, on the lunar surface. Protons in this energy range (E <100 MeV) contribute to some extent at larger shielding depths also. As an illustration, at a shielding depth of 5 g.cm^{-2} they account for 29% of the total production of ^{132}Xe. For isotopes ^{131}Xe, ^{130}Xe and ^{129}Xe the contributions from the low energy protons are, 25%, 26% and 18% of the total production of these isotopes respectively at this shielding depth. At still larger ·shielding depths the low energy protons are essentially cut off by ionisation losses in the medium and they amount to only ~10% of the total production at a shielding depth of 24 g.cm^{-2}.
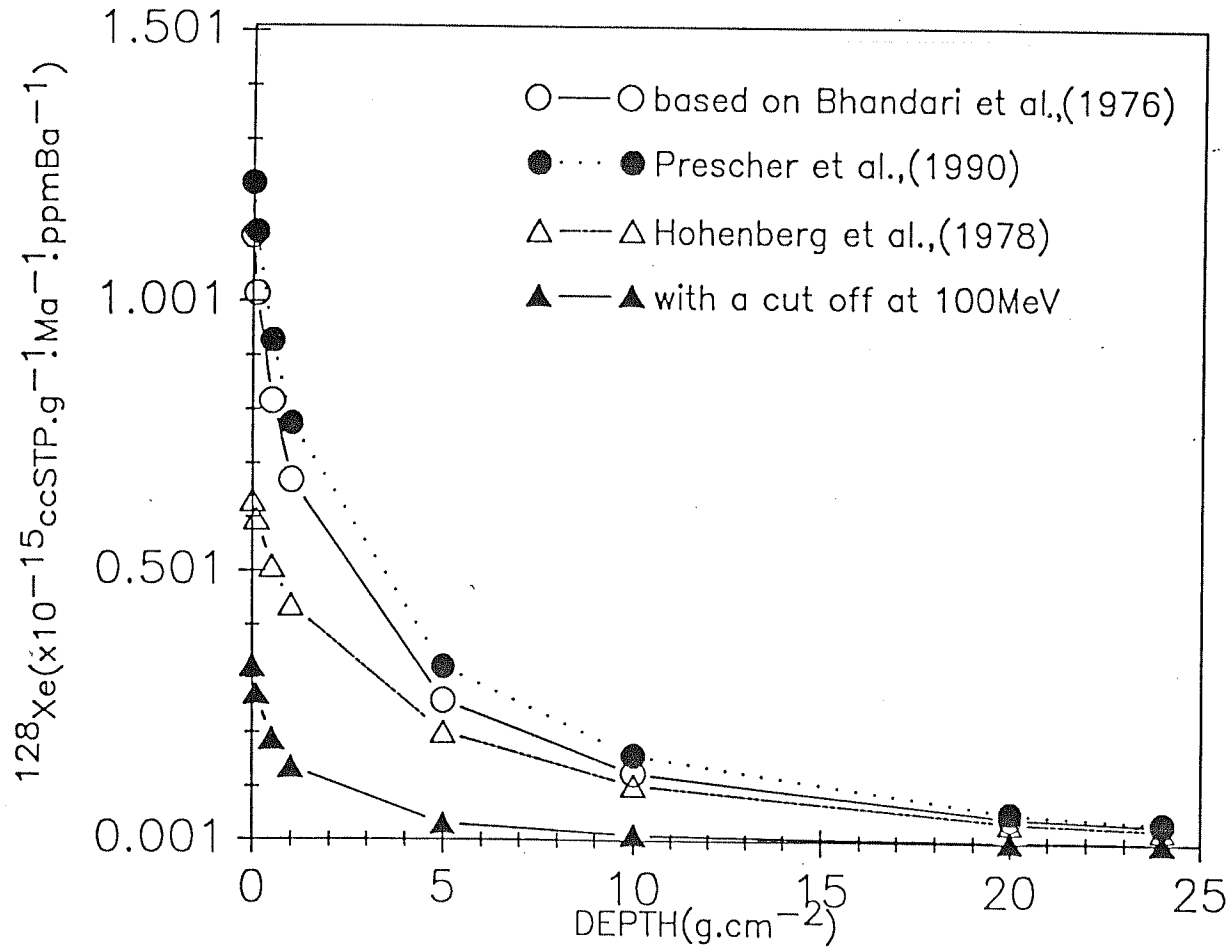
Fig.3.11 ^{128}Xe production rates in lunar surface material calculated by different models for R_o = 100 MV and an integrated proton flux of 100 protons $cm^{-2}.s^{-1}$.
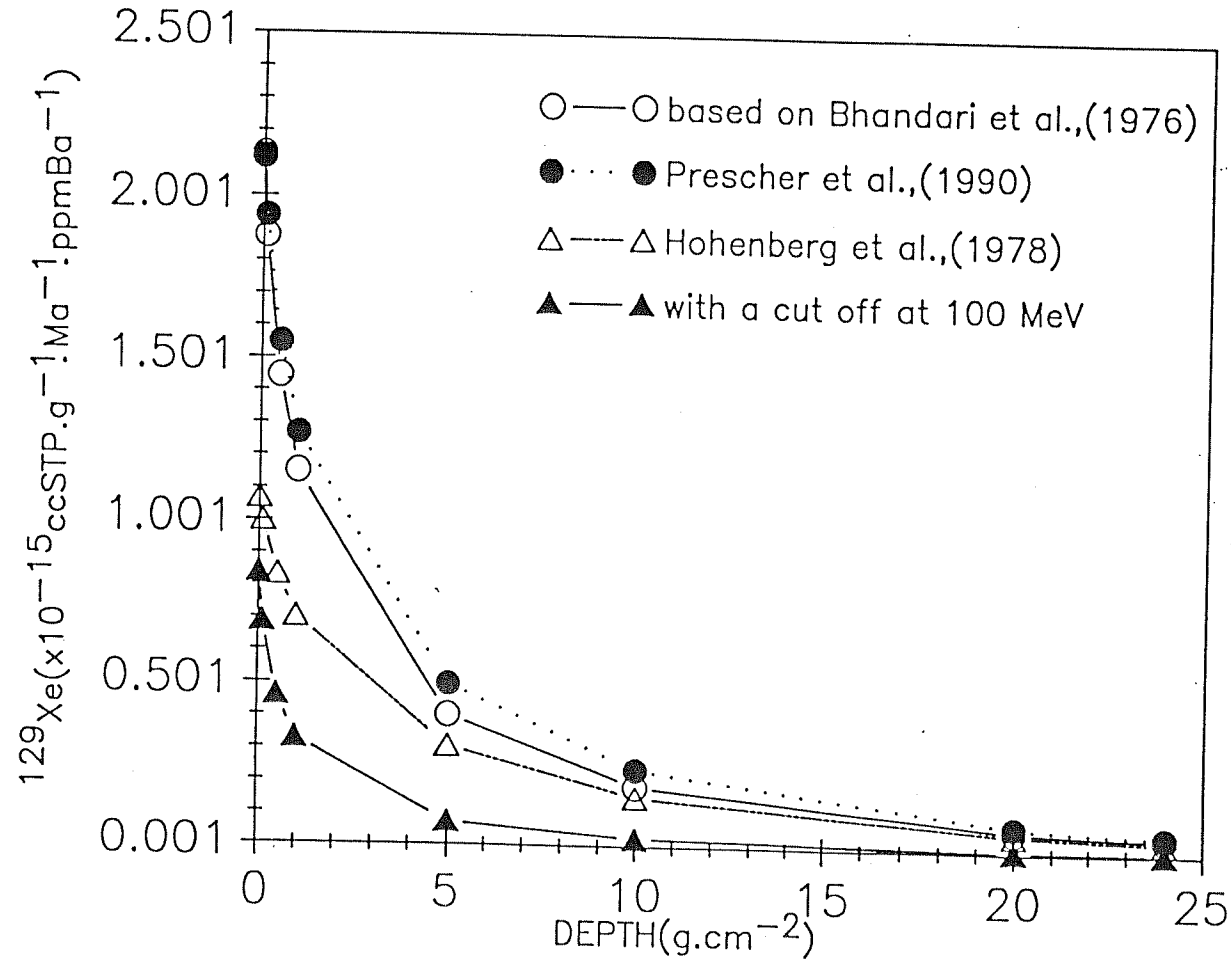
Fig.3.12 ^{129}Xe production rates in lunar surface material calculated by different models for R_o = 100 MV and an integrated proton flux of 100 protons $cm^{-2}.s^{-1}$.
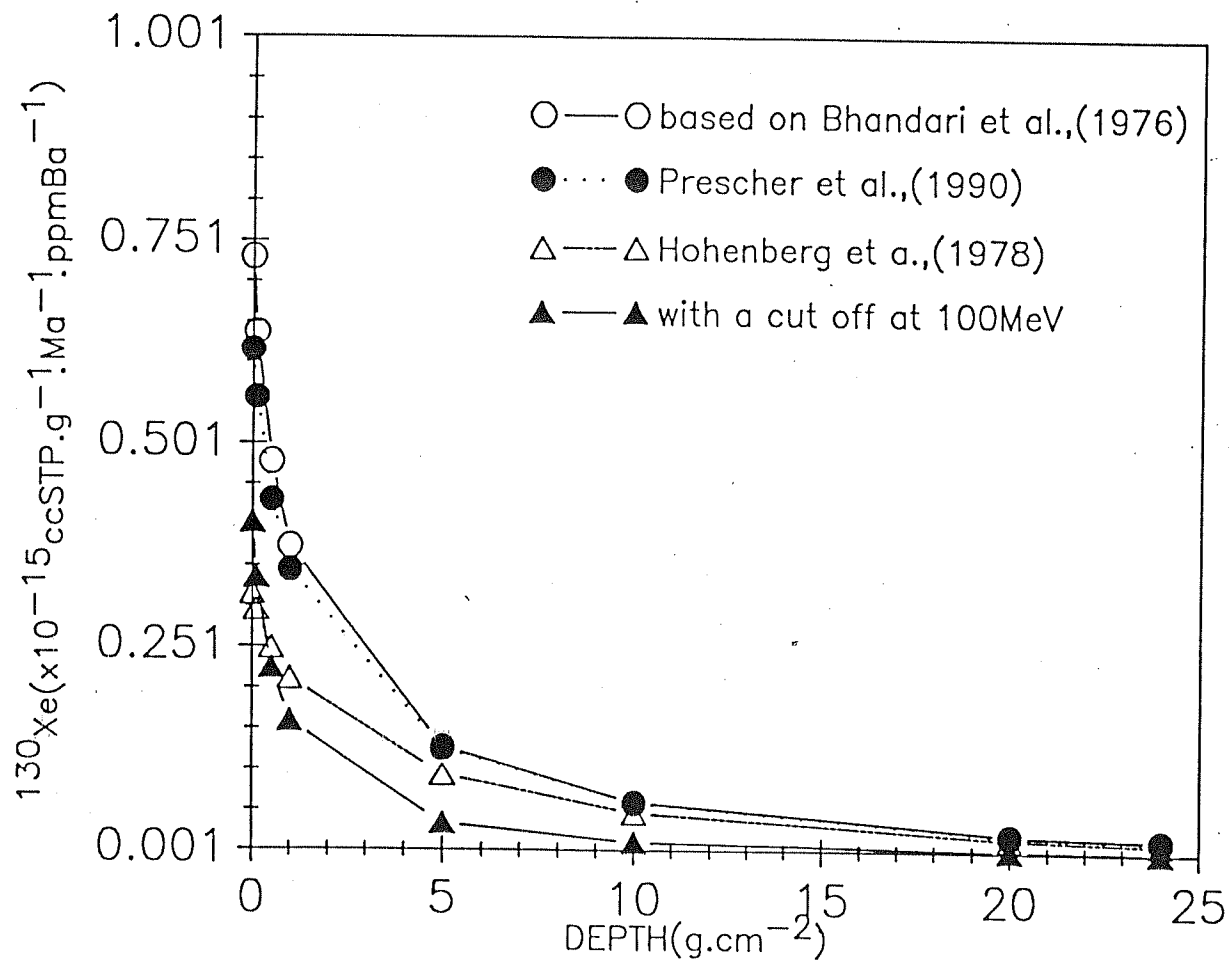
Fig.3.13 ^{130}Xe production rates in lunar surface material calculated by different models for R_o = 100 MV and an integrated proton flux of 100 protons cm^{-2}.s^{-1}.
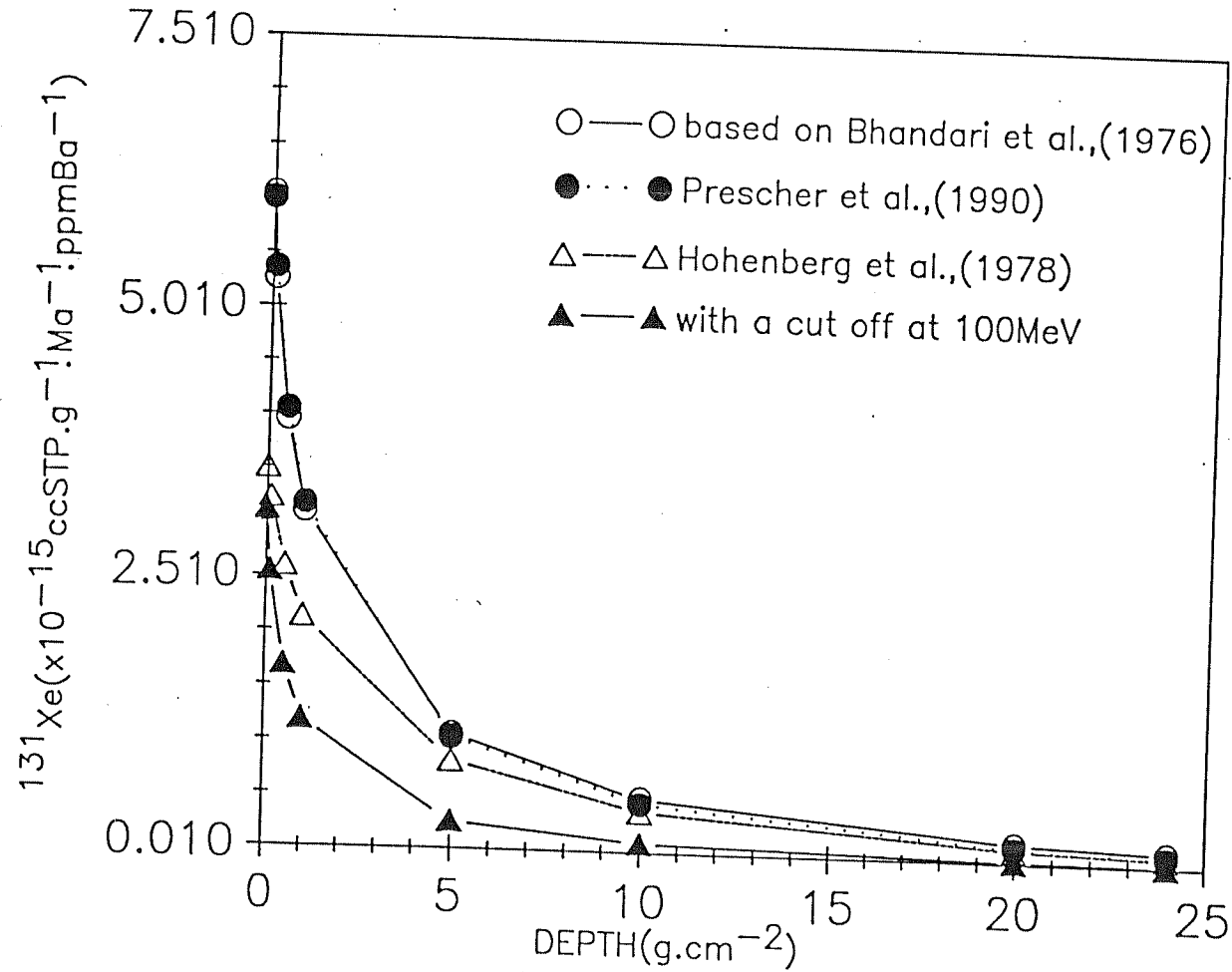
Fig.3.14 ^{131}Xe production rates in lunar surface material calculated by different models for R_o = 100 MV and an integrated proton flux of 100 protons $cm^{-2}.s^{-1}$.
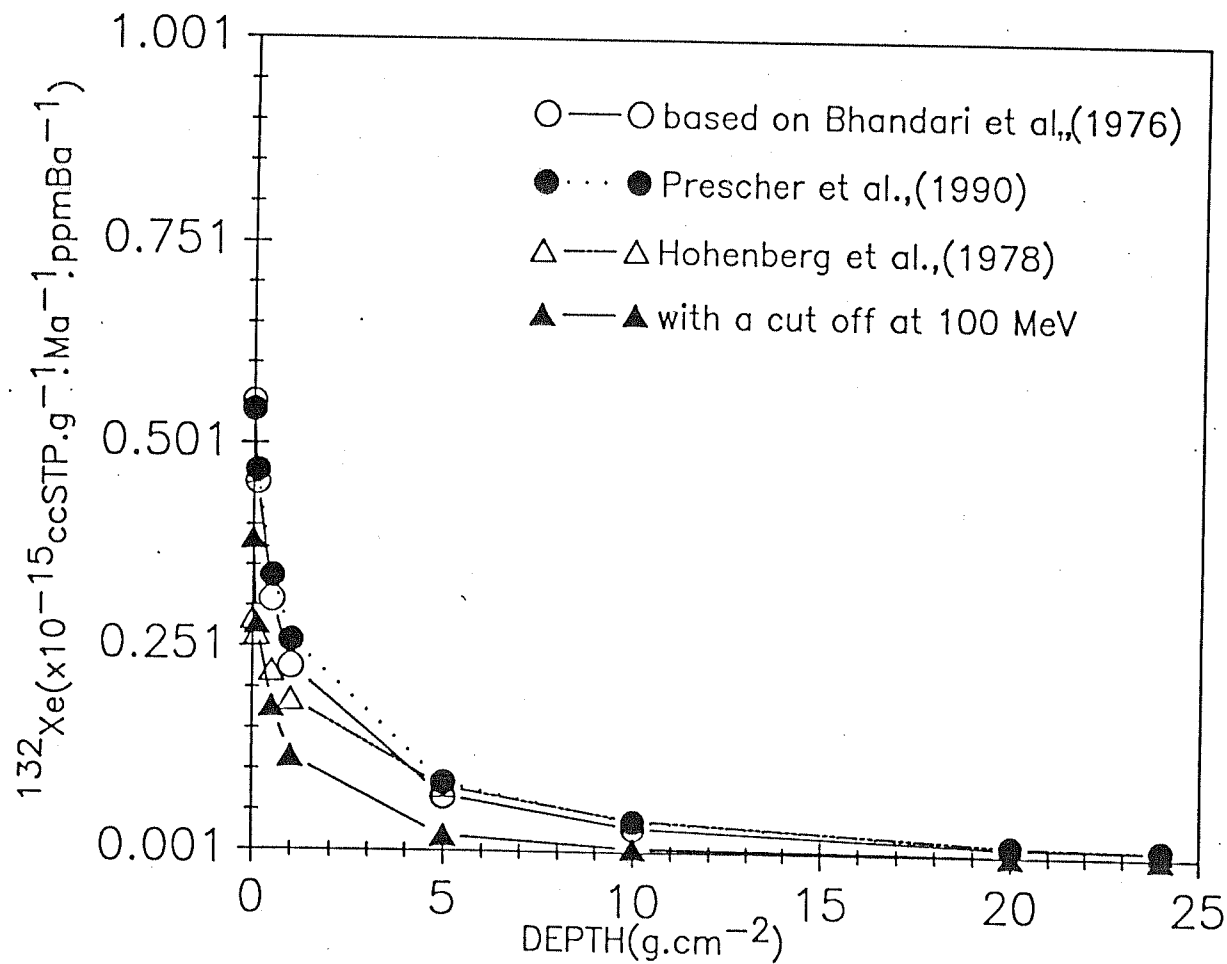
Fig.3.15 ^{132}Xe production rates in lunar surface material calculated by different models for R_o = 100 MV and an integrated proton flux of 100 protons cm^{-2}.s^{-1}.

3.2a. Comparison of the Present Calculations with Earlier estimates

The SCR xenon production rates, calculated on the basis of the Bhandari et al.,(1976) model, discussed above, are in good agreement with those calculated by using models developed by Michel and Brinkmann (1980). The Michel calculations for SCR xenon production are presented in Prescher et al.,(1991). These calculations are based on an improved stopping calculations making use of the most recent stopping-power tables [R.Michel Person. Communic.,(1990)], though, the effects of this change are not very significant. The surface production rates of ^{130}Xe are 0.617×10^{-15} ccSTP.g^{-1}.Ma^{-1}.ppmBa^{-1} in comparison to the PRL value of 0.731×10^{-15} ccSTP.g^{-1}.Ma^{-1}.ppmBa^{-1} calculated for identical exposure conditions on the lunar surface.. At larger shielding depths also the production rate calculations by the above two models agree reasonably well. For example, at a shielding depth of 20 g.cm^{-2} the PRL and Hannover production rate values are, respectively, 0.022 and 0.020×10^{-15} ccSTP.g^{-1}.Ma^{-1}.ppmBa^{-1}.

The agreement between the production rate calculations at PRL [using the Bhandari et al.,(1976)] and the Hannover calculations [using Michel and Brinkmann (1980)] is obvious from Figures 3.11, 3.12, 3.13, 3.14 and 3.15. In these diagrams the production rates of isotopes ^{128}Xe, ^{129}Xe, ^{130}Xe, ^{131}Xe and ^{132}Xe calculated by using Bhandari et al.,(1976) and Michel and Brinkmann (1980) and those estimated by Hohenberg et al.,(1978) are shown as a function of shielding depth on the lunar surface. The assumed SCR spectrum have R$_o$ =100 MV. Also shown are the PRL calculations with the protons having E >100 MeV cut off, so that
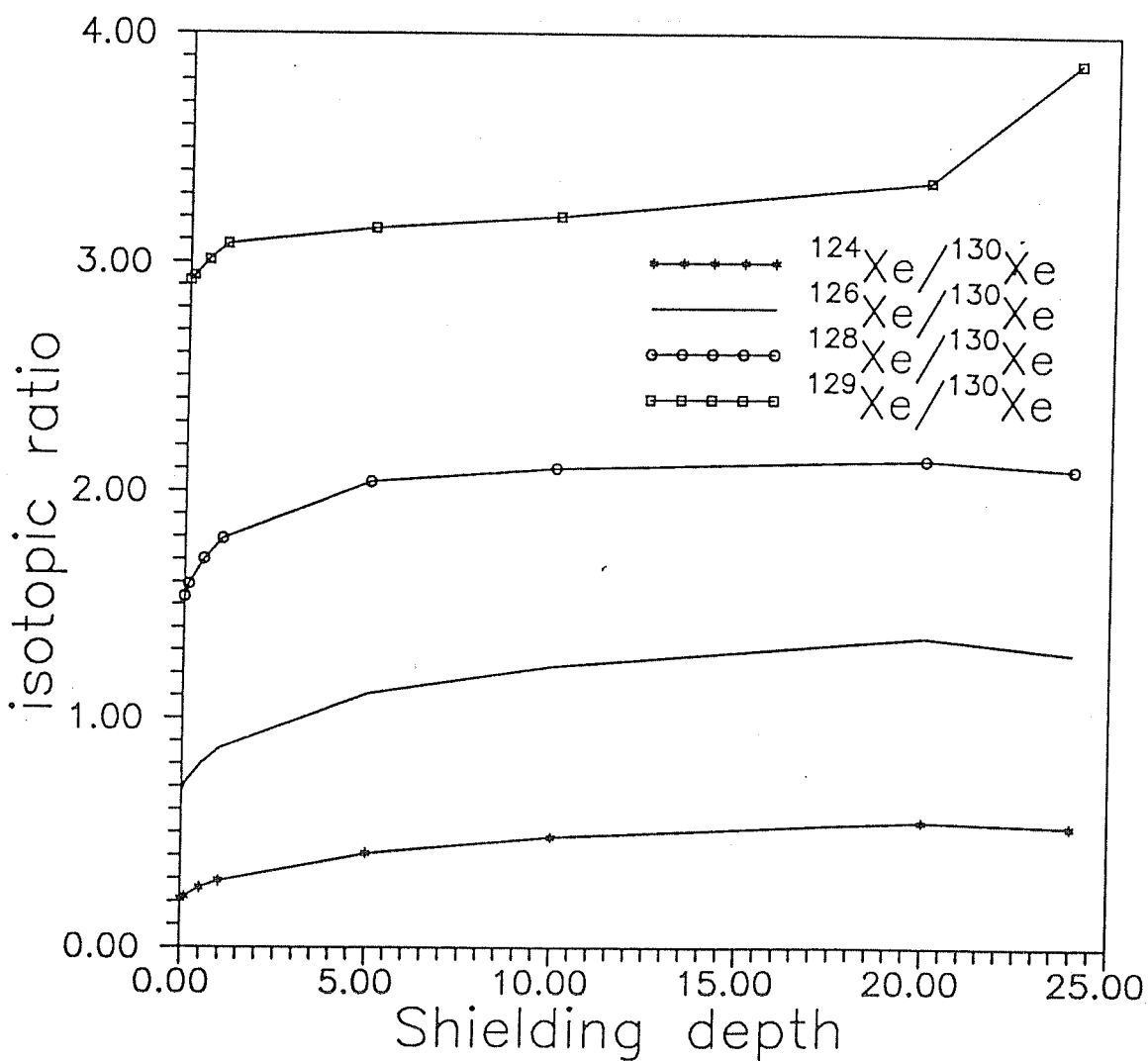
Fig.3.16 $^{124}Xe/^{130}Xe$, $^{126}Xe/.^{130}Xe$, $^{128}Xe/^{130}Xe$ and $^{129}Xe/^{130}Xe$
production ratios as a function of depth in lunar
surface material for R_o = 100 MV and integral proton
flux J = 100 protons $cm^{-2}s^{-1}$.
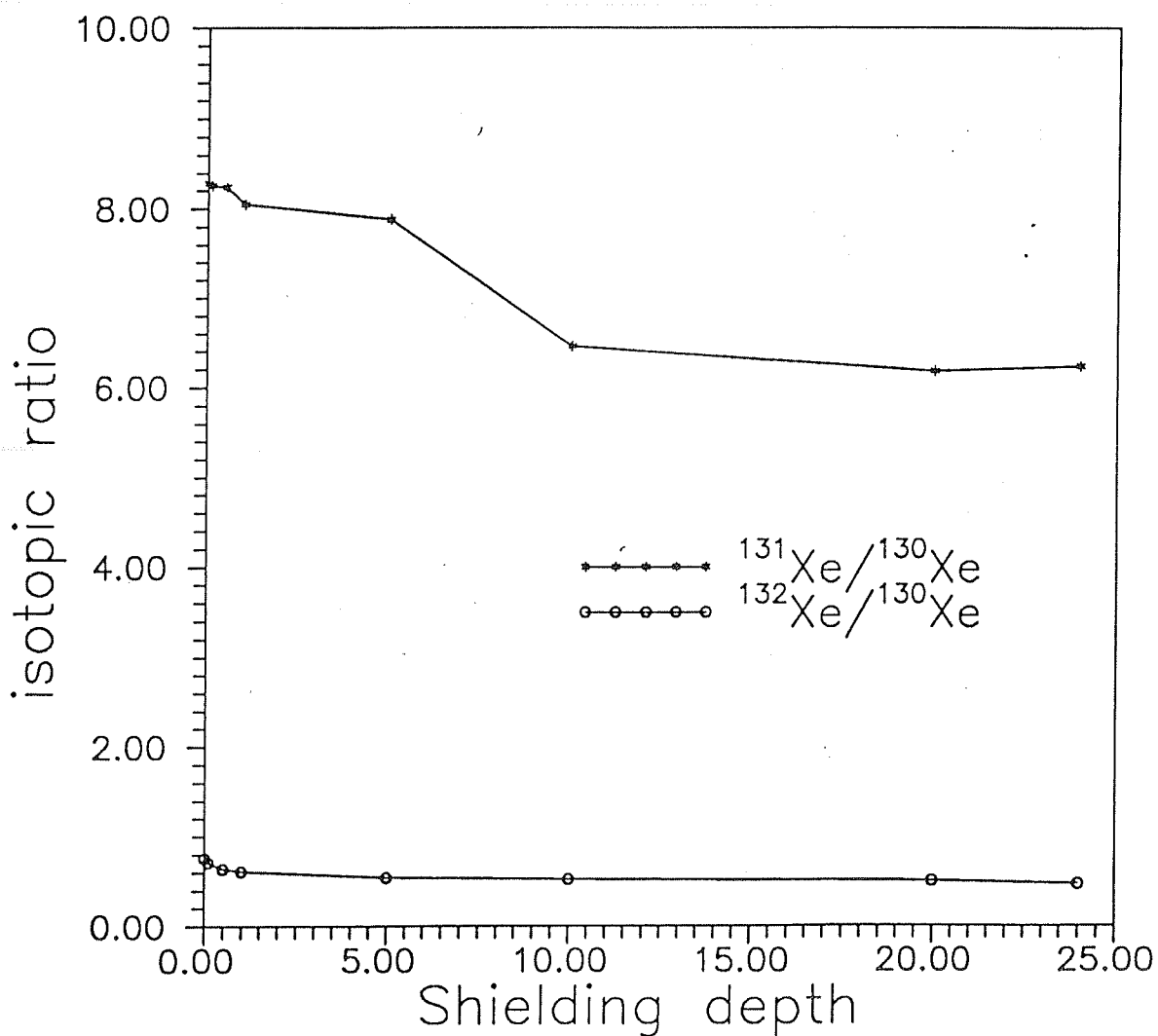
Fig.3.17 ^{131}Xe/^{130}Xe and ^{132}Xe/^{130}Xe ratios as a function of shielding

depth in lunar surface material

for R_o = 100MV and integral proton flux J = 100 protons

cm^{-2}s^{-1}.

100

the contribution from the low energy protons alone can be separately estimated.

There is some systematic behaviour which the isotopic ratios of production rates exhibit. Supposing A is the mass number of the normalizing isotope the isotopes lighter than A have isotopic ratios, $^M Xe/^A Xe$, increasing with shielding depths whereas the isotopes heavier than A have isotopic ratios, $^M Xe/^A Xe$, decreasing with shielding depths. This fact is illustrated in Fig 3.16 which shows $^{124}Xe/^{130}Xe$, $^{126}Xe/^{130}Xe$, $^{128}Xe/^{130}Xe$ and $^{129}Xe/^{130}Xe$ and Fig.3.17 shows the $^{131}Xe/^{130}Xe$ and $^{132}Xe/^{130}Xe$ ratios as a function of shielding depth. All lighter isotope ratios exhibit the same behaviour as the 129/130 ratio and the heavier isotope ratios vary much like the 132/130 ratio.

3.2b. Concluding Remarks on the SCR Xenon Production Rate Calculations

From the study of oriented lunar rocks, exposed to the sun on the lunar surface under known irradiation geometry it is interesting to note that the major isotopes ^{129}Xe, ^{131}Xe and ^{132}Xe are produced with significant abundances by SCR protons. Isotopic excesses are observed only at these isotopes in the surface samples of lunar rocks 61016, 64435 and 79215. The theoretical production rates conform to this observation if comparatively lower rigidities are chosen for consideration. If a harder SCR spectrum is used in the calculations the isotopes ^{130}Xe and ^{128}Xe are also produced with relatively larger abundances and as a matter of fact the predicted production rates for the above two isotopes become higher than that of ^{132}Xe at $R_o = (or >) 100$ MV.

Thus our results suggest that the SCR proton spectra seem to be soft and that values of R_o are some what less than 100 MV. These conclusions conform the latest observations by Nishiizumi et al.,(1990) based on the study of radioactive nuclides in lunar samples.

The isotopic ratios also show some variation with the characteristic rigidity of the SCR spectrum assumed. Compared to ^{130}Xe, on the one hand, the production of the lighter isotopes ^{124}Xe, ^{126}Xe, ^{128}Xe and ^{129}Xe decreases and the production of ^{131}Xe and ^{132}Xe, on the other hand, increases as the rigidity of the spectrum adopted in the calculations is increased.

The errors of the present calculations are around 20% where absolute concentrations are concerned and about 5% in the case of isotopic ratios. A major contributing factor to the errors is the uncertainty in the excitation functions of the various isotopes in the proton energy range of 50 to 200 MeV. This can be improved by enriching the data base with more experimental cross-section measurements in the proton energy range of 50 to 200 MeV where no measured cross-section values exist.

In conclusion, to accurately calculate the lunar cosmogenic xenon, three processes should be separately considered. These are the production of xenon by SCR and GCR particles and the thermal neutron capture reactions on ^{130}Ba leading to the production of xenon isotopes ^{131}Xe. Using the data already discussed and the production of xenon by high energy protons (corresponding to GCR particles) which will be discussed in the next section, the SCR and GCR production rates can be estimated satisfactorily. There is scope for further improvement as and

when the experimental cross-sections in the E =50 to 200 MeV become available. Further the agreement in calculations between the PRL and Hannover xenon production rates show that if reliable cross-section values are available for all the energy ranges of interest, existing models can predict the cosmogenic production rates in extraterrestrial matter quite accurately. The discrepancies between the Hohenberg et al.,(1978) calculations and the present calculation also emphasizes this inference.

3.3. SCR Xenon Spallation Ratios Deduced from Study of Lunar Rocks 61016, 64435 and 79215

When a rock is exposed to the Sun, directly without any shielding, on the lunar surface, the top most grain layers get implanted with solar wind (SW) and solar flare (SF) gases. The typical range of the SW particles are ~ 2 to 3 x 10^3 A^o in silicate grains. Another process occurring simultaneously with the above mentioned process is that the surfaces of these rocks get continually eroded by micro meteorite (and to some extent by SW ion bombardment at the rate of about ~1 mm/m.y on an average) [Burnett and Woolum (1977), Hörz et al.,(1975) and Bhandari et al.,(1975)]. This process of erosion constantly generates fresh surfaces and one may find about 10^3-10^4 years equivalent of implanted SW in the top layers [Yaniv and Marti (1981)]. The SF particles, on the other hand, are more energetic and get deeply implanted into the top layers of the lunar rock up to ~ 10 to 20 μm [Yaniv and Marti (1981)]. This fact is based on the range energy relationship of these Solar Energetic Particles (SEP) in silicate grains, Lal (1972). The SF particles seem to have

rigidity dependent energy spectrum [Reedy (1987)]. For purposes of the study here, we assume that the isotopic composition of the implanted SF xenon, and of SW-xenon are similar to each other.

It is natural to assume that such lunar rocks which contain significant amounts of implanted solar gases (SW +SF) also contain cosmogenic nuclides produced by energetic solar flare protons, the Solar Cosmic Rays (SCR). The presence of these SCR-produced nuclides in such rocks can be detected under certain favourable conditions if the rocks have simple exposure history and if the samples are retrieved under documented conditions. The pre-requisites for detecting the SCR effects in a rock are that (1) since these rocks get exposed to the sun for short time periods only, their total GCR exposure ages, the combined period for which they are exposed to the GCR particles at the surface and at low shielding depths, should be small (about a few million years) and (2) they should have enough target concentrations for the production of the cosmogenic nuclide of interest. In addition, these rocks should not have changed their orientation during the exposure to solar particles on the lunar surface. In such an event the shielding conditions of the sample would not remain the same throughout the course of SCR irradiation and the measured signals will be the cumulative effect of the irradiations under different shielding conditions on the lunar surface. Whether a given lunar rock satisfies the above conditions can be verified experimentally, using particle track techniques [Bhandari et al., (1976)] and ^{21}Ne isotopes {Yaniv and Marti (1981)]. Only in rocks satisfying these conditions one can expect to detect SCR effects. In the other cases SCR effects are likely to get mixed

up in the overwhelming background of trapped gases and that of GCR produced isotopes and it is difficult to disentangle them in such cases.

By nuclear track studies, counting techniques and rare gas mass spectrometric measurements, Bhandari et al.,(1976) and Nautiyal et al.,(1981) had earlier shown that lunar rocks 61016, 64435 and 79215 contain nuclides produced by SCR protons. Samples from known depths of these three lunar rocks 61016, 64435 and 79215 are carefully studied (as part of an earlier lunar sample program at PRL under Prof. N.Bhandari) for the xenon isotopic composition to examine if these rocks contain resolvable amounts of SCR produced xenon isotopes. A detailed description of the analysed samples can be found in Bhandari et al., (1976). The procedure used for resolving the various components is described in Appendix IV of this thesis.

3.3a. Discussion on the Lunar Rock Xenon Data

Three samples each, from (a) the surface, (b) intermediate depth and (c) deeper shielding positions of the rocks 61016, 64435 and 79215 have been analysed mass spectrometrically (earlier these samples were analysed for nuclear tracks [Bhandari et al., (1976)]. The surface samples are designated as R1 samples, the intermediate depth position samples as R2 samples and the samples from deeper depths are called R3 samples, hereafter. The results of these measurements are given in Tables 3.6, 3.7 and 3.8. The xenon isotopic amounts are expressed in units $[x10^{-12}ccSTP.g$ rock material$^{-1}]$.

The R1 samples have more xenon concentrations as

Table 3.6 : ^{130}Xe concentrations and isotopic composition of Xe measured in samples from lunar rock 61016. Amounts are expressed in units [x10^{-12}ccSTP.g rock material^{-1}]

^{130}Xe [x10^{-12}ccSTP.g^{-1}]	$\dfrac{^{124}Xe}{^{130}Xe}$	$\dfrac{^{126}Xe}{^{130}Xe}$	$\dfrac{^{128}Xe}{^{130}Xe}$	$\dfrac{^{129}Xe}{^{130}Xe}$	$\dfrac{^{131}Xe}{^{130}Xe}$	$\dfrac{^{132}Xe}{^{130}Xe}$	$\dfrac{^{134}Xe}{^{130}Xe}$	$\dfrac{^{136}Xe}{^{130}Xe}$
SAMPLE = R1, Shielding depth = 0.5 to 3 mm									
19.71 ±1.00	0.041 0.0012	0.065 0.0015	0.512 0.011	7.221 0.136	5.917 0.112	6.990 0.130	2.483 0.053	2.135 0.048
SAMPLE = R2, Shielding depth = 4 to 7.5mm									
7.74 ±0.39	0.078 0.002	0.144 0.004	0.524 0.015	5.926 0.136	4.875. 0.107	5.838 0.123	2.201 0.055	1.810 0.049
SAMPLE = R3, Shielding depth = 16 to 18 mm									
2.81 ±0.14	0.120 0.004	0.192 0.006	0.609 0.016	6.082 0.140	5.014 0.120	5.951 0.131	2.220 0.056	1.881 0.051

Table 3.7 : ^{132}Xe concentrations and isotopic composition of Xe measured in samples from lunar rock 64435. Amounts are expressed in units [x10^{-12}ccSTP.g rock material^{-1}]

^{130}Xe [x10^{-12}ccSTP.g^{-1}]	$\dfrac{^{124}Xe}{^{130}Xe}$	$\dfrac{^{126}Xe}{^{130}Xe}$	$\dfrac{^{128}Xe}{^{130}Xe}$	$\dfrac{^{129}Xe}{^{130}Xe}$	$\dfrac{^{131}Xe}{^{130}Xe}$	$\dfrac{^{132}Xe}{^{130}Xe}$	$\dfrac{^{134}Xe}{^{130}Xe}$	$\dfrac{^{136}Xe}{^{130}Xe}$

ROCK 64435

SAMPLE = R1, Shielding depth = 0 to 1 mm

| 26.49 ±1.32 | 0.0370 0.0015 | 0.045 0.002 | 0.541 0.015 | 7.163 0.165 | 5.974 0.149 | 6.964 0.153 | 2.471 0.067 | 2.112 0.059 |

SAMPLE = R2, Shielding depth = 4.5 to 7.5 mm

| 9.37 ±0.47 | 0.058 0.002 | 0.077 0.003 | 0.551 0.019 | 6.704 0.201 | 5.691 0.170 | 6.694 0.187 | 2.308 0.074 | 1.982 0.067 |

SAMPLE = R3, Shielding depth = 7.5 to 9.0 mm

| 8.86 ±0.44 | 0.047 0.002 | 0.072 0.003 | 0.603 0.021 | 6.366 0.178 | 5.021 0.151 | 6.345 0.177 | 2.415 0.077 | 2.138 0.072 |

Table 3.8 : ^{130}Xe concentrations and isotopic composition of Xe measured in samples from lunar rock 79215. Amounts are expressed in units [x10^{-12}ccSTP.g rock material^{-1}]

^{130}Xe [x10^{-12}ccSTP.g^{-1}]	$\dfrac{^{124}\text{Xe}}{^{130}\text{Xe}}$	$\dfrac{^{126}\text{Xe}}{^{130}\text{Xe}}$	$\dfrac{^{128}\text{Xe}}{^{130}\text{Xe}}$	$\dfrac{^{129}\text{Xe}}{^{130}\text{Xe}}$	$\dfrac{^{131}\text{Xe}}{^{130}\text{Xe}}$	$\dfrac{^{132}\text{Xe}}{^{130}\text{Xe}}$	$\dfrac{^{134}\text{Xe}}{^{130}\text{Xe}}$	$\dfrac{^{136}\text{Xe}}{^{130}\text{Xe}}$
			ROCK 79215					
		SAMPLE = R1, Shielding depth = 0 to 1.5 mm						
24.19 ±1.21	0.331 0.009	0.598 0.016	1.095 0.026	3.365 0.074	6.656 0.120	2.935 0.062	0.818 0.019	0.639 0.016
		SAMPLE = R2, Shielding depth = 2 to 5 mm						
20.15 ±1.01	0.358 0.010	0.696 0.018	1.201 0.029	2.319 0.053	6.226 0.131	1.906 0.040	0.422 0.010	0.322 0.008
		SAMPLE = R3, Shielding depth = 5 to 8 mm						
18.62 ±1.00	0.393 0.010	0.721 0.019	1.251 0.030	1.971 0.045	6.201 0.130	1.450 0.030	0.351 0.008	0.242 0.006

compared to the R2 and R3 samples, in all the three rocks. In the case of rocks 61016 and 64435 the R1 samples have about 3 to 4 times more xenon concentrations than the R2 and R3 samples. This is as expected because the surface samples of these rocks have trapped or implanted solar (SW + SF) gases, besides the xenon trapped in all the three samples, at the time of formation of the rock (referred to as intrinsically trapped, hereafter). The intrinsically trapped component is assumed to be the same in all the three samples R1, R2 and R3 taken from the same rock. It is also assumed that there is no isotopic fractionation occurring during this trapping process between R1, R2 and R3 samples at the time of formation of the rock. This intrinsically trapped component can be corrected by subtracting the xenon concentrations measured in the R3 samples from the ones measured in the respective R1 samples. Here, the GCR contribution also gets correspondingly corrected as the GCR produced xenon amounts in R1 and R3 are nearly equal. The GCR production between 0 g.cm^{-2}(R1) and 10 g/cm^{-2} (~R3) are not much different (considering the scope of errors involved in some of these measurements).

A look at the raw data of the lunar rock measurements, presented in Tables 3.6, 3.7 and 3.8 gives clues about the components contributing to the samples from various depths. The lighter isotopic ratios $^{124}Xe/^{130}Xe$, $^{126}Xe/^{130}Xe$ and $^{128}Xe/^{130}Xe$ increases as the shielding depths increase from R1 to R3 sample. All the three rocks show the same trends as far as the lighter xenon isotope ratios are concerned. One explanation for this trend is that the lighter isotopes are less abundant in trapped xenon, which can be of SW or SF composition, or a mixture of the

above two.

The ^{M}Xe/^{130}Xe ratios, for M=129, 131 and 132, on the other hand, decrease as the shielding depth of the sample from the surface increases. All these isotopic ratios are highest in the R1 samples of all the three rocks studied here. In the R3 sample these isotopic ratios are lower than the corresponding ratio in the R1 sample. The R2 xenon isotopic ratios ^{M}Xe/^{130}Xe for M=129, 131 and 132 are generally in between the corresponding ratios of the R2 and R3 samples in the same rock. A plausible explanation is that there is some mechanism of producing the isotopes ^{129}Xe, ^{131}Xe and ^{132}Xe in the surface samples. The production of the above isotopes is maximum at the surface samples (R1 samples) and falls off steeply as the shielding depth of the sample increases. The solar cosmic ray (SCR) particles satisfy the constraints elaborated above. As the energy of these particles are low the isotopic production due to them is confined to a few millimeters in the top surfaces of the extraterrestrial body with which they interact [Lal and Venkatavardhan (1967), Amin et al., (1968) and Shedlovsky et al., (1970)].

The ^{136}Xe/^{130}Xe and ^{134}Xe/^{130}Xe ratios on the other hand show no systematic behaviour, but in these cases also the isotopic ratios at the surface are higher than the isotopic ratios in R2 and R3 samples.

As shown in Tables 3.9, 3.10 and 3.11 the R1-R3 xenon concentrations are much higher than the measured R3 xenon concentrations. In the case of rock 61016 the R1-R3 xenon amounts are about 86% of the xenon amounts in R1 and it is ~6 times higher than the xenon amounts in R3 sample. For rock 64435 it is about

Table 3.9 : Measured solar Xenon and excesses over trapped and GCR produced Xe in lunar rock 61016. All the gas amounts are given in units $[\times 10^{-12} ccSTP.g$ rock material$^{-1}]$.

	^{130}Xe	^{124}Xe	^{126}Xe	^{128}Xe	^{129}Xe	^{131}Xe	^{132}Xe	^{134}Xe	^{136}Xe
R1-R3	16.90	0.471	0.742	8.378	125.24	102.53	121.05	42.70	36.79
	±1.01	0.051	0.078	0.564	7.76	6.36	7.50	2.71	2.36
SOLAR TRAPPED	19.07	0.553	0.494	9.611	121.17	95.12	115.60	42.70	34.67
	±1.01	0.051	0.078	0.564	7.76	6.36	7.50		2.36
EXCESS OVER TRAPPED			0.248		4.07	7.41	5.45		
					±11.00	±9.00	±11.00		
R1-R2	11.97	0.204	0.167	6.034	96.46	78.89	92.58	31.90	28.07
	1.07	0.060	0.096	0.60	8.11	6.64	7.84	2.86	2.47
SOLAR TRAPPED	14.25	0.413	0.369	7.182	90.54	71.08	86.38	31.9	25.91
	1.07	0.060	0.096	0.600	8.11	6.64	7.84		2.47
EXCESS OVER TRAPPED					5.92	7.81	6.2		
					±11.5	±9.4	±11.0		

Table 3.10 : Measured solar Xenon and excesses over trapped and GCR produced Xe in lunar rock 64435. All the gas amounts are given in units $[\times 10^{-12}\,ccSTP.g\ \text{rock material}^{-1}]$.

	^{130}Xe	^{124}Xe	^{126}Xe	^{128}Xe	^{129}Xe	^{131}Xe	^{132}Xe	^{134}Xe	^{136}Xe
R1-R3	17.63	0.564	0.554	8.987	133.35	113.76	128.26	44.07	37.02
	±1.29	0.066	0.090	0.882	11.42	9.19	11.31	3.92	3.39
SOLAR TRAPPED	19.68	0.570	0.510	9.919	125.05	98.16	119.30	44.07	35.77
	±1.29	0.066	0.090	0.882	11.42	9.2	11.30		3.39
EXCESS OVER TRAPPED					8.3	15.6	8.96		
					±15.0	±13.0	±15.0		
R1-R2	17.12	0.437	0.471	9.167	126.93	104.93	121.76	48.83	37.39
	±1.29	0.068	0.092	0.880	11.56	9.35	11.43	3.93	3.38
SOLAR TRAPPED	19.57	0.567	0.506	9.863	124.35	97.61	118.63	43.83	35.58
	±1.29	0.068	0.092	0.880	10.56	9.0	11.40		3.38
EXCESS OVER TRAPPED					2.58	7.32	3.13		
					±15.0	13.00	15.00		

Table 3.11: Measured solar Xenon and excess as over trapped and GCR produced Xe in lunar rock 79215. All the gas amounts are given in units $[\times 10^{-12} \text{ccSTP. rock material}^{-1}]$.

	^{130}Xe	^{124}Xe	^{126}Xe	^{128}Xe	^{129}Xe	^{131}Xe	^{132}Xe	^{134}Xe	^{136}Xe
R1–R3	5.57	0.69	1.03	3.20	44.70	45.55	44.0	13.26	10.95
	±1.56	0.63	1.15	2.01	4.94	10.85	4.16	1.15	0.90
SOLAR TRAPPED	5.92	0.172	0.153	2.98	37.61	29.53	35.89	13.26	10.76
	±1.56	0.63	1.15	2.01	4.94	10.85	4.16		0.90
EXCESS OVER TRAPPED		0.518	0.887	0.22	7.09	16.02	8.00		
		±0.89	1.63	2.84	7.00	15.00	6.00		
R1–R2	4.04	0.80	0.45	2.29	34.67	35.56	32.59	11.29	8.97
	±1.57	0.62	1.14	1.99	5.14	10.94	4.38	1.18	0.93
SOLAR TRAPPED	5.04	0.146	0.131	2.54	32.02	25.14	30.55	11.29	9.16
	±1.57	0.62	1.14	1.99	5.14	10.94	4.38		0.93
EXCESS OVER TRAPPED		0.65	0.319		2.65	10.42	2.04		
		±0.88	1.61		7.3	15.0	6.2		

66% of the gas amount in R1 which is higher than the R3 xenon amounts by a factor of ~2 (for the isotope ^{130}Xe which is used for normalization purposes). The R2 and R3 xenon amounts are nearly equal in the case of 64435. In case of 61016, as well, the difference between xenon concentrations in R2 and R3 samples is not as large as that between R1 and R2 samples or that between R1 and R3 samples. The rock 79215 has xenon concentrations decreasing from R1 to R2 to R3 sample, though the decrease is much less compared to the other rocks 61016 and 64435. Some of these differences may be due to the intrinsically trapped xenon because these rocks are lunar breccias. Table 3.10 shows the R1-R3 amounts for the Apollo 16 lunar rock 64435. Table 3.11 shows the results for the Apollo 17 lunar rock 79215. In the case of the normalising isotope ^{130}Xe the R1-R3 amounts in 79215 is about 23% of the ^{130}Xe amount in the R1 sample and the corresponding figures are respectively 86% in rock 61016 and 66% in 64435. The rock 79215 contains large quantities of GCR produced xenon isotopes as can be seen from higher ^{M}Xe/^{130}Xe ratios for M=124, 126 and 128. These isotopes are indicative of GCR spallation reactions and their concentrations in the trapped xenon are small. Further, the above fact is also evident from lower ^{M}Xe/^{130}Xe ratios for values of M=131, 132, 134 and 136. All these isotopes are abundant in trapped xenon and the latter two (^{134}Xe and ^{136}Xe) are indicators of fission from ^{238}U and/or ^{244}Pu. As these rocks are formed less than 3.6 by ago (formation age) [Stettler et al., (1973)] we rule out any ^{244}Pu fission contribution to the measured xenon concentrations in these samples. Also the trapped xenon amounts in this rock are small in comparison with 64435, probably due to

differences in mineral gas retentivities. At this stage, the ^{134}Xe concentration is used for calculating the trapped solar Xe content in the R1 sample by assuming that all the ^{134}Xe (or ^{136}Xe) in R1-R3 represents essentially is trapped solar xenon (SW). This isotope ^{134}Xe is used here since smaller errors are associated with this isotope compared to ^{136}Xe (in fact, the results obtained here are not sensitive whether ^{134}Xe (or ^{136}Xe) is used to estimate the solar implanted xenon amounts). The implanted solar gases are assumed to be having SUCOR composition [Eberhardt et al., (1972)]. These implanted solar gas amounts thus estimated are subtracted from the R1-R3 gas amounts to obtain the SCR produced xenon isotope concentrations.

The argument that most of the xenon concentrations at the R1-R3 stage are of solar origin can be substantiated by the isotopic ratios. The ^{124}Xe/^{130}Xe, ^{126}Xe/^{130}Xe and ^{128}Xe/^{130}Xe ratios in this fraction (R1-R3) are somewhat similar to the values deduced by Eberhardt et al., (1972) for the lunar soil 12001. For example the ^{124}Xe/^{130}Xe and ^{128}Xe/^{126}Xe ratios in the R1-R3 fractions are respectively 0.028 and 0.496 in case of 61016 and 0.032 and 0.509 in case of rock 64435 (the corresponding SUCOR values are 0.029 and 0.504). This inference is valid in the case of the R1-R2 xenon fraction also. In case of lunar rock 79215, however, the ^{124}Xe/^{130}Xe and ^{126}Xe/^{130}Xe ratios are higher than the SUCOR (Solar) ratios but the ^{128}Xe/^{130}Xe ratio in this rock matches the SUCOR value. The deviation in the ^{124}Xe/^{130}Xe and ^{126}Xe/^{130}Xe ratios in this rock are misleading as this rock has a higher GCR exposure age of 180 Ma [Rao et al., (1979)] and the determination of trapped amounts of these isotopes are prone to

errors. This fact also becomes evident from the larger errors in the isotopic concentration of the isotopes ^{124}Xe and ^{126}Xe in this rock.

The major isotope ratios ^{129}Xe/^{130}Xe, ^{131}Xe/^{130}Xe and ^{132}Xe/^{130}Xe on the other hand are markedly different from the SUCOR values. As an illustration, in the case of 61016 these ratios are 7.41, 6.07 and 7.16 [and for 64435 the corresponding values are 7.56, 6.45 and 7.28] (taking errors into consideration) compared to the SUCOR values of 6.354, 4.988 and 6.062 for these isotopic ratios. The rock 79215 also have the 129/130, 131/130 and 132/130 ratios well above the SUCOR values. The values of the above isotopic ratios in 79215 (R1-R3) fraction are respectively 8.03, 8.18 and 7.90.

3.3b. SCR Spallation Spectra Inferred from Lunar Rocks 61016, 64435 and 79215

The isotopes ^{129}Xe, ^{131}Xe and ^{132}Xe remaining after the correction of the GCR produced xenon amounts and the trapped solar wind amounts, are attributed to SCR production. It may be argued that the isotopic excesses seen above at isotopes ^{129}Xe, ^{131}Xe and ^{132}Xe are not due to fission process. The fission correction to ^{129}Xe is negligible. We do not know the precise fission spectrum for cosmic ray induced fission of ^{238}U and from the observed ^{136}Xe and ^{134}Xe in these samples this fission spectrum cannot be deduced. The ^{238}U spontaneous fission contribution to the ^{136}Xe$_f$ is very small in these samples. A similar correction for the isotope ^{129}Xe to account for the radiogenic ^{129}Xe from ^{129}I is not warranted as these contributions are the same for (R1, R2 and R3)

116

samples. Also, the time of formation of these rocks are much later in lunar history and they did not incorporate any live ^{129}I, (and ^{224}Pu) nuclides at the time of their formation.

The ^{129}Xe, ^{131}Xe and ^{132}Xe excesses obtained following the procedure elaborated in the previous paragraphs are listed in Table 3.12. These isotopic excesses are attributed by SCR protons. The errors quoted are only the lower limits of the isotopic excesses. The ^{129}Xe : ^{131}Xe : ^{132}Xe obtained from the three rocks are, respectively:

0.75 : 1.36 : 1.000 - deduced from 61016 R1-R3

0.95 : 1.26 : 1.000 - deduced from 61016 R1-R2

0.93 : 1.74 : 1.000 - deduced from 64435 R1-R3

0.82 : 2.34 : 1.000 - deduced from 64435 R1-R2

0.88 : 2.000 : 1.000 - deduced from 69215 R1-R3

1.30 : 5.110 : 1.000 - deduced from 79215 R1-R2

Based on these we estimate the average SCR produced xenon spectra in lunar rocks to be

$$^{129}Xe : {}^{131}Xe : {}^{132}Xe = 0.94 : 2.30 : 1.000.$$

The isotopic ratios deduced above based on the lunar rock data are not very different from the production rate ratios calculated by us in lunar surface material.

There seems to be a correlation between the SCR production rates calculated here and the SCR xenon production rate ratios deduced from the study of lunar rocks 61016, 64435 and 79215. We have seen in section 3.2 that at lower rigidities of the SCR proton spectra ($R_0 < 100$ MeV) the xenon isotopes produced with greater abundance are ^{129}Xe, ^{131}Xe and ^{132}Xe. The SCR spallation spectra obtained from the lunar rock studies also

117

Table 3.12 : Solar Cosmic Produced ^{132}Xe concentrations and isotopic ratios estimated in lunar rocks 61016, 64435 and 79215.

ROCK	^{132}Xe [X10^{-12}ccSTP.g rock material^{-1}]	^{129}Xe/^{132}Xe	^{131}Xe/^{132}Xe	^{132}Xe
61016 (R1-R3)	5.45 ±11.00	0.75 ±2.54	1.36 ±3.23	1.000
61016 (R1-R2)	6.20 ±11.00	0.95 ±2.45	1.26 ±2.70	1.000
64435 (R1-R3)	8.96 ±15.00	0.93 ±2.19	1.74 ±3.14	1.000
64435 (R1-R2)	3.13 ±15.00.	0.82 ±6.2	2.34 ±12.00	1.000
79215 (R1-R3)	8.00 ±6.00	0.89 ±1.13	2.00 ±2.50	1.000
79215 (R1-R2)	2.04 ±6.20	1.30 ±5.32	5.11 ±17.20	1.00

brings us to the same conclusion. The xenon production rates calculated using the Michel and Brinkmann (1980) which are discussed in the paper Prescher et al., (1991) and the present calculations using Bhandari et al., (1976) are good estimates of the xenon production rates in lunar surface material, available in literature today.

Based on the ^{131}Xe excesses deduced in these rocks and using the production rate values estimated in this study the SCR exposure ages of these rock are calculated. The Ba contents of these rocks are taken to be respectively 145 ppm (130 ppm Ba and 15 ppm La) for rock 61016 [Laul and Schmitt (1973)], 25 ppm (Ba+La) for rock 64435 [Hubbard et al.,(1973) and Laul and Schmitt (1973)]and 100 ppm for rock 79215 [Laul et al.,(1974)].

The estimated SCR exposure ages of all the three rocks are, respectively, 8.4±10.2 for the lunar rock 61016 and 17.5±16.5 for the rock 79215. The SCR exposure ages of these rocks are found to be 1.8 Ma for rock 61016 [Rao et al., (1979)] based on the ^{3}He and ^{21}Ne measurements, 0.8 Ma for rock 64435 based on ^{3}He and ^{21}Ne measurements [Venkatesan et al., (1980)] and 4 Ma for rock 79215 [Bhandari et al., (1976)] based on nuclear track measurements.

Though the errors associated with the numbers are very large (due to the subtraction of SW) the facts that (i) in the case of all three rocks 61016, 64435 and 79215 we have got similar results; (ii) the SCR produced xenon concentrations deduced from these rocks are somewhat consistent with the theoretically predicted production rate values for these well studied rocks having known SCR exposure histories. We conclude that our

arguments are in the right direction. Still a word of caution has to be added here that these are only suggestive and very careful studies on well documented samples are needed before the above facts can be considered established. The attempts made here are probably the first steps in that direction.

CHAPTER IV

Results and Discussions

Part II (High Energy)

Production Cross-sections of xenon at p-energies >600 MeV and Production Profiles as a function of depth based on Simulation Experiments

4.1 High Energy Measurements

In the first part of this chapter the thin target cross-sections for the production of stable xenon isotopes on Ba targets irradiated with 600 MeV, 800 MeV, 1200 MeV and 2600 MeV protons are discussed. These irradiated thin target Ba glasses are obtained from proton irradiation experiments carried out at different accelerators in Europe and USA (i.e. CERN synchrocyclotron, Saclay accelerator and Los Alamos accelerator) on different occasions. The experimental details regarding irradiation, flux monitoring etc. are described in Chapter 2. In the later sections of this Chapter (sections 4.2a and 4.2b) I have discussed the results of the measurement of Ba glass targets from the Simulation (thick target) Experiments. In these "Thick Target" irradiation experiments three spherical meteoroid mock-ups of radii 5 cm, 15 cm and 25 cm have been irradiated with 600 MeV protons at the CERN synchrocyclotron, simulating the space irradiation conditions of meteoroids. The complete experimental details of this irradiation are given by Michel et al.,(1989 and 1986), Dragovitsch (1987) and Peiffer (1986). However relevant information for the Ba/Xe system are outlined in Chapter 2 and Appendix II and III.

4.1a   Thin target Production Cross-sections of Xe Isotopes on Ba at Proton energies of 600, 800, 1200 and 2600 MeV

Table 4.1 shows the cross-sections for the production of ^{126}Xe by protons having energies of 600 MeV, 800 MeV, 1200 MeV and 2600 MeV on Ba. These cross-section values include the contributions from all possible reaction channels leading to the production of this isotope. As the irradiated Ba targets have been fabricated from natural barium glass containing all the stable Ba isotopes it is energetically possible that many reaction channels contribute a given end product.

Figures 4.1, 4.2, 4.3 and 4.4 show the energy dependence of the production cross-sections for xenon isotopes ^{124}Xe, ^{126}Xe, ^{128}Xe, ^{129}Xe, ^{130}Xe, ^{131}Xe ^{132}Xe and ^{134}Xe. The heaviest xenon isotope ^{136}Xe, is not produced in both the high and low energy spallation reactions on barium. The experimental cross-section values only are plotted in these figures. The energy region 50 MeV <E <600 MeV, where no cross-section values are available, are joined by straight lines. The following points may be inferred from these figures: (i) production cross-sections for all xenon isotopes, in general, increase with increasing proton energies, though, the increases are different for different isotopes; (ii) the variations in production cross-sections at energies higher than 600 MeV are much smaller compared to the change between 50 and 600 MeV and (iii) in the low energy region (proton energies <50 MeV) the measured excitation functions exhibit structures. The isotopes ^{129}Xe and ^{132}Xe are chosen for discussion because the production cross-sections are relatively higher for these isotopes. The cross-section for the production of these isotopes

122

Table 4.1 : Thin target cross-sections for ^{126}Xe and isotopic composition for the production of stable Xe isotope at 600 MeV, 800 MeV and 2600 MeV from Ba. The errors in the isotopic ratios are above 1-2%.

ENERGY MeV	^{126}Xe [mb]	$\frac{^{124}Xe}{^{126}Xe}$	$\frac{^{128}Xe}{^{126}Xe}$	$\frac{^{129}Xe}{^{126}Xe}$	$\frac{^{130}Xe}{^{126}Xe}$	$\frac{^{131}Xe}{^{126}Xe}$	$\frac{^{132}Xe}{^{126}Xe}$	$\frac{^{134}Xe}{^{126}Xe}$
600	54.5 ±3.83	0.725	1.131	1.131	0.681	1.229	0.530	0.038
800	85.4 ±6.1	0.719	1.125	1.125	0.728	1.276	0.595	0.047
1200	65.5 ±4.8	0.698	1.188	1.188	0.829	1.415	0.690	0.059
2600	31.2 ±2.3	0.612	1.362	1.420	1.061	1.901	0.974	0.087
600*	50.2 ±7.1	0.679	1.123	0.905	0.619	1.140	0.327	0.032
730**	43.0 ±10.0	0.721	1.139	1.121	0.721	1.309	0.549	0.049
1000***	30.0 ±	0.714	1.130	1.060	0.741	1.180	0.569	0.051

* represents cross-section values measured by Kaiser (1977).

** represents cross-section values measured by Funk et al., (1967) and

*** represents cross-section values measured by Shukolyukov et al., (1988).

123
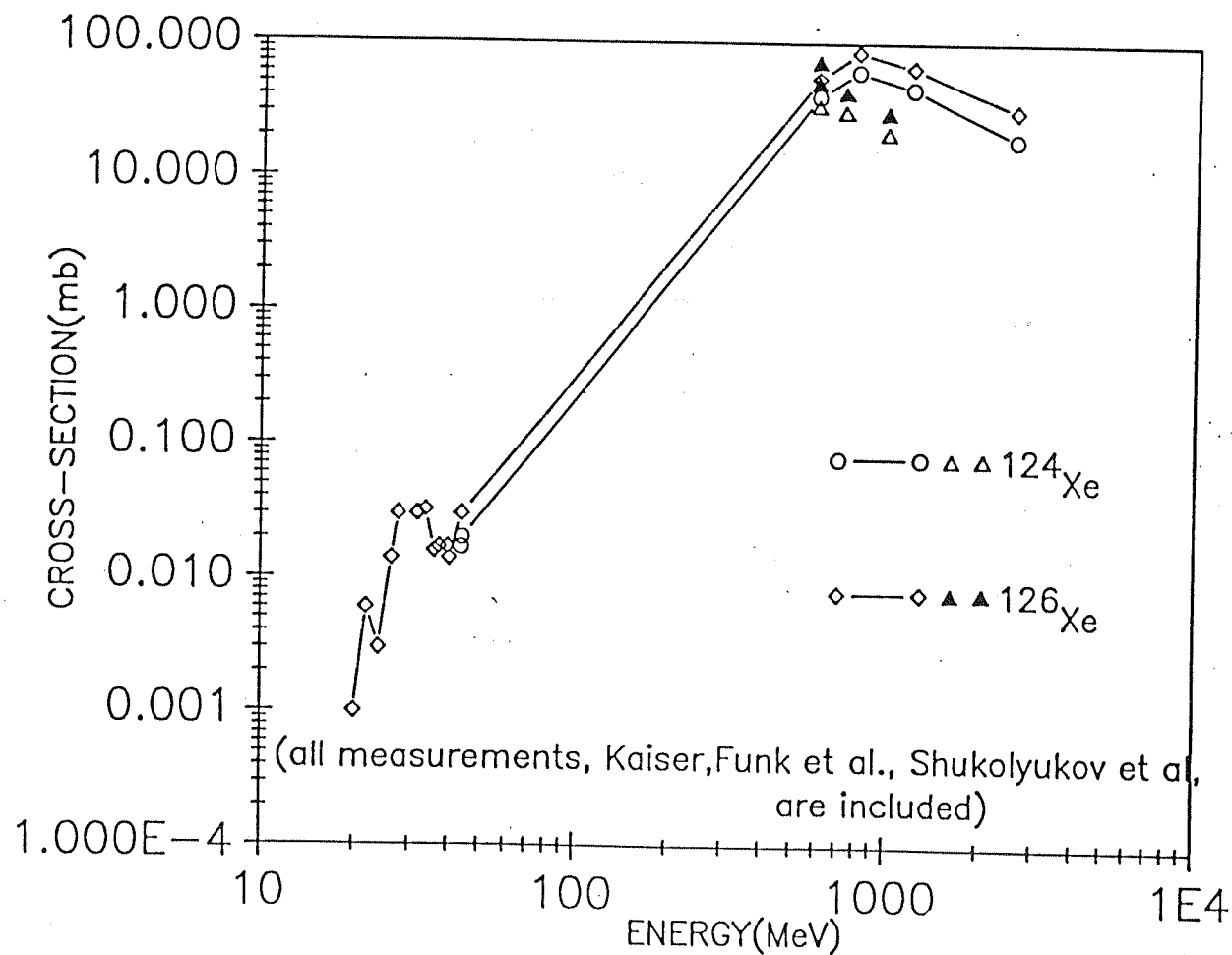
Fig 4.1   Cross-sections for the production of [124]Xe and [126]Xe on Ba
targetsin the proton energy range up to 2600 MeV.   Measurements by
Kaiser(1977), Shukolyukov et al.,(1988) and Funk et al.,(1967) are also
indicated.
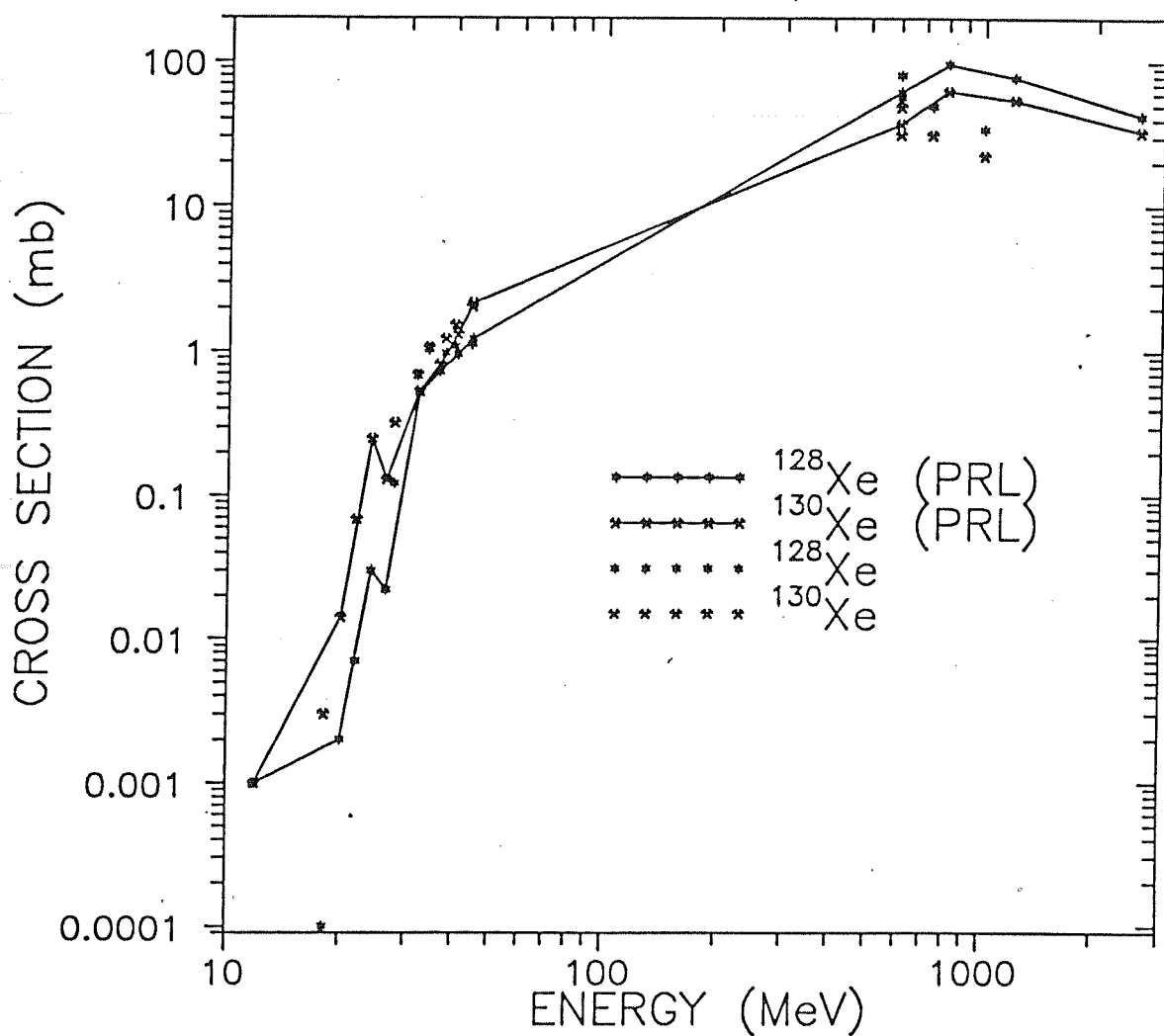
Fig 4.2   Cross-sections for the production of [128]Xe and [130]Xe on
           Ba targets in the proton energy range up to 2600 MeV.
           Measurements by Kaiser(1977), Shukolyukov et al.,(1988)
           and Funk et al.,(1967) are also indicated.

125
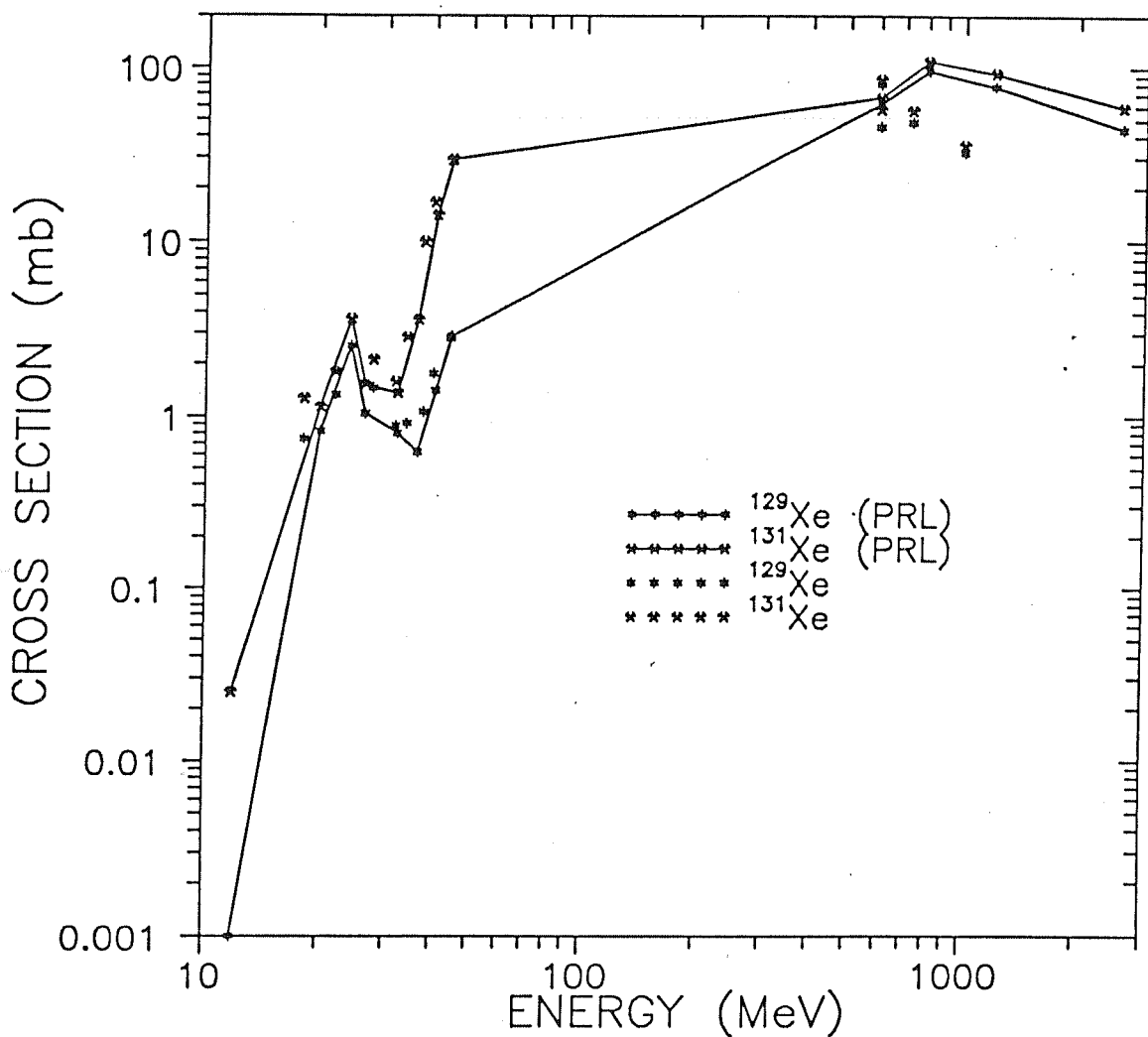
Fig 4.3   Cross-sections for the production of [129]Xe and [131]Xe on

Ba targets in the proton energy range up to 2600 MeV.

Measurements by Kaiser(1977), Shukolyukov et al.,(1988)

and Funk et al.,(1967) are also indicated.

126
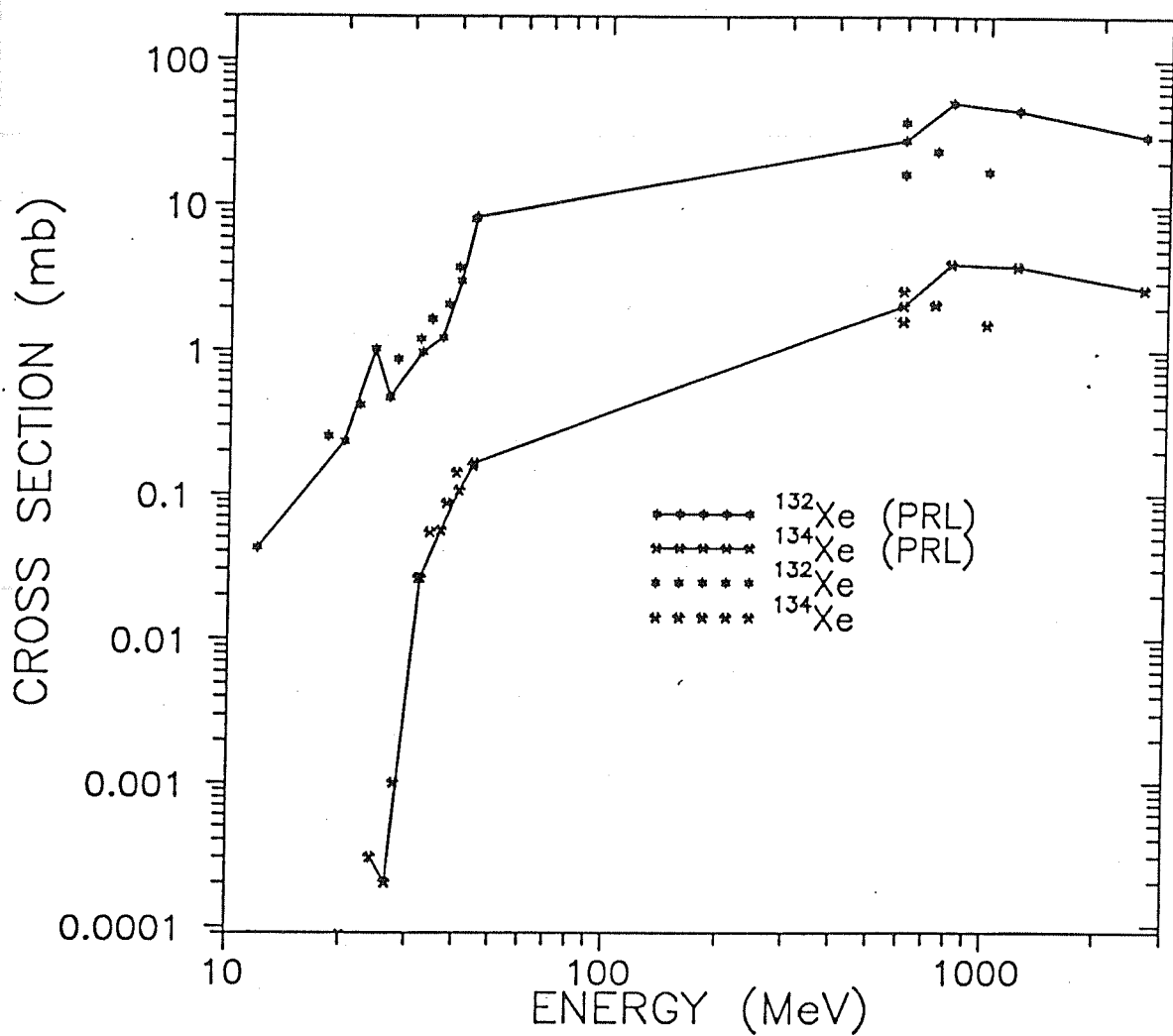
Fig 4.4   Cross-sections for the production of [132]Xe and [134]Xe on
Ba targets in the proton energy range up to 2600 MeV.
Measurements by Kaiser(1977), Shukolyukov et al.,(1988)
and Funk et al.,(1967) are also indicated.

at 45 MeV are, respectively, 2.88 ±0.43 mb and 29.3 ±4.39 mb. The corresponding values at 600 MeV are 62.7 ±4.4 mb and 69.8 ±4.9 mb. As the bombarding energy increases, the cross-section values of ^{129}Xe and ^{131}Xe at 800 and 1200 MeV are respectively 96.0 ± 6.0 mb and 78.0 ± 5.8 mb (^{129}Xe) and 109.0 ± 7.8 mb and 93.0 ± 6.8 mb (for ^{131}Xe). At 2600 MeV the production cross-sections are much lower than the above values, i.e. 59.3 ± 4.5 mb and 44.3 ± 3.4 mb. for ^{131}Xe and ^{129}Xe respectively.

The ^{126}Xe cross-sections remain almost constant at ~60. mb in the energy range of 600 MeV to 1200 MeV, but it is much lower at 2600 MeV i.e. 31.2 ± 2.3 mb.

^{126}Xe is essentially a high energy product, produced by spallation reactions on Ba targets and rare earth elements (r.e.e's) and is ideal for normalizing purposes while discussing xenon produced in high energy proton induced reactions. An added advantage is that the abundance of this isotope in trapped gases is extremely small so even a small contribution to this isotope in an extraterrestrial sample are detectable. The cross-section values obtained here are comparatively higher than the values reported earlier by Kaiser (1977), Funk and Rowe (1967) and Shukolyukov and Gorin (1988).

4.1b. Thin target spallation yields at high energies :

The Figure 4.5 shows the high energy xenon spallation spectrum measured here. The spallation spectra measured by Kaiser (1977) at 600 meV, Funk and Rowe (1967) at 730 MeV and Shukolyukov and Gorin (1988) at 1000 MeV are also plotted for purposes of comparison. In the following discussion it may be noted that the
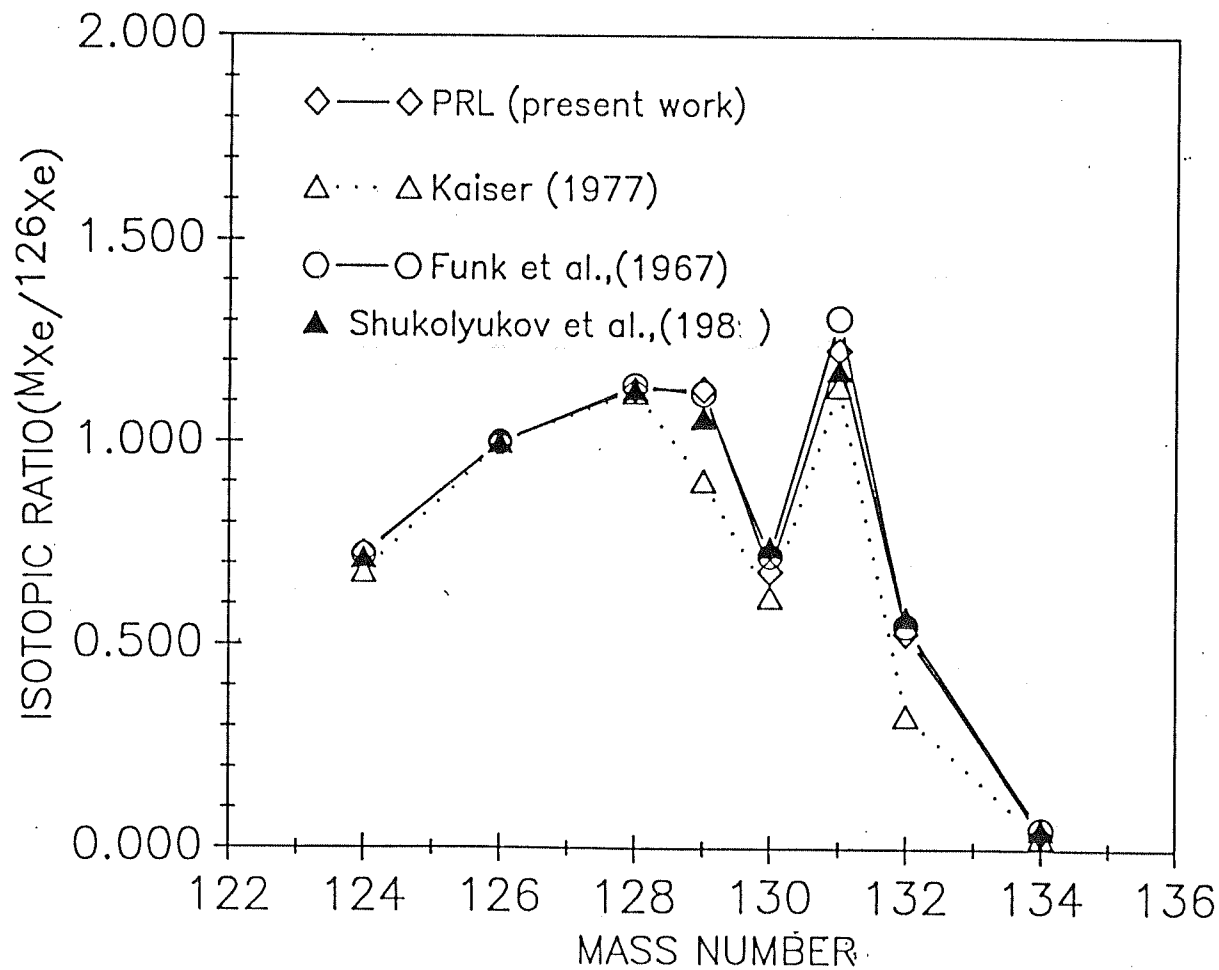
Fig 4.5   Xenon spallation spectra at high energies. The spallation spectra measured by Kaiser(1977), Funk et al.,(1967) and Shukolyukov et al.,(1988) are also shown for comparison.

errors in the isotopic ratios measured here are only 1-2%.

The minor isotope ratios $^{124}Xe/^{126}Xe$ and $^{128}Xe/^{126}Xe$ at 600, 800, 1200 and 2600 MeV are similar to each other. As an illustration, the $^{128}Xe/^{126}Xe$ values measured by us at 600 MeV is 1.131 in comparison with the value of 1.123 measured by Kaiser (1977) at 600 MeV, 1.139 measured by Funk and Rowe (1967) at 730 MeV and 1.130 measured by Shukolyukov and Gorin (1988) at 1 GeV. The $^{129}Xe/^{126}Xe$ ratio of 1.131 measured by us at 600 MeV agree reasonably well with the value of 1.121 measured by Funk and Rowe (1967) but this isotopic ratio is somewhat higher than those measured by Kaiser (1977) and Shukolyukov and Gorin (1988). The $^{129}Xe/^{126}Xe$ ratios measured by these authors are, respectively 0.905 and 1.06. In fact it is more appropriate to compare the 1 GeV measurements by Shukolyukov and Gorin (1988) with the thin target spallation spectra measured by us at 800 MeV or at 1200 MeV. The $^{129}Xe/^{126}Xe$ ratios measured by us at these energies are, respectively, 1.125 and 1.188 in comparison to the Shukolyukov measurement of 1.06 at 1000 MeV.

The $^{130}Xe/^{126}Xe$, $^{131}Xe/^{126}Xe$ and $^{132}Xe/^{126}Xe$ isotopic ratios measured by us at 600 MeV are significantly different from the isotopic ratios measured by the above authors. The $^{131}Xe/^{126}Xe$ ratio at 600 MeV for example, is 1.229 (our measurement), 1.14 [Kaiser (1977). But this ratio is found to be 1.31, by Funk and Rowe (1967) at 730 MeV and 1.18 by Shukolyukov and Gorin (1988) at 1000 MeV. It may be emphasized here that the deviations in isotopic ratios measured by us, from the earlier measurements, occur at the major isotopic ratios. The determination of these isotopic ratios, in the present

experiments, have the advantages of larger signals, negligible blank corrections and nominal m.d. corrections and we consider these measurements as superior to those by Kaiser (1977) and Shukolyukov and Gorin (1988).

The production ratios for xenon isotopes show systematic behaviour. Above 600 MeV, the $^{124}Xe/^{126}Xe$ ratio decreases with increasing energies, where as the $^{128}Xe/^{126}Xe$, $^{129}Xe/^{126}Xe$, $^{130}Xe/^{126}Xe$, $^{131}Xe/^{126}Xe$, $^{132}Xe/^{126}Xe$ and $^{134}Xe/^{126}Xe$ ratios increases. The Fig. 4.6 shows the percentage deviation of the isotopic ratios from the 600 MeV values. These deviations are defined using the following equation

$$\frac{(^iXe/^{126}Xe)_E - (^iXe/^{126}Xe)_{600MeV}}{(^iXe/^{126}Xe)_{600MeV}} \times 100 = \delta(^iXe/^{126}Xe)$$

and the results are plotted in the Fig.4.6.

From the Fig. 4.6 it becomes clear that the isotopic ratios at energies higher than 600 MeV are systematically different from those at 600 MeV. These variations in the isotopic ratios are such that the lighter isotopes, for eg. ^{124}Xe, production have less as compared to the heavier isotopes. The magnitude of deviation of the isotopic ratios from the 600 MeV value increases as the proton energies increase from 600 MeV upwards. Also, this deviation increases as the mass number of the xenon isotope increases from 124 to 132. In this connection it may be pointed out that the xenon production ratios on the lunar surface show similar variations with shielding depth [Prescher et al.,(1991)]. The spallation spectra for the production of all the stable xenon isotopes are shown in the Table 4.1. Also listed are

131
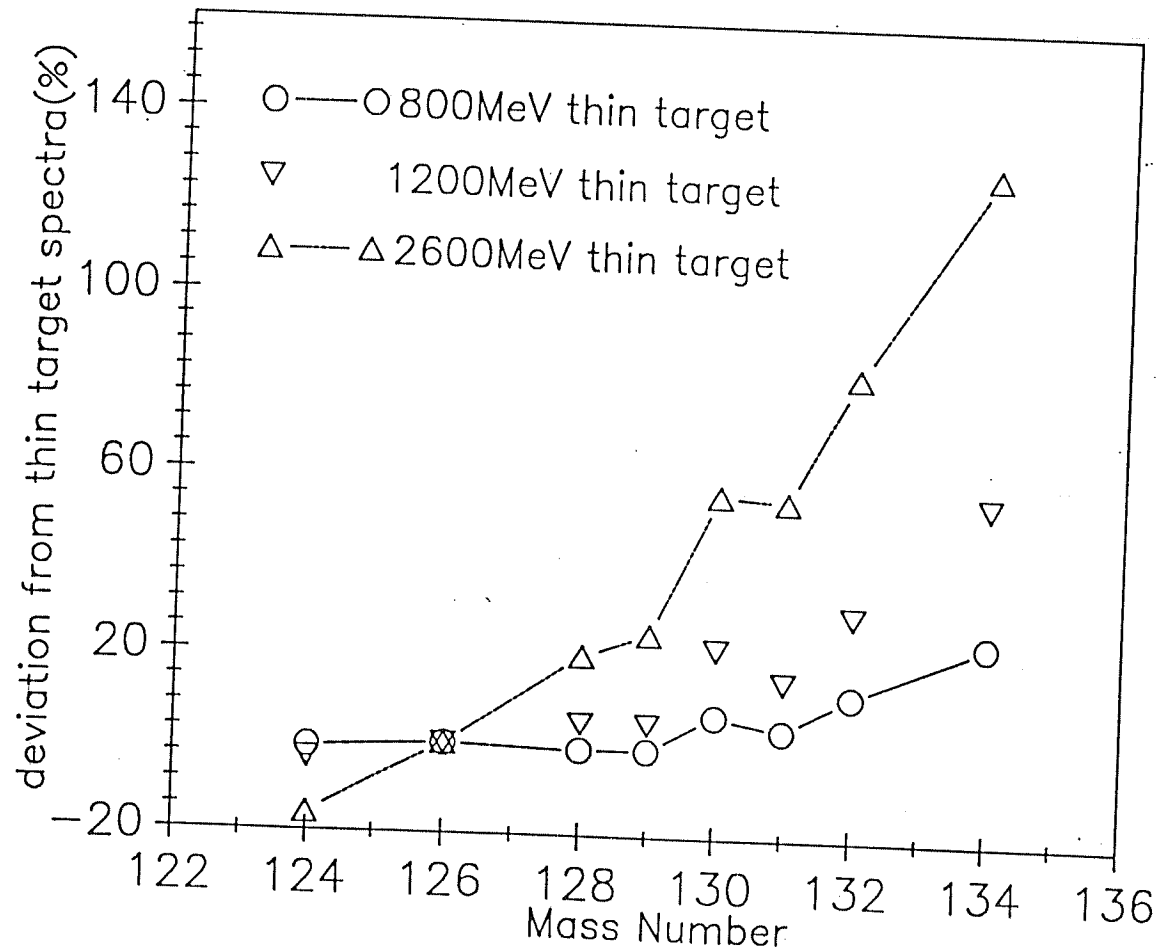
Fig 4.6   Percentage deviation of the measured spallation spectra at 800 MeV, 1200 MeV and 2600 MeV from the thin target isotopic ratios.

the ^{126}Xe production cross sections and spallation spectra measured at 600 MeV by Kaiser(1977), at 730 MeV by Funk and Rowe (1967) and at 1 GeV by Shukolyukov and Gorin (1988).

The isotopic ratios measured by Kaiser(1977), Funk and Rowe (1967) and Shukolyukov and Gorin (1988) differ marginally from the values measured by us at 600 MeV. Between the results from different irradiations experiments, some kind of variation may be expected. In case of Shukolyukov and Gorin (1988) the published data does not provide the ^{126}Xe production cross section at 730 MeV. So only the isotopic ratios at this energy can be compared with the published results of other authors. There is an agreement between the isotopic ratios measured by Shukolyukov and Gorin (1988) and those measured by Funk and Rowe (1967) at the same energy. The spallation spectra derived by both the above authors are marginally different from the spallation spectra measured by us at 600 MeV.

4.2 Production Profiles of Xe Isotopes as a function of depth in Model Meteoroids

In this section the results of the measurement of Ba glass samples from the 5 cm and 25 cm spherical meteoroid models irradiated with 600 MeV protons at the CERN accelerator are discussed. These irradiations have been carried out as a part of the experiments SC/1 and SC/2 at the CERN synchrocyclotron. As already discussed in section 2.2a of chapter II, during the course of these irradiation experiments the meteoroid mock-ups were made to translate and rotate in two perpendicular directions so that they get uniform isotropic irradiation, similar to the exposure

133

conditions of meteorites in space. Also, a defocussed beam is used which further ensures homogeneity of irradiation of the meteorite body. Much of the information relevant to the present study is presented in Chapter II and in Appendix II and III. Complete experimental details and the results of the measurements on other target foils are given elsewhere [Michel et al.,(1989 and 1986), Dragovitsch (1987) and Peiffer (1986)].

The present work includes the results from the measurement of xenon isotopes on Ba targets from the 5 cm diorite sphere and from the 25 cm grano diorite (gabbro) sphere. The Ba glass samples irradiated inside the 15 cm sphere are not dealt with here. These samples were measured at MPI, Mainz.

Both the data sets based on the results of the measurement of Ba glass targets from the irradiation of the 5 cm and 25 cm meteoroid models are discussed separately. The meteoroid models are used as a medium for simulating the secondary particle field generation inside the body of a meteoroid, irradiated in space by GCR particles. This enables us to directly compare the results obtained from these simulation experiments with the depth profiles of cosmogenic nuclides in meteorite cores. In the case of the less energetic SCR particles the secondary production is insignificant and the production depth profiles can be determined by direct energy loss calculations on the incident particles. The major difference between the above mentioned laboratory simulation experiments and the space irradiation of meteorites by GCR particles is that the meteorites receive particles with an energy spectrum (which itself is a function of space and time), where as in the laboratory simulation experiments

the thick targets receive mono energetic protons from an accelerator. The GCR particles consist of 10% α particles also. These particles also "deposit" energy in the irradiated meteorite resulting in the production of cosmogenic nuclides. This effect has not been taken into consideration in the calculations presented here (the effect of the α-particles can be accounted later by the consideration that nuclear reactions induced by charged particles are of the same nature as p-induced reactions at the same energy/nucleon values). Another aspect which differentiates the laboratory irradiations from that of the meteoroids is the fact that meteoroids have irregular shapes and the thick targets used in laboratory experiments are regular shaped bodies. To convert the results obtained from the laboratory simulation experiments into the space irradiation conditions of meteorites the above factors should be considered.

The production depth profile of a cosmogenic isotope is determined by the shape of the underlying excitation function and the depth, size and energy dependence of the primary and secondary nucleon fields within the thick target body. The availability of a broad range of neutron and proton energies in the thick target bodies makes it possible for a wide range of nuclear reactions, such as compound nuclear reactions in statistical equilibrium, pre-equilibrium reactions, spallation and fragmentation reactions to take place in these bodies. The measured concentrations of a cosmogenic nuclide is a superposition of all these different reaction channels. Hence a simplistic way of looking at the various product nuclides as "low energy" or "high energy" product is not very meaningful.

4.2a Xenon Production Profiles (experimentally measured) in the 5 cm Diorite Sphere

Five Ba glass samples, Ba 0111, Ba 0211, Ba 0311, Ba 0411 and Ba 0511 from known depth positions (depths are measured from the centre of the sphere on either side) of -3.9 cm, -1.9 cm, +0.1 cm, +2.1 cm and +4.1 cm, irradiated inside diorite sphere of radius R =5 cm, have been analysed in this study. The results of these measurements are given in Table 4.2. The ^{126}Xe gas amounts are expressed in units [x10^{-10}ccSTP.g^{-1}] and the isotopic ratios w.r.t ^{126}Xe are also listed. The blank corrections are lesser than 1% of the gas amounts measured in the irradiated samples and they could be neglected as they do not have any significant effect on the data. The 1600^OC re-extraction of gases from the Ba glass samples are equal to the system blank levels showing that the xenon extraction from the sample is complete in the first heating step itself. These re-runs are done immediately after the analysis of the Ba glass targets.

The ^{136}Xe concentrations measured in all irradiated samples are extremely small. The measured amounts of this isotope in the irradiated Ba glass sample is found to be equal to the ^{136}Xe concentrations measured in a similar amount of unirradiated blank Ba glass. Hence, the ^{136}Xe measured in the irradiated Ba glass samples is treated as trapped from the atmosphere. Based on these ^{136}Xe amounts corrections are made at all the other isotopes for the atmospheric trapped xenon contribution using standard air composition. The corrections at all stable xenon isotopes are found to be lesser than 1% of the measured concentrations of these isotopes.

136

Table 4.2 : Measured ^{126}Xe amounts and Isotopic composition of Xe from Ba targets at different depths from the granodiorite sphere irradiated with 600 MeV protons. The distances of the targets are measured from the centre. The isotopic composition of Xe produced from 600 MeV thin target Ba glass are included for comparison.

SAMPLE MeV	Depth position (cm)	^{126}Xe [x10^{-8}cc STP/g]	$\dfrac{^{124}Xe}{^{126}Xe}$	$\dfrac{^{128}Xe}{^{126}Xe}$	$\dfrac{^{129}Xe}{^{126}Xe}$	$\dfrac{^{130}Xe}{^{126}Xe}$	$\dfrac{^{131}Xe}{^{126}Xe}$	$\dfrac{^{132}Xe}{^{126}Xe}$	$\dfrac{^{134}Xe}{^{126}Xe}$
Ba0111	-3.9	2.307 ±0.346	68.51 0.69	116.25 1.16	118.65 1.19	70.65 0.71	135.39 1.35	56.75 .0.57	3.89 0.04
Ba0211	-1.9	2.252 ±0.338	70.06 1.05	115.10 1.73	118.37 1.78	70.95 1.06	136.32 2.04	55.99 0.84	3.70 0.06
Ba0311	+0.1	2.086 ±0.313	67.94 0.68	116.39 1.16	120.62 1.21	71.43 0.71	139.19 1.39	57.54 0.58	3.89 0.04
Ba0411	+2.1	2.018 ±0.303	70.41 1.06	118.02 1.77	120.52 1.81	71.57 1.07	137.93 2.07	57.74 0.87	3.83 0.06
Ba0511	+4.1	2.217 ±0.333	70.25 0.70	114.44 1.14	117.33 1.17	70.44 0.70	130.92 1.31	55.89 0.56	3.88 0.04
Ba11	600 MeV thin target	–	71.30 ±0.70	114.40 1.10	114.70 1.10	68.80 0.70	128.20 1.30	54.30 0.60	3.90 0.02

The ^{126}Xe amounts decrease from surface to centre by about 6% in the case of the 5 cm diorite sphere. In case of isotope ^{131}Xe also, though it has a comparatively high production cross-section at all energies (both low and high) there is a decrease in the centre production rate compared to the surface samples and this decrease is by ~6% in the absolute values. However, if one considers errors it is only marginal. The surface and centre production rates of this isotope are, respectively, 5.09 ±0.76 (at a shielding depth of 1.1 cm inside the diorite sphere, R =5 cm) and 4.74 ±0.72 x10^{-10}ccSTP.gBa^{-1}.Ma^{-1} (at a distance of 0.1 cm from the centre of the diorite sphere).

Fig.4.7 and 4.8 show the variation of the xenon isotopic ratios as a function of depth in the diorite sphere. Though the ^{M}Xe/^{126}Xe (M = 124 to 134) isotopic ratios in the diorite remain the same at all depths of the diorite sphere (taking the errors into consideration) these isotopic ratios are different from the 600 MeV thin target ratios. For example, the ^{129}Xe/^{126}Xe and ^{131}Xe/^{126}Xe ratio measured in Ba glass samples kept near the surface and near the centre of the diorite sphere are, respectively, 1.17 ± 0.01 and 1.21 ± 0.01 (for ^{129}Xe/^{126}Xe) and 1.30 ± 0.01 and 1.39 ± 0.01 for (^{131}Xe/^{126}Xe) as compared to the 600 MeV thin target production rate ratio of 1.14 ± 0.01 and 1.28 ± 0.01. In Table 4.2 the isotopic ratios measured at 600 MeV are also given. Compared to the thin target isotopic ratios the ^{124}Xe/^{126}Xe ratio decreases with increasing shielding depth inside the diorite (R =5 cm) sphere. This isotopic ratio is the highest at the surface of the spherical body of radius 5 cm. The ^{134}Xe/^{126}Xe ratios remain the same in the thin and thick target

138
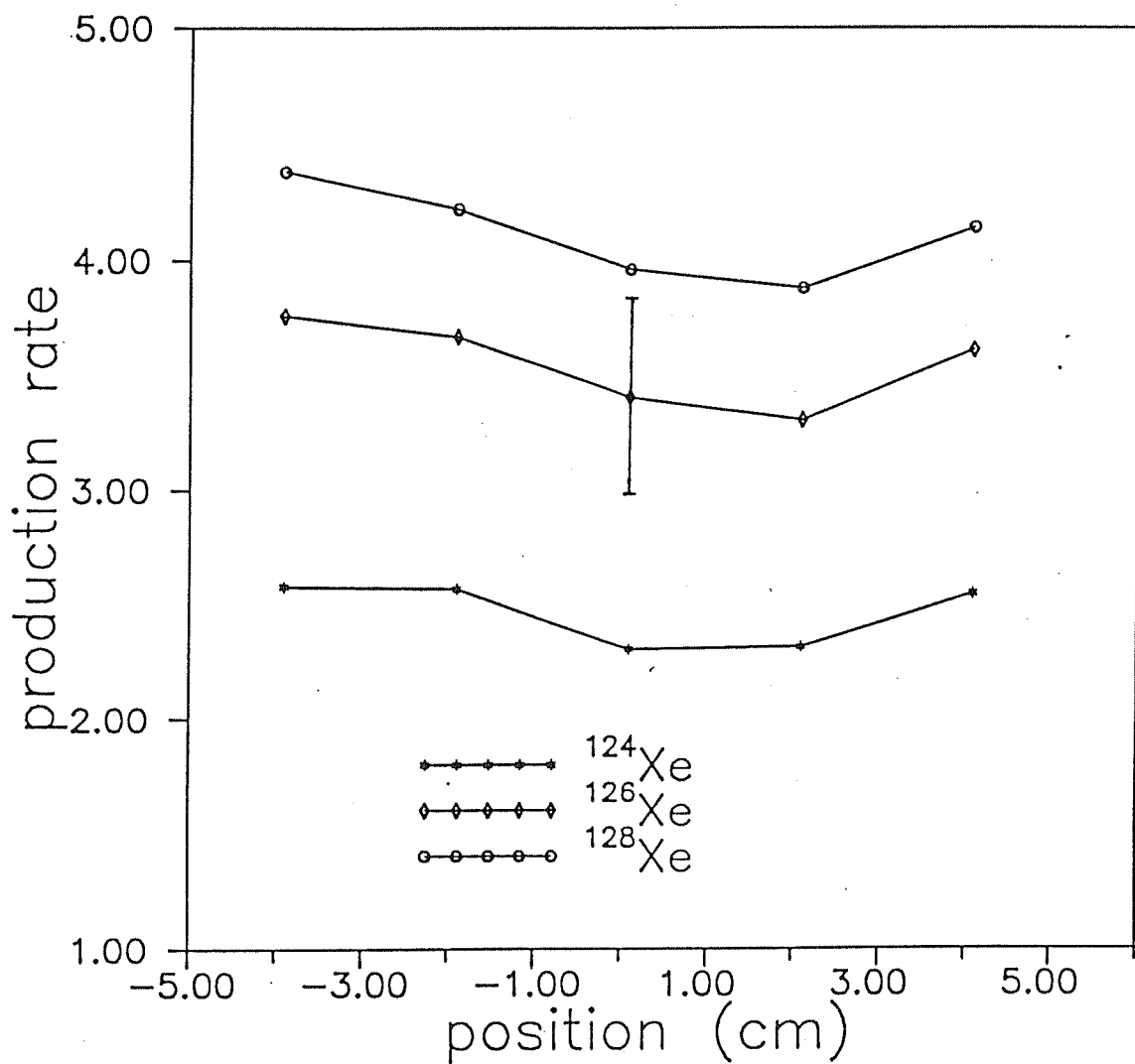
Fig 4.7a ^{124}Xe, ^{126}Xe, and ^{128}Xe production rates as a function of depth in the diorite sphere (R =5 cm), isotropically irradiated with 600 MeV protons at the CERN synchrocyclotron. The lines joining data points are only eye guides. Typical errors are indicated on one of the data points.
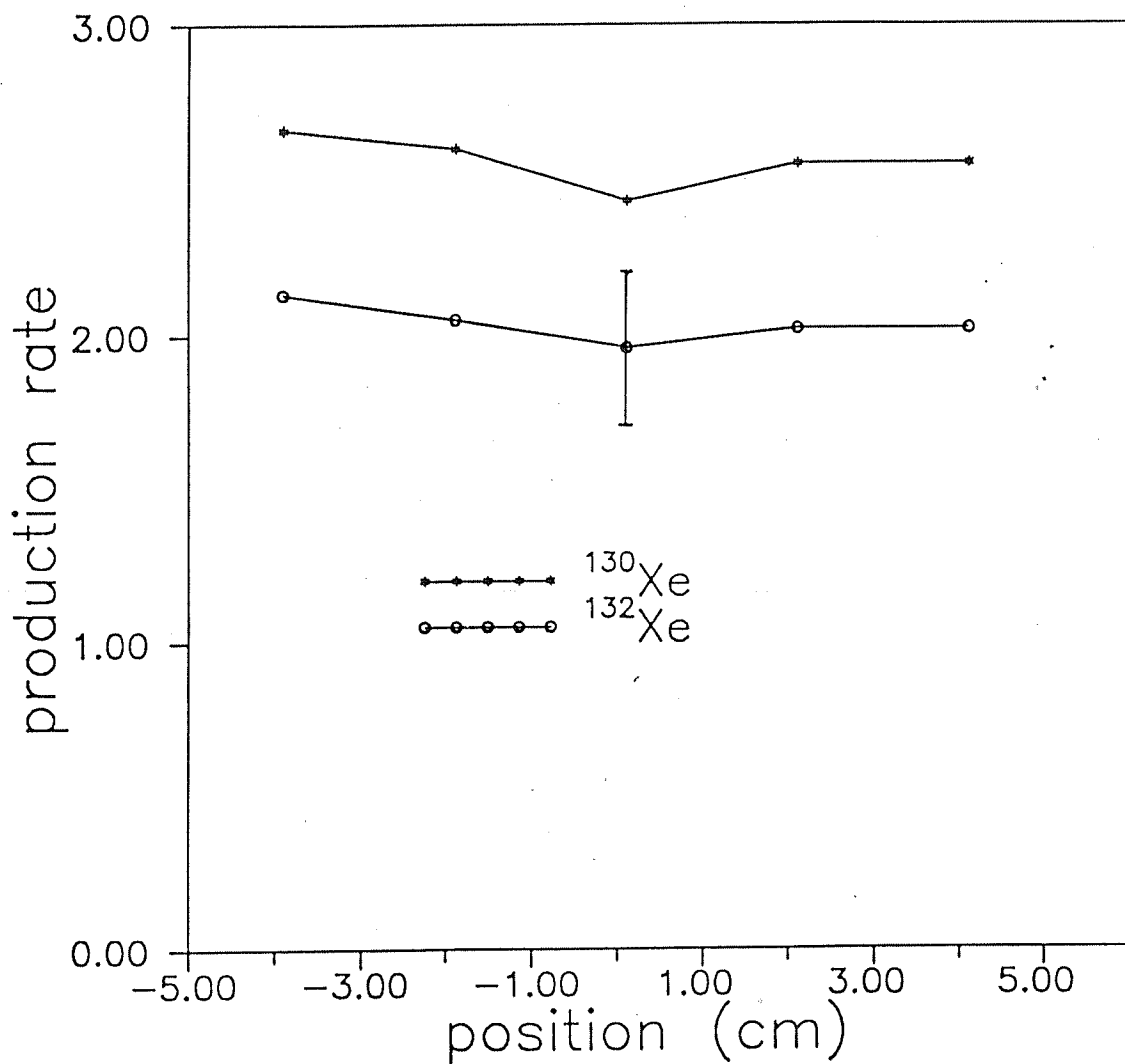
Fig 4.7b ^{130}Xe and ^{132}Xe production rates as a function of depth in the diorite sphere (R =5 cm) isotropically irradiated with 600 MeV protons at the CERN synchrocy£otron. The lines joining data points are only eye guides. Typical errors are indicated on one of the data points.
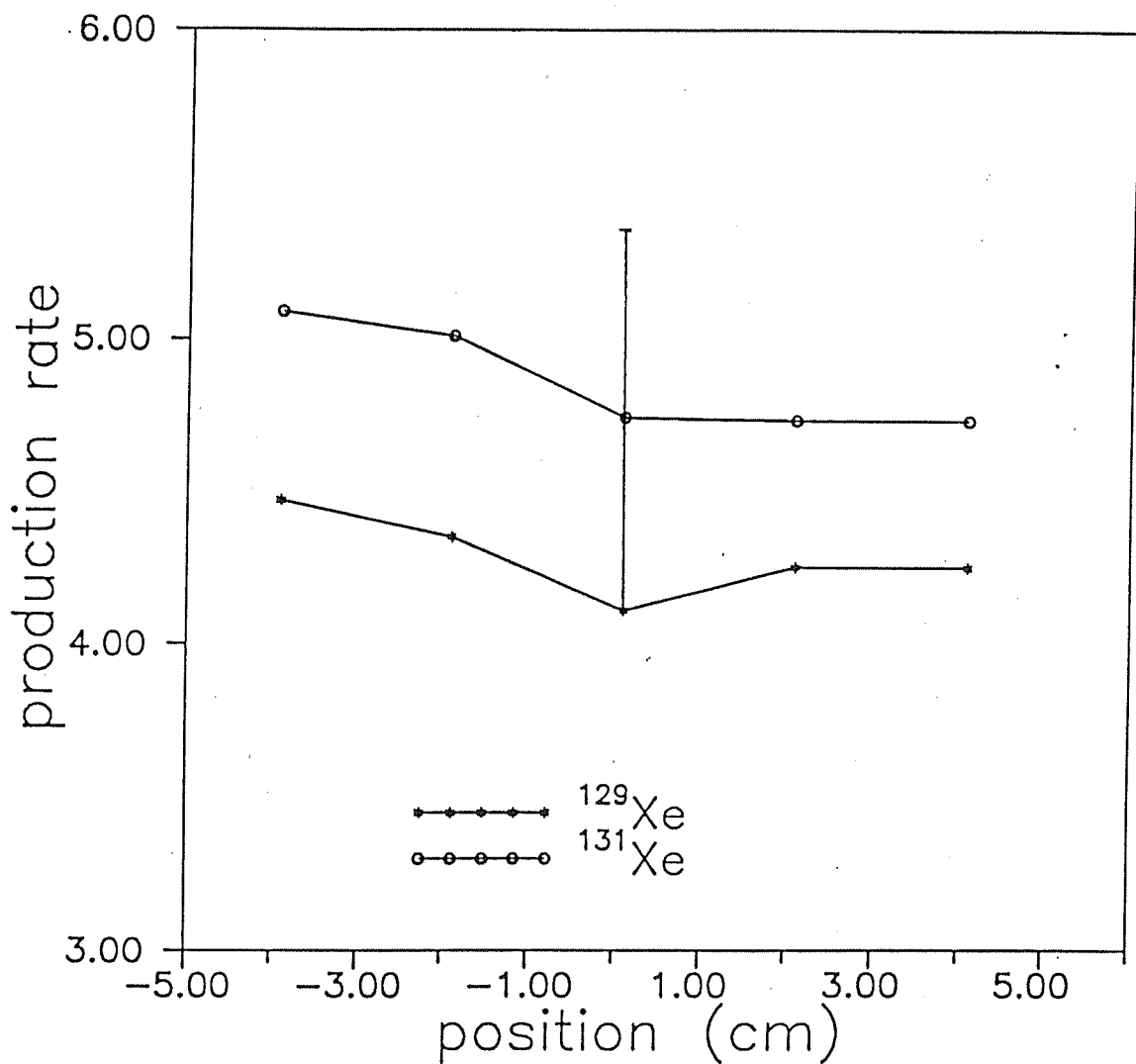
Fig 4.8 ^{129}Xe and ^{131}Xe production rates as a function of depth in the diorite sphere (R =5 cm) isotropically irradiated with 600 MeV protons at the CERN synchrocyclotron. The lines joining data points are only eye guides. Typical errors are indicated on one of the data points.

irradiations. The $^{132}Xe/^{126}Xe$ ratio also does not show significant variations but it is consistently higher than the 600 MeV thin target production ratio. All the other isotopic ratios, viz. $^{128}Xe/^{126}Xe$, $^{129}Xe/^{126}Xe$, $^{130}Xe/^{126}Xe$ and $^{131}Xe/^{126}Xe$ show somewhat higher values than the thin target production ratios at all shielding depths. In general, all the isotopic ratios increase with increasing shielding depth in the diorite sphere. The changes in isotopic ratios are significant since the isotopic ratios can be measured more accurately than the absolute concentrations. The change in xenon isotopic ratios with shielding depth has been successfully used in determining the burial depth of lunar samples [Kaiser (1977)]. A similar approach can be carried out in the meteoric case also. More discussion on this topic will be taken up while discussing the measured xenon depth production profiles in the 25 cm sphere.

Table 4.3 gives the production rates of the various stable xenon isotopes measured at various depths inside the diorite sphere. These production rates are expressed in units $[x10^{-10}ccSTP.gBa^{-1}.Ma^{-1}]$. The values obtained for the 600 MeV thin target are also shown in the same units, to facilitate an easier comparison. Such a comparison can also show how much is the total contribution from the secondary particles at each shielding depth.

All xenon isotopes, ^{124}Xe to ^{134}Xe, have a higher production rate than the thin target production at all depths, including zero depth i.e. the surface of the model meteoroid. [The Ba glass samples at distances of -3.9 cm and 4.1 cm from the centre of the 5 cm diorite sphere, or in other words at depths of

Table 4.3 : The Xe isotope production rates in $[\times 10^{-10} ccSTP.g^{-1}.Ma^{-1}]$ measured as a function of depth, based on the results of the measurement of Ba glass samples from the isotropically irradiated R=5cm diorite sphere.

SAMPLE	Depth position (cm)	^{124}Xe	^{126}Xe	^{128}Xe	^{129}Xe	^{130}Xe	^{131}Xe	^{132}Xe	^{134}Xe
Ba0111	-3.9	2.58 ±0.39	3.76 0.56	4.38 0.66	4.47 0.67	2.66 0.40	5.09 0.76	2.13 0.32	0.15 0.02
Ba0211	-1.9	2.57 ±0.39	3.67 0.55	4.22 0.63	4.35 0.66	2.60 0.40	5.01 0.75	2.05 0.30	0.14 0.02
Ba0311	+0.1	2.31 ±0.35	3.40 0.52	3.96 0.60	4.11 0.62	2.43 0.36	4.74 0.72	1.96 0.29	0.13 0.02
Ba0411	+2.1	2.32 ±0.35	3.30 0.49	3.88 0.62	4.25 0.60	2.55 0.39	4.73 0.72	2.02 0.31	0.14 0.02
Ba0511	+4.1	2.55 ±0.39	3.61 0.54	4.14 0.62	4.25 0.63	2.55 0.39	4.73 0.72	2.02 0.31	0.14 0.02
Ba11	600 MeV thin target	1.91 ±0.29	2.70 0.41	3.12 0.47	3.14 0.47	1.90 0.28	3.52 0.53	1.51 0.22	0.11 0.02

1.1 cm and 0.9 cm from the surface of the diorite sphere, are considered as the surface samples in the following analysis]. The production rates at the surface samples are consistently higher by about 35% for all xenon isotopes. At the centre they are consistently higher by about 25 to 30%. For all xenon isotopes ([124]Xe to [132]Xe), the production rates measured in Ba glasses kept at the centre are slightly lower than the production rates measured in Ba glass sample kept near the surface, though the changes are only marginal. It may be noted here that these decreases and increases in production rates of the isotopes [124]Xe to [132]Xe are small and much emphasis cannot be given to these changes in productions rates. However, some trends about the depth dependence of the xenon production in bodies of smaller size can be obtained. These results suggest that in bodies of small size (R ~5 cm) there is relatively small contribution by secondary particles to xenon isotope production. As a best approximation it can be stated that the production rates of all xenon isotopes at all shielding depths in a very small body (R ~5 cm) are higher than the thin target production rates but there is no significant change in the xenon production rate with shielding depth in similar sized bodies (R ~5 cm). The observed increase in production rates are by about 30%.

The thick target production rates as deduced here for the xenon isotopes in units of [$\times 10^{-10}$ccSTP.gBa^{-1}.Ma^{-1}] are given in the Table 4.3. The thin target production rates are also included for purposes of comparison. It has to be mentioned here that the xenon isotopes are produced from different Ba isotopes by losing a minimum of 3 to 7 nucleons and a maximum of 5 to 15

nucleons from the compound nucleus formed by the absorption of the incoming proton and the target nuclide. Below, the depth profiles obtained for xenon in the study are compared with those obtained for other cosmogenic nuclides. A more detailed description of the depth profiles of radio nuclides and of rare gas He and Ne isotopes deduced from the same irradiation experiments can be obtained from Michel et al.,(1989 and 1986). From the dependence of the production of a cosmogenic nuclide on shielding depth, few generalizations about the nature of the underlying reactions can be made. For the products with masses close to that of the target the depth profiles have a maximum near the centre. This seem to be true for ΔA values of ~8-10. In case of cosmogenic nuclides belonging to this category, which have ΔA ~8-10, as the radius of the irradiated object is increased, from 5 cm to 25 cm the production rates at the centre increases by ~3.5 times in the case of ^{60}Co (from Co) [Michel et al., (1989)]. On the other hand, products farther away from the target nuclide mass, which are produced mostly by high energy particles, are minimum at the centre of the model meteoroid. These products have ΔA values of ~20 to 30. The production rates further decrease as the size of the irradiated body increases. For example the depth profile for the production of ^{196}Au from Au and for the production of ^{54}Mn from Co have their maximum at the centre of the model meteoroid. The production depth profiles for ^{169}Yb from Au and ^{75}Se from Rh, in contrast, have their minimum at the centre of the meteoroid mockup. The production profiles of ^{7}Be from Al, Mg, Si and Fe are all constant within the limits of statistical errors [Michel et al., (1989 and 1986)].

To understand the secondary particle contribution to the production of a cosmogenic nuclide at a particular depth we have calculated, for each xenon isotope $(^M Xe_{thick} - {}^M Xe_{thin})/^M Xe_{thin}$. The numerator in the above . expression represent the total secondary production and the denominator here represents the production by primaries alone. The Table 4.4 gives the values calculated in this fashion for each isotope at five different depths inside the 5 cm diorite sphere. Fig. 4.9 shows percentage deviations of the spallation spectrum measured in Ba glass samples near the surface and near the centre of' the diorite sphere. It can be seen that at the centre of the 5 cm body the production of all isotopes are higher by about 20 to 30% than the thin target production. The Fig. 4.10 and 4.11 show the isotopic ratios $^M Xe/^{126} Xe$ (M =124 to 132) for the production of Xe as a function of shielding depth in the diorite .sphere. From fig the 4.10 and 4.11 it becomes clear that the isotopic ratios show maximum variation in case of the $^{131} Xe/^{126} Xe$, $^{129} Xe/^{126} Xe$ and $^{132} Xe/^{126} Xe$, in the order in which these ratios are affected.

4.2b Xenon Production Profiles (experimentally measured) in the 25 cm Gabbro Sphere

Seven of the nine Ba glass samples, Ba 0122, Ba 0312, Ba 0412, Ba 0522, Ba 0612, Ba 0712 and Ba 0922 from depth positions of -25.4 cm, -13.3 cm, -7.3 cm, -1.4 cm, 4.8 cm, 10.8 cm and 22.6 cm irradiated inside the gabbro sphere of radius R=25 cm are measured in this study. The results from these measurements are given in the Table 4.5. The $^{126} Xe$ concentrations are expressed in units [x10^{-8} ccSTP.gBa^{-1}] and the isotopic ratios w.r.t $^{126} Xe$ are

146

Table 4.4 : Measured $[(^M Xe_{thick} - {}^M Xe_{thin})/{}^{Xe}Xe_{thin}]$ at different depth positions inside a diorite sphere of radius R=5 cm. The numerator here is an indication as to how much the secondary neutrons and protons together contribute to the production at each shielding depths.

SAMPLE	Depth position (cm)	^{124}Xe	^{126}Xe	^{128}Xe	^{129}Xe	^{130}Xe	^{131}Xe	^{132}Xe	^{134}Xe
Ba011	-3.9	0.35	0.40	0.40	0.42	0.40	0.45	0.41	0.39
Ba0211	-1.9	0.34	0.36	0.35	0.38	0.37	0.42	0.36	0.29
Ba0311	+0.1	0.21	0.26	0.27	0.31	0.28	0.35	0.29	0.25
Ba0411	+2.1	0.21	0.22	0.24	0.26	0.24	0.29	0.26	0.19
Ba0511	+4.1	0.33	0.34	0.33	0.35	0.34	0.34	0.33	0.33
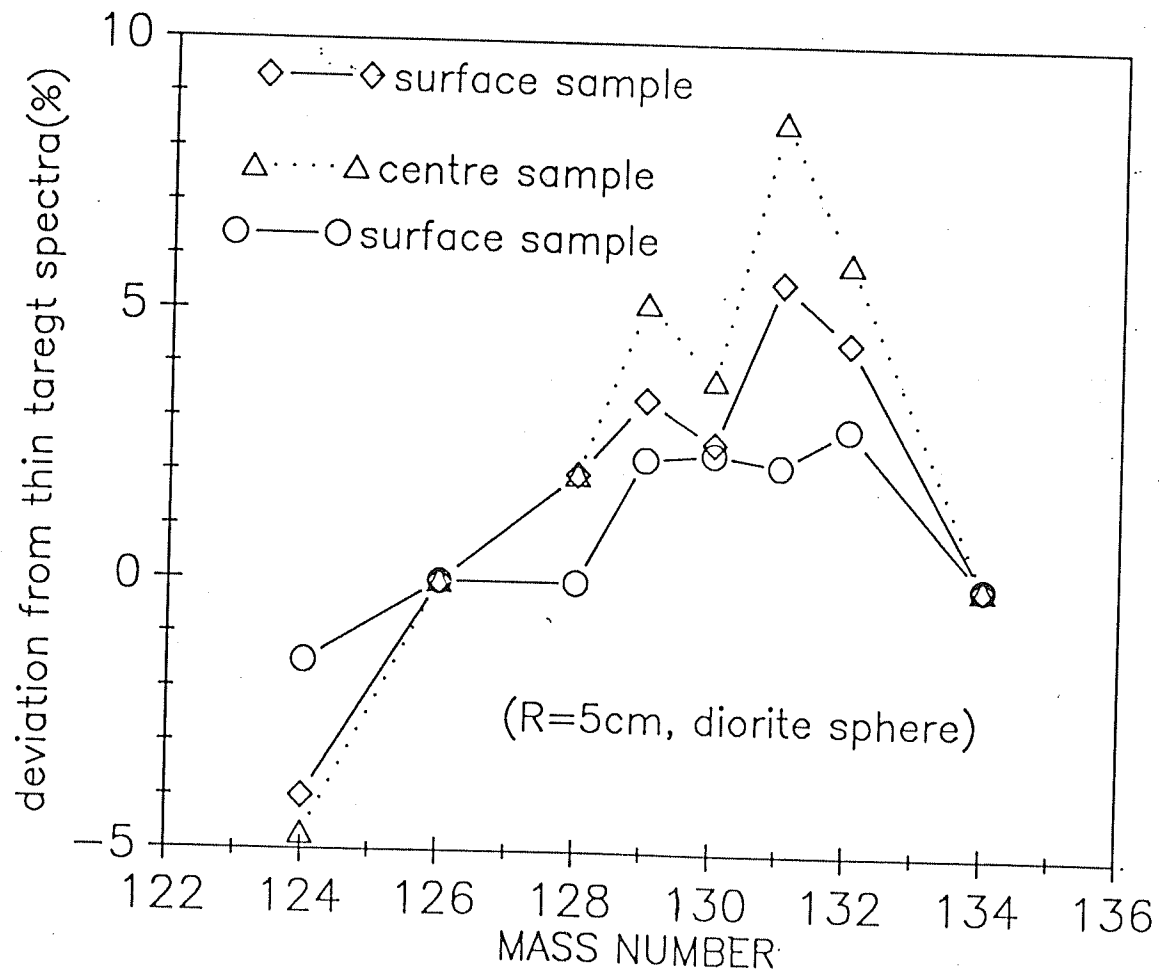
Fig 4.9   Percentage deviation of the spallation spectra measured in Ba glasses from diorite sphere (R =5 cm), irradiated with 600 MeV protons, from the thin target spallation spectra at 600 MeV.
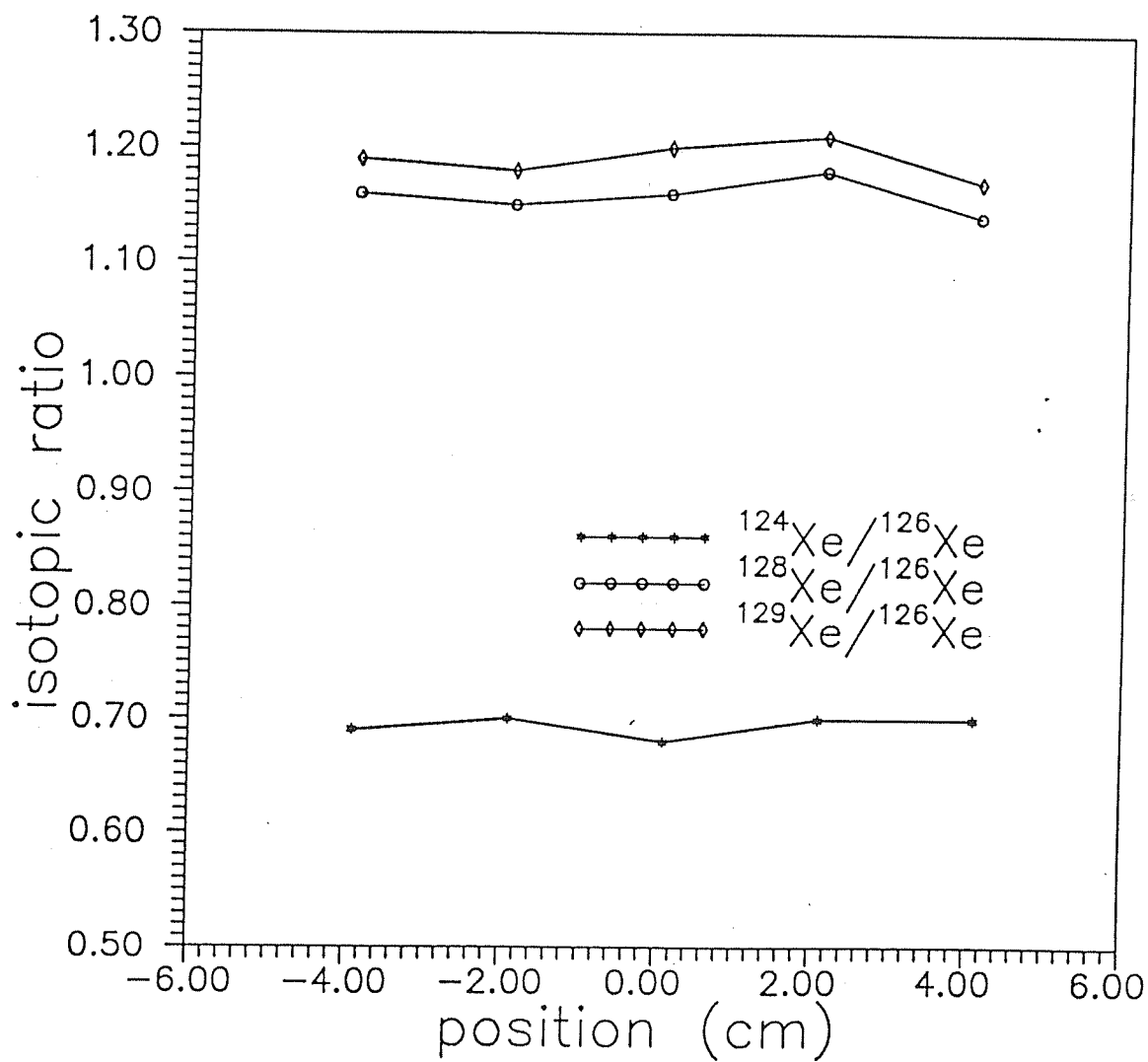
Fig 4.10 ^{124}Xe/^{126}Xe, ^{128}Xe/^{126}Xe and ^{129}Xe/^{126}Xe ratios as a function of depth in the diorite sphere (R =5 cm) irradiated isotropically with 600 MeV protons at the CERN synchrocyclotron.
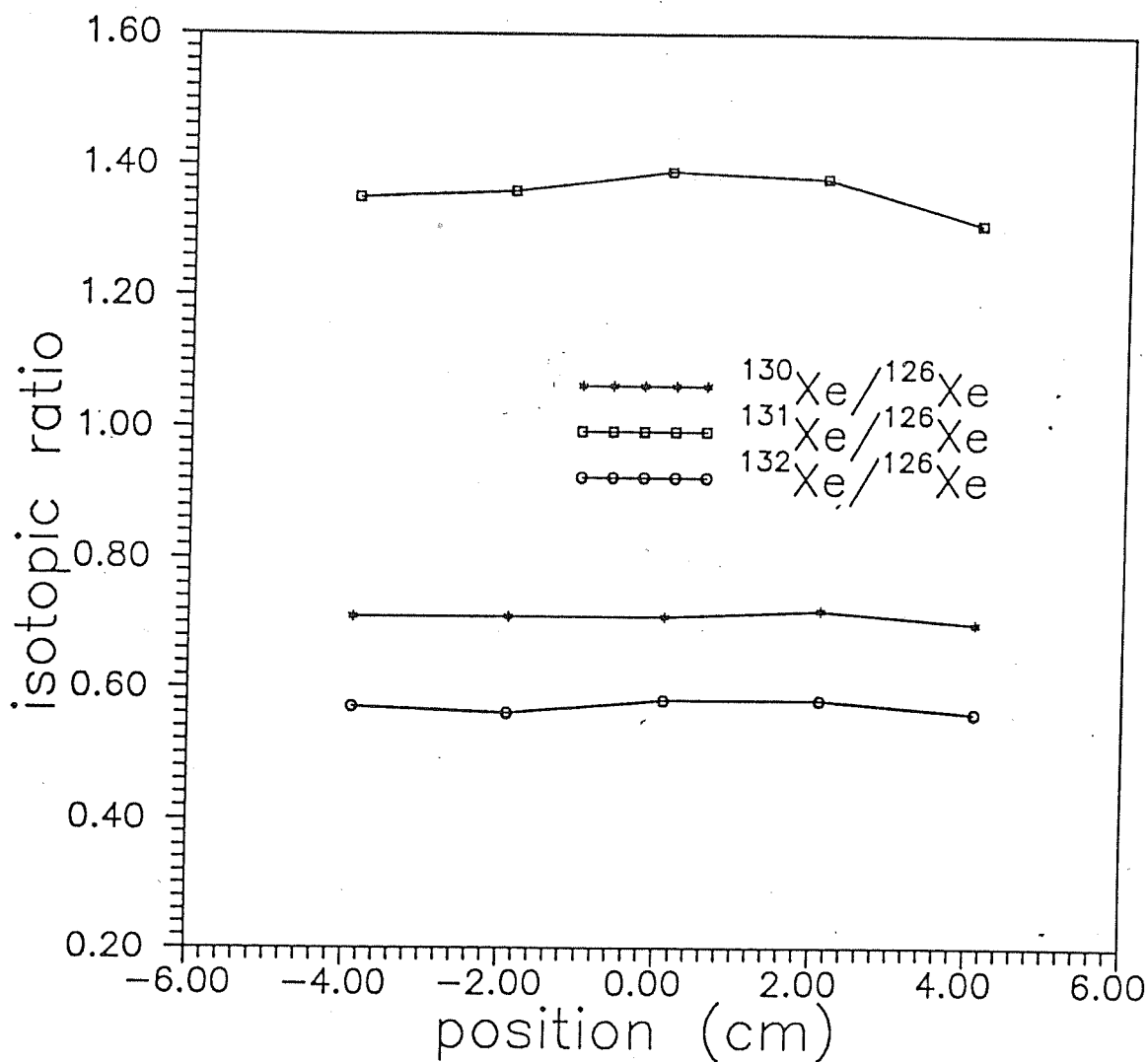
Fig 4.11 ^{130}Xe/^{126}Xe, ^{131}Xe/^{126}Xe and ^{132}Xe/^{126}Xe ratios as a function of depth in the diorite sphere (R =5 cm) irradiated isotropically with 600 MeV protons at the CERN synchrocyclotron.

Table 4.5 : Measured ^{126}Xe amounts and Isotopic composition of Xe from Ba targets at different depths from the gabbro sphere irradiated with 600 MeV protons. The distances of the targets are measured from the centre of the sphere.

SAMPLE MeV	Depth position (cm)	^{126}Xe [x10^{-8}cc STP/g]	$\frac{^{124}Xe}{^{126}Xe}$	$\frac{^{128}Xe}{^{126}Xe}$	$\frac{^{129}Xe}{^{126}Xe}$	$\frac{^{130}Xe}{^{126}Xe}$	$\frac{^{131}Xe}{^{126}Xe}$	$\frac{^{132}Xe}{^{126}Xe}$	$\frac{^{134}Xe}{^{126}Xe}$
Ba0122	-25.4	7.91 ±1.18	64.47 0.64	127.82 1.28	142.15 1.42	78.89 0.79	180.71 1.81	68.41 0.68	4.90 0.05
Ba0312	-13.3	10.27 ±0.72	64.80 0.70	132.40 1.30	148.30 1.50	82.30 0.80	189.60 2.00	71.9 0.70	4.80 0.20
Ba0412	-7.3	12.91 ±0.90	62.50 0.60	135.5 1.40	150.00 1.50	85.80 0.90	204.80 2.10	75.50 0.80	4.90 0.2
Ba0522	-1.4	11.41 ±1.71	62.06 0.62	133.35 1.33	148.99 1.49	85.21 0.85	203.55 2.03	74.51 0.75	4.78 0.05
Ba0612	+4.8	12.70 ±0.88	62.40 0.60	133.90 1.40	149.90 1.50	84.90 0.90	201.00 2.00	74.90 0.80	4.70 0.20
Ba0712	+10.8	10.45 ±0.73	64.30 0.60	131.40 1.30	145.90 1.50	82.10 0.80	184.40 1.90	71.10 0.70	4.90 0.20
Ba0922	+22.6	6.86 ±1.02	64.82 0.65	127.98 1.28	135.88 1.36	77.81 0.78	173.11 1.73	64.85 0.65	4.09 0.04
Ba11	600 MeV thin target	–	71.30 ±0.70	114.40 1.10	114.70 1.10	68.80 0.70	128.20 1.30	54.30 0.60	3.90 0.02

also listed in Table 4.5. The blank corrections on these measurements are much less than 1% of the measured signals. The $1600^{O}C$ re-extractions of the Ba glass samples yielded signals equivalent to the system blanks showing that the xenon extraction from the samples are total. The $\cdot^{136}Xe$ amounts measured in these samples are extremely small as discussed in the previous case and this is of atmospheric origin. As in the former case the ^{136}Xe concentrations are used for correcting the atmospheric trapped xenon in the barium glass samples. These corrections are, however,found to be much less than 1% of the measured xenon concentrations.

The Table 4.5 gives the absolute concentrations and isotopic composition of the xenon measured from the Ba glasses irradiated inside the gabbro (R =26 cm) sphere. The isotopic ratios for the production of xenon measured using the thin target Ba glass are also indicated for comparison. The production of all isotopes increase from surface to centré significantly and the amounts by which the production increases vary from isotope to isotope. This variation is found to be maximum for isotope ^{131}Xe and the isotopes adjoining ^{131}Xe follow next. There is a systematic increase as the masses are increased from ^{124}Xe to ^{131}Xe and for isotopes heavier than ^{131}Xe (^{132}Xe for eg.) the production at the centre is not as pronounced as in the case of ^{131}Xe. The Table 4.6 shows the variation in production rate at different depths. The samples Ba 0122 and Ba 0922 at distances of -25.4 cm and 22.6 cm from the centre of the gabbro sphere (R= 26 cm) are treated as surface samples (similar to the case of the diorite sphere). The increase in production at depths

Table 4.6 : The Xe isotope production rates in $[\times 10^{-10} \mathrm{ccSTP.g^{-1}.Ma^{-1}}]$ measured as a function of depth, based on the results of the measurement of Ba glass samples from the isotropically irradiated R=25cm gabbro sphere.

SAMPLE	Depth position (cm)	$^{124}\mathrm{Xe}$	$^{126}\mathrm{Xe}$	$^{128}\mathrm{Xe}$	$^{129}\mathrm{Xe}$	$^{130}\mathrm{Xe}$	$^{131}\mathrm{Xe}$	$^{132}\mathrm{Xe}$	$^{134}\mathrm{Xe}$
Ba0122	-25.4	1.68 ±0.26	2.59 0.39	3.32 0.54	3.69 0.55	2.05 0.30	4.60 0.70	1.77 0.27	0.13 0.02
Ba0312	-13.3	2.18 ±0.15	3.37 0.23	4.46 0.32	5.00 0.35	2.77 0.20	6.39 0.46	2.43 0.18	0.16 0.01
Ba0412	-7.3	2.65 ±0.19	4.23 0.29	5.74 0.41	6.36 0.45	3.64 0.26	8.68 0.61	3.20 0.22	0.21 0.02
Ba0522	-1.4	2.32 ±0.35	3.74 0.56	5.00 0.75	5.58 0.84	3.19 0.48	7.62 1.15	2.79 0.42	0.18 0.03
Ba0612	+4.8	2.60 ±0.19	4.16 0.29	5.58 0.39	6.25 0.43	3.54 0.25	8.38 0.59	3.12 0.22	0.20 0.02
Ba0712	+10.8	2.21 ±0.15	3.43 0.23	4.50 0.32	5.01 0.35	2.82 0.20	6.39 0.42	2.44 0.18	0.17 0.01
Ba0299	+22.6	1.45 ±0.22	2.25 0.34	2.88 0.43	3.06 0.46	1.75 0.26	3.89 0.59	1.47 0.22	0.09 0.01
600 MeV Thin Target		1.91 ±0.29	2.70 0.41	3.12 0.47	3.14 0.47	1.90 0.28	3.52 0.53	1.51 0.22	0.11 0.02

corresponding to all other samples are indicated in the Table 4.7.

The production rates for all the isotopes in units $[x10^{-10}ccSTP.gBa^{-1}.Ma^{-1}]$ are expressed in the Table 4.7. Fig. 4.12. shows the production rates of ^{124}Xe, ^{126}Xe and ^{128}Xe as a function of depth in the gabbro sphere (R =26 cm), irradiated with 600 MeV protons. The Fig. 4.13 shows similar plots for isotopes ^{129}Xe and ^{131}Xe and Fig. 4.14 show the depth dependence of ^{132}Xe and ^{134}Xe production rates in the gabbro sphere (R =26.1 cm). The production rates measured for the thin target, 600 MeV Ba glass, are also included for comparison purposes. It may be pointed out that at the surface of the gabbro sphere (R =25 cm) the measured production rates are almost the same as those for the thin target except for the isotope ^{131}Xe which shows slightly enhanced production even at the surface of the 25 cm meteoroid body. As we move towards the centre from either side the production rates increases sharply and at a distance of about 5 to 7 cm away from the centre the production rates are high by about 40% to 150% depending on the isotope, compared to their surface production rates. The increase is maximum (~150% for the isotope ^{131}Xe and on either side of this isotope, as the mass number decreases or increases, the increase in production rate with increasing shielding depth inside the gabbro sphere are less pronounced. At the centre (corresponding to Ba 0522 at distance of -1.4 cm from the centre of the 26 cm sphere, in this case) the xenon isotopes (excluding ^{131}Xe) have production rates which are higher by about 20% to 120%. The ^{131}Xe production rates at the surface and centre of the gabbro sphere are, respectively, 4.6 ±0.7 $x10^{-10}ccSTP.gBa^{-1}.Ma^{-1}$ and 7.62 ±1.15 (in the same units as

Fig 4.12 ^{124}Xe, ^{126}Xe and ^{128}Xe production as a function of depth in the gabbro sphere (R =26 cm), isotropically irradiated with 600 MeV protons at the CERN synchrocyclotron. The lines joining data points are only eye guides. Typical errors are indicated on some of the symbols.

Fig 4.13 ^{129}Xe and ^{131}Xe production as a function of depth in the gabbro sphere (R =26 cm), isotropically irradiated with 600 MeV protons at the CERN synchrocyclotron.   The lines joining data points are only eye guides. Typical errors are indicated on some of the symbols.
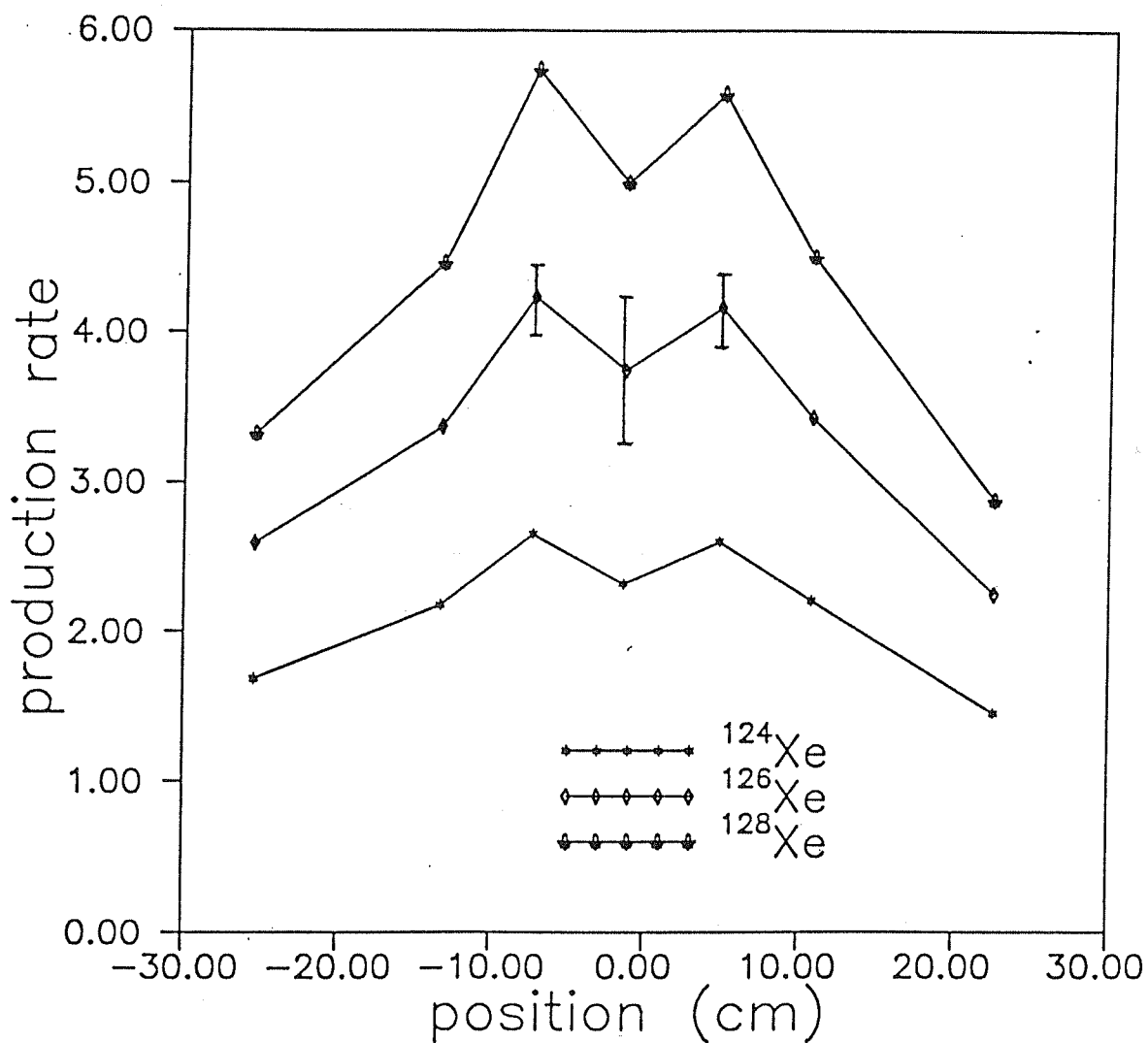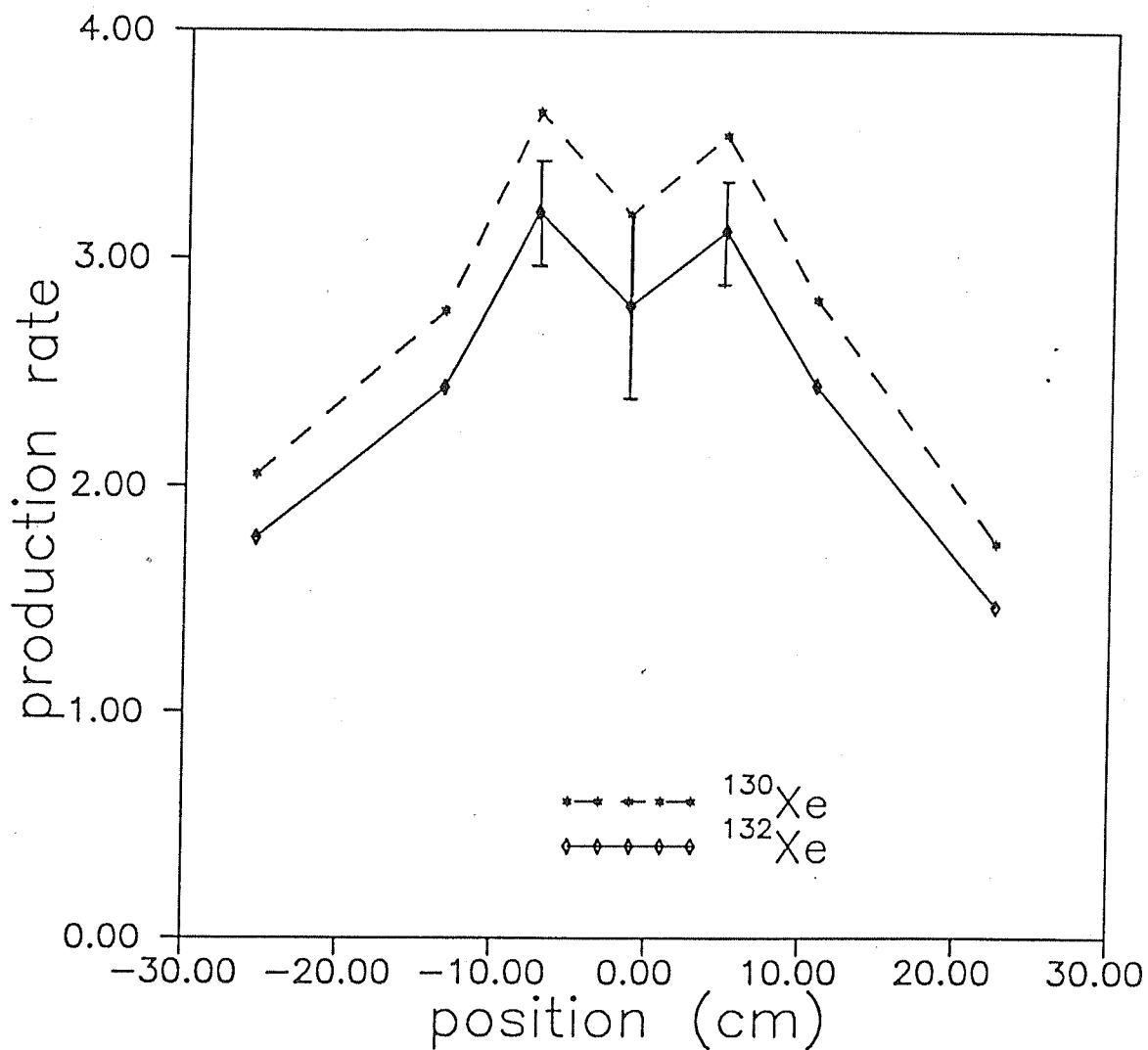
Fig 4.14 ^{130}Xe and ^{132}Xe production as a function of depth in the
gabbro sphere (R =26 cm), isotropically irradiated with
600 MeV protons at the CERN synchrocyclotron.   The
lines joining data points are only eye guides. Typical
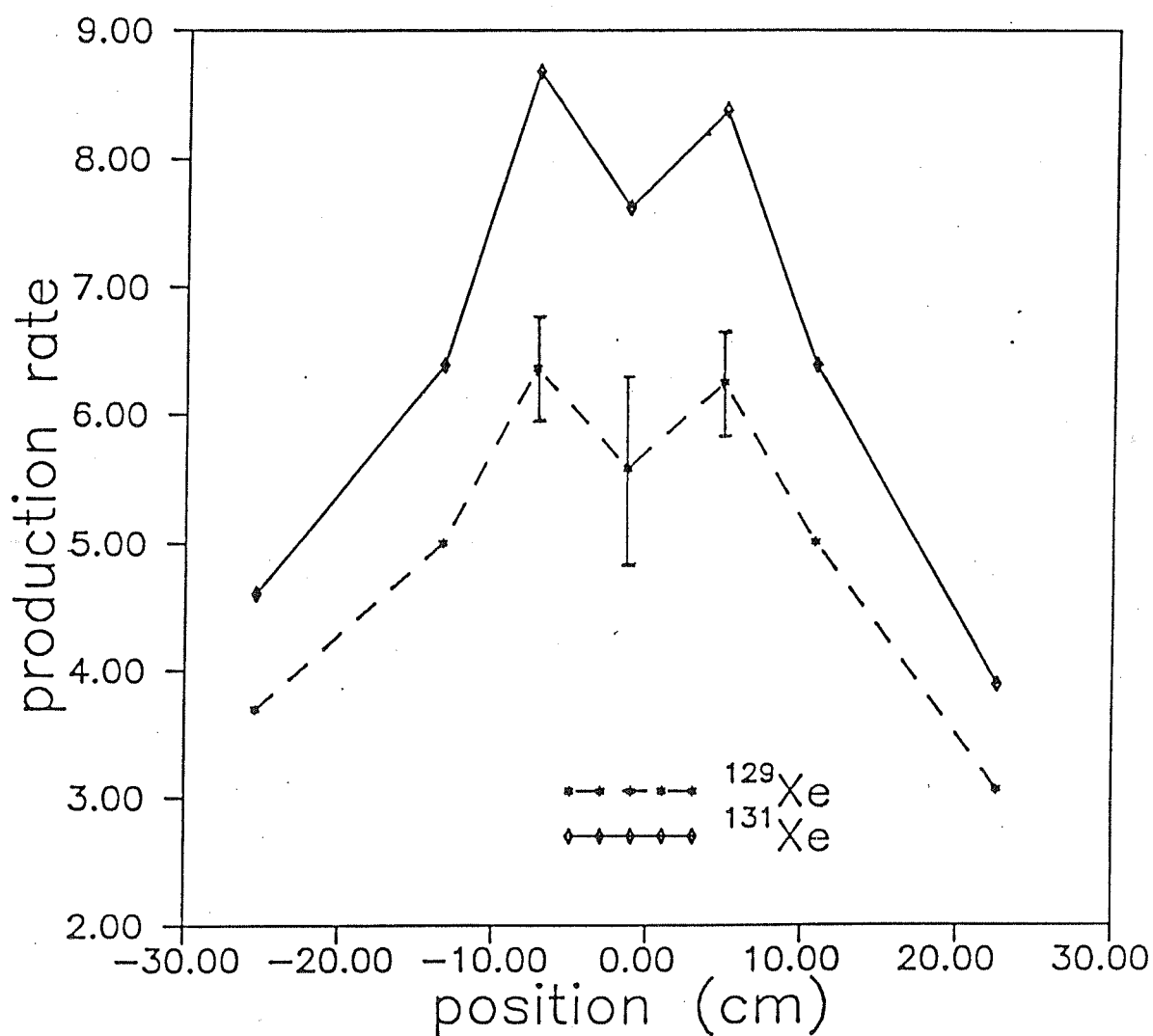errors are indicated on some of the symbols.

157

above). The corresponding thin target production rate value is 3.52 ±0.53 x10^{-10}ccSTP.gBa^{-1}.Ma^{-1}. In the case of the isotope ^{129}Xe the production rates measured in barium glasses kept near the surface (at a distance of 25.4 cm away from the centre of the gabbro sphere) and near the centre (at a distance of 1.4 cm from the centre) are, 3.69 ±0.55 and 5.58 ±0.84 when compared to the 600 MeV thin target production rate of 3.14 ± 0.47 [all the above production rates are expressed in units x 10^{-10}ccSTP.gBa^{-1}.Ma^{-1}]. The increase in production between the surface and the centre for Ba glass samples is the lowest for ^{124}Xe, only about 20%. And as the masses are increased the production rates increase more with depth, this increase reaches a maximum at ^{131}Xe and decreases further as we move on to heavier xenon isotopes. This behaviour is consistent with the systematics of spallation reactions. As the isotopes near the valley of nuclear stability are approached the production cross-section increase. The ^{131}Xe production is the maximum because the cross-sections for the production of this isotope is higher as compared to the cross-sections for the other xenon isotopes in both p- and n- induced reactions at low and medium energies.

These results suggest that a small body of size about 50 cm is sufficient for the generation of significant secondary nucleon cascade and in such a body there is an appreciable production of xenon isotopes due to the secondary particle interactions. These secondary particles have, obviously, much lower energies than the incoming primary proton beam.

A very significant effect obtained from the study of depth production profiles of xenon isotopes is the change in the

isotopic ratios with shielding depth inside the mock-up meteoroid. Fig.4.15 shows the isotopic ratios $^{124}Xe/^{126}Xe$, $^{128}Xe/^{126}Xe$ and $^{129}Xe/^{126}Xe$ as a function of depth in the gabbro (R =25 cm) sphere. Fig.4.16 shows a similar plot for isotopic ratios $^{130}Xe/^{126}Xe$, $^{131}Xe/^{126}Xe$ and $^{132}Xe/^{126}Xe$. The $^{131}Xe/^{126}Xe$ ratio shows the largest variation. The change in value of this isotopic ratio is from 1.73 ± 0.02 at the surface to 2.04 ± 0.02 at the centre of the 26 cm mock-up meteoroid ie. an increase of about 18%. The surface value of 1.73 ± 0.02 is higher by about 35% as compared to the thin target production ratio of 1.28 ± 0.02 for this isotopic ratio. The change in the isotopic ratio $^{132}Xe/^{126}Xe$ is ~15% between the surface and centre of the 26 cm (radius) gabbro sphere. The surface and centre values of $^{132}Xe/^{126}Xe$ ratios are 0.65 ± 0.01 and 0.75 ± 0.01 respectively. The $^{130}Xe/^{126}Xe$ ratios also show significant variations between the surface and centre of the gabbro sphere (R ~ 26 cm). The values of these isotopic ratios at the centre and near surface of the gabbro sphere are, respectively, 0.85 ± 0.01 and 0.78 ± 0.01 for $^{130}Xe/^{126}Xe$ and 1.49 ± 0.02 and 1.36 ± 0.01 in the case of $^{129}Xe/^{126}Xe$.

Fig. 4.17 shows the percentage deviation of the spallation spectra for xenon measured in the surface and centre samples of the gabbro (R =25 cm) sphere. These deviations are defined with respect to 600 MeV thin target production ratios using the equation

$$\frac{(^{i}Xe/^{126}Xe)_{E} - (^{i}Xe/^{126}Xe)_{600MeV}}{(^{i}Xe/^{126}Xe)_{600\ MeV}} \times 100 = \delta(^{i}Xe/^{126}Xe)$$

The percentage deviations are given in Table 4.8.

Table 4.8 : The increased production of ^{126}Xe production at various depths inside the gabbro sphere compared to the surface samples measured. Also given are the changes in the ^{M}Xe/^{126}Xe ratio from the surface sample at the same depths inside the gabbro sphere.

SAMPLE	Depth position (cm)	^{126}Xe [x10^{-8}cc STP/g] %	$\dfrac{^{124}\text{Xe}}{^{126}\text{Xe}}$ %	$\dfrac{^{128}\text{Xe}}{^{126}\text{Xe}}$ %	$\dfrac{^{129}\text{Xe}}{^{126}\text{Xe}}$ %	$\dfrac{^{130}\text{Xe}}{^{126}\text{Xe}}$ %	$\dfrac{^{131}\text{Xe}}{^{126}\text{Xe}}$ %	$\dfrac{^{132}\text{Xe}}{^{126}\text{Xe}}$ %	$\dfrac{^{134}\text{Xe}}{^{126}\text{Xe}}$ %
	-25.4	–	–	–	–	–	–	–	–
	-13.3	30.0	0.5	3.6	4.3	4.3	4.9	5.1	-2.0
	-7.3	63.0	-3.0	6.0	5.5	8.7	13.3	10.4	0
	-1.4	44.0	-3.7	4.3	4.8	8.0	12.6	8.9	-2.4
	-1.4	66.0	-4.3	4.2	9.6	9.5	17.6	15.0	17.0
	+4.8	85.0	-3.7	4.6	10.3	9.1	16.0	15.5	15.0
	+10.8	52.0	-1.0	2.7	7.4	5.5	7.7	9.6	20.0
	+22.6	–	–	–	–	–	–	–	–

Fig 4.15   Measured isotopic ratios $^{124}Xe/^{126}Xe$, $^{128}Xe/^{126}Xe$ and
$^{129}Xe/^{126}Xe$ as a function of depth in the gabbro (R =26
cm) sphere.
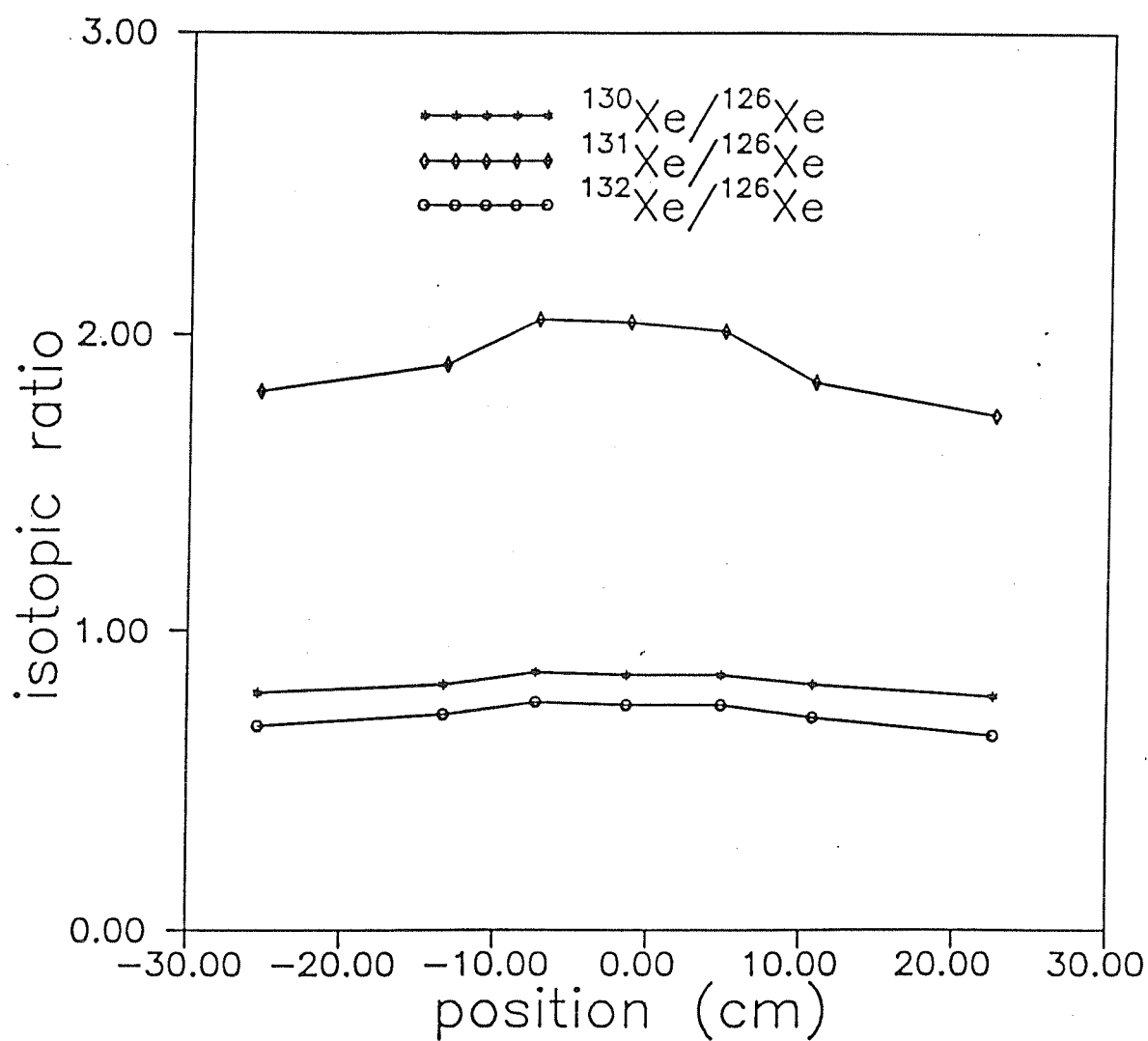
Fig 4.16   Measured isotopic ratios ^{130}Xe/^{126}Xe, ^{131}Xe/^{126}Xe and
      ^{132}Xe/^{126}Xe   as a function of depth in the gabbro (R =26
      cm) sphere.
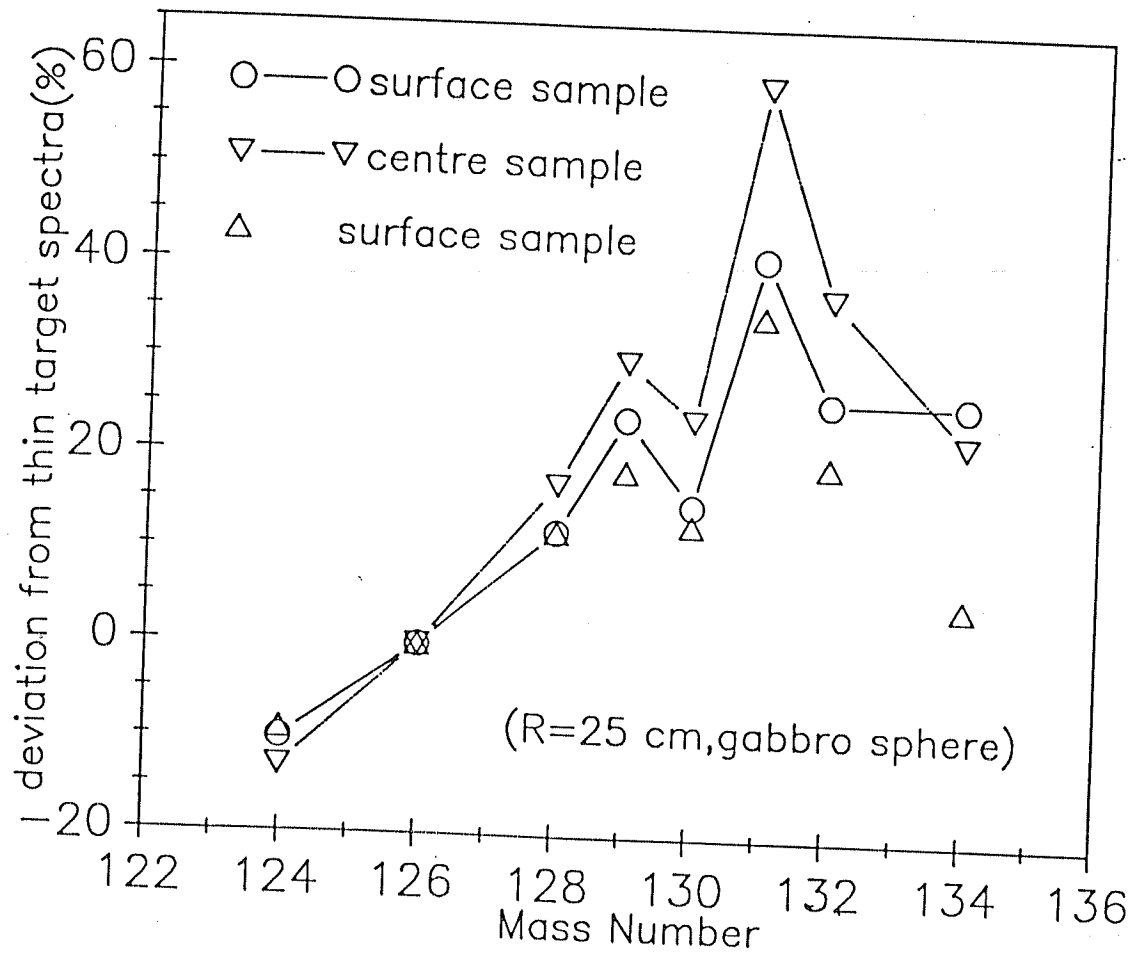
Fig 4.17   Percentage deviation of the spallation spectra measured
in Ba glass samples near the centre and near the
surface of the gabbro (R =26 cm) sphere.

Another interesting aspect which becomes clear from the Fig. 4.17 is that at comparatively higher depths inside a thick target body of diameter 50 cm the relative yields for the production of ^{131}Xe is much larger as compared to the other xenon isotopes. There is general tendency among xenologists to attribute any excess at ^{131}Xe isotope to (n,γ) reactions on ^{130}Ba. The thick target used in the present experiments are not large enough to thermalize the energetic secondary neutrons produced during the knock-on phase and the relatively low energy neutrons produced in the evaporation process of de-excitation of the residual nucleus. Also there is no water in the gabbro sphere to modulate neutrons. Our results show that a considerable portion of the ^{131}Xe excess have to be attributed to production by low energy protons and neutrons. Also it may be recalled here that we have already shown that the production cross-sections for isotopes ^{131}Xe, ^{129}Xe and ^{132}Xe by low energy protons are higher compared to other xenon isotopes.

The availability of medium energy neutrons and protons, produced as secondary particles in the 50 cm (diameter) gabbro body allows a large number of nuclear reactions involving these particles energetically possible. And in this case the effects due to thermalized neutrons can be ruled out as much larger objects are needed for this purpose. Hence the increases in production rates are due to secondary protons and neutrons. With neutrons in the energy range of a few MeV to 20-30 MeV the following reactions are possible, involving Ba targets.

Reaction	Q-value
^{130}Be (n, 2n)...^{129}Xe	-6.7 MeV
^{132}Ba ((n, α)^{129}Xe	+5.9 MeV
^{130}Ba (n, 3n)...^{128}Xe	-13.6 MeV
^{130}Ba (n, p)...^{130}Xe	+3.34 MeV
^{132}Ba (n, p)...^{132}Xe	+1.66 MeV
^{135}Ba (n, α)^{132}Xe	+6.99 MeV
^{132}Ba (n, 2n)...^{131}Xe	-8.1 MeV
^{134}Ba (n, α)^{131}Xe	+4.92 MeV
^{137}Ba (n, α)^{134}Xe	+5.84 MeV

Incidentally, these are the same isotopes in which we observe considerable variations in the isotopic ratios w.r.t ^{126}Xe. It is reasonable to infer that the observed effects, at least partly, are produced by neutrons having E <30 MeV. As far as the xenon isotopes are concerned such effects are observed for the first time and they may have important implications in the case of meteorites.

In the case of lunar samples the changes in isotopic ratios ^{M}Xe/ ^{126}Xe (M = 128, 129 and 131) had been successfully used in deriving the burial depths of these samples [Kaiser (1977)]. Lavielle and Marti (1989) used the combined determination of ^{78}Kr/^{83}Kr ratio and ^{22}Ne/^{21}Ne ratio in core samples of St.Severin chondrite to get a better discrimination of depth and size. For the interior samples they observed that the ^{78}Kr/^{83}Kr and ^{22}Ne/^{21}Ne ratios correlates linearly. In meteorites showing cosmogenic effects in xenon it is advantageous to use the depth dependence of the isotopic ratios of xenon for deducing such

information. The isotopic ratios $^{M}Xe/^{126}Xe$ (M =129, 130, 131 and 132) can be used for this purpose. This technique can now be extended to the case of meteorite samples and the shielding depths of the measured samples inside its parent body can be deduced from the measured values of the cosmogenic $^{129}Xe/^{126}Xe$, $^{130}Xe/^{126}Xe$, $^{131}Xe/^{126}Xe$ and $^{132}Xe/^{126}Xe$ ratios. The isotope ^{129}Xe has contributions in some cases from ^{129}I and so this isotopic ratio may be less favourable in applications of the kind discussed above. But, if the ^{129}Xe amounts from extinct ^{129}I are accountable, this isotopic ratio can be made use of in deducing the shielding depths of meteorite samples (because the fission contribution to this isotope is nominal).

Kaiser (1977), Hohenberg et al., (1970), Bogard et al., (1971), Lugmair and Marti (1972) and Srinivasan (1974) have shown that in meteorites and lunar samples with Ba/Ce ratio ≥ 2 the cosmogenic xenon due to Ba targets predominates the isotopic composition of the observed xenon spectra. So the picture emerging from the present analysis is not largely affected by the contribution from rare earth elements to the production of xenon isotopes, in general.

The availability of neutrons in the energy range of few MeV to 20-30 MeV, in the lunar surface, make the reactions listed above energetically possible for the lunar case also. The ^{131}Xe anomaly observed in lunar samples by Hohenberg et al., (1970), Pepin et al., (1970), Kaiser and Rajan (1973), Kaiser and Bermann(1972), Eberhardt et al., (1974), Marti and Lugmair (1971) and Eugster et al., (1970), can at least partially, be explained as due to reactions of the kind listed above.

CHAPTER V

CONCLUSIONS

In this study, the cross-sections for the production of xenon isotopes on Ba targets by protons having energies from 12 to 45 MeV (in the low-energy region) and 600 to 2600 MeV (in the high-energy region) are accurately measured using stacked foil irradiation techniques as well as different combinations of "thin" and "thick" target irradiation methods. Based on these cross-section measurements (along with some theoretically estimated ones), excitation functions for several xenon isotopes are constructed and the results are used to estimate the SCR production rates for xenon isotopes in the case of lunar surface samples.

The low proton energy range of 12 MeV <E <45 MeV (low-energy region) has been systematically investigated using Ba targets and our results show that there is a significant production of xenon isotopes in the p-induced reactions on Ba. Prior to our experiments, xenologists have assumed that low-energy proton induced reactions on barium targets did not produce xenon isotopes. The isotopes ^{129}Xe, ^{131}Xe and ^{132}Xe have relatively larger yields compared to other xenon isotopes. The measured cross-sections for the production of ^{129}Xe, ^{131}Xe and ^{132}Xe at ~24 MeV, for example, are, 2.53 ±0.38 mb, 3.62 ±0.54 mb and 1.01 ±0.15 mb as compared to the ^{130}Xe production cross-section of 0.25 ±0.04 mb and 0.03 ±0.004 mb for ^{128}Xe. The enhanced production of these three isotopes at p-energies of about 24 MeV as evident from the

larger values of $^M\text{Xe}/^{130}\text{Xe}$ (M = 129, 131 and 132) at these energies indicate that pre-equilibrium α-emission reactions play a significant role in the low energy region. These reactions favourably produce the isotopes ^{129}Xe, ^{131}Xe and ^{132}Xe.

The calculation of SCR production rates carried out for the xenon isotopes in the case of lunar surface indicate higher production rates for the isotopes ^{129}Xe, ^{131}Xe and ^{132}Xe compared to other xenon isotopes, in the topmost surface layers. For all xenon isotopes our SCR xenon production rates are higher by approximately a factor of 2 compared the earlier estimates by Hohenberg et al., (1978). The xenon production rate calculations obtained here agree reasonably well with those obtained by Michel et al., (1980). The Hohenberg . et al., (1978) calculations have underestimated the xenon production in lunar surface material because the low energy contributions (from protons having E <60 MeV) on barium targets have not been taken into consideration. The present calculations carried out with a cut off energy of 100 MeV shows that protons having energy <100 MeV accounts for as much as 70% of the total production of ^{132}Xe on the lunar surface. The production rates of these isotopes in lunar surface material are, respectively, 6.05 $\times 10^{-15}\text{ccSTP.g}^{-1}.\text{Ma}^{-1}.\text{ppmBa}^{-1}$ (^{131}Xe) and 0.731 $\times 10^{-15}\text{ccSTP.g}^{-1}.\text{Ma}^{-1}.\text{ppmBa}^{-1}$. The contribution of protons having E <100 MeV in the ^{131}Xe and ^{130}Xe production rates given above are, 3.13 $\times 10^{-15}\text{ccSTP.g}^{-1}.\text{Ma}^{-1}.\text{ppmBa}^{-1}$ and 0.404 $\times 10^{-15}\text{ccSTP.g}^{-1}.\text{Ma}^{-1}.\text{ppmBa}^{-1}$ (protons in this energy range (E <100 MeV) contribute ~50% of the total production of ^{131}Xe and ^{130}Xe on the lunar surface). Further, our results suggest that the SCR

proton spectra are soft and values of characteristic rigidity $R_0 \sim 100$ MV are more likely for the SCR protons during the last few million years.

The xenon data from documented samples of oriented lunar rocks 61016, 64435 and 79215 (which are known to contain records of SCR exposure on the lunar surface) are analysed in an attempt to delineate the SCR xenon spallation yields from known Ba contents in these rocks. Detailed analysis of the rock data here show that these rocks contain qualitative indications for the presence of SCR produced xenon isotopes. The SCR produced xenon spectrum is deduced to be ^{129}Xe : ^{131}Xe : ^{132}Xe = 0.94 : 2.30 : 1.000 (large errors are associated with these numbers). Further we calculate the SCR exposure ages of these rocks based on the xenon production rates (theoretically estimated) and they roughly agree with the ages deduced for these rocks by other techniques.

The cross-section measurements (thin target) carried out by us at 600, 800, 1200 and 2600 MeV show that in the energy range 600 MeV $<$E $<$1200 MeV, the production cross sections remain almost constant but at still higher p-energies the xenon production cross-sections decrease significantly. Another important observation at these energies is that the relative yields for various xenon isotopes change considerably. These changes are such that that the heavier xenon isotope production is enhanced as compared with the lighter xenon isotopes. Many of these effects at high energies have not been considered earlier while estimating the cosmogenic xenon production rates in moon and meteorite samples.

169

The production rates of xenon isotopes as a function of depth measured in the diorite (R =5 cm) and gabbro spheres (R =26 cm) irradiated isotropically with 600 MeV protons at the CERN synchrocyclotron (in order to simulate the conditions of space irradiation in the laboratory), show the following results. In mock-up meteoroid bodies of small size (R ~5 cm) the production rates remain fairly constant at all shielding depths. Whereas in the case of mock-up meteoroid bodies of larger size (R ~26 cm) there is a significant enhancement the in production of some xenon isotopes from the surface to the centre of the body. The enhancement in the production is maximum for the isotope ^{131}Xe and the isotopes ^{129}Xe, ^{130}Xe and ^{132}Xe also show significant enhancement at the center of the mock-up object. For example, the calculated production rates using the measured in barium glass samples irradiated near the surface and near the centre of the gabbro sphere (R =26 cm) are, respectively, 4.60 ±0.70 x10^{-10}ccSTP.g^{-1}.Ma^{-1} and 7.62 ±1.15 x10^{-10}ccSTP.g^{-1}.Ma^{-1} (for ^{131}Xe) and 3.69 ±0.55 x10^{-10}ccSTP.g^{-1}.Ma^{-1} and 5.58 ±0.84 x10^{-10}ccSTP.g^{-1}.Ma^{-1} (for ^{129}Xe). Our results, further, demonstrate that the isotopic ratios of xenon change systematically with shielding depth inside the irradiated mock-up meteoroid. The changes in the isotopic ratios ^{M}Xe/^{126}Xe (M = 124 to 132) show a maximum for the isotope ^{131}Xe followed by ^{132}Xe, ^{130}Xe and ^{129}Xe isotopes. In the case of ^{131}Xe/^{126}Xe the change in the isotopic ratio between the centre and the surface of the 25 cm body is about 18%. Further, the present study indicates that the neutron reactions (n,p), (n,2n), (n,α) and (n,3n) with the

barium target isotopes ^{130}Ba, ^{132}Ba, ^{134}Ba and ^{135}Ba play an important role in favouring the production of ^{131}Xe, ^{132}Xe, ^{130}Xe and ^{129}Xe isotopes in these mock-up model objects. These results suggest that such type of phenomena must be occurring in the cosmic ray irradiation of the meteoroids in space.

In addition to the enhancement in the absolute production rates at the centre of the spherical object as seen in the "thick" target experiments, the isotopic ratios show systematic variations with shielding depth inside the meteoroid mock-ups. This systematic behaviour in the isotopic variations of cosmogenic xenon can be utilized in deducing the shielding depths in the case of meteorite samples under favourable conditions. In this case, since at least four isotopic ratios, viz ^{129}Xe/^{126}Xe, ^{130}Xe/^{126}Xe, ^{131}Xe/^{126}Xe and ^{132}Xe/^{126}Xe can be employed for the above purposes the self consistency of the results can be monitored. Since the possibility of (n,γ) reactions due to thermalized neutrons is ruled out in the case of artificial meteoroid mock-ups of radii 26 cm, the effects observed in the experiments at the ^{131}Xe isotope have to be explained by more energetic neutrons. Thus the ^{131}Xe anomaly seen in lunar samples can at least partially, be explained as due to the (n,p), (n,2n), (n,α) and (n,3n) reactions as mentioned in Chapter **IV**.

Our results show that with the available excitation functions for proton induced reactions on Ba, the production rates of cosmogenic anuclides can be estimated reasonably well using the existing models. The simulation experiments carried out have used both the thin and thick target approaches and have contributed in

171

a significant way to the understanding of the production profiles of cosmogenic nuclides as a function of depth in moon and meteorite samples. Using the results of xenon production cross-sections over a wide range of energies, obtained in the present studies, the cosmogenic xenon production in extraterrestrial matter can now be estimated accurately.

APPENDIX I

(a) Elemental composition of the Ba glass targets used in the low energy irradiation experiments

---

Element (Z) :	Ba(56)	B(5)	O(8)	Al(13)	Si(14)	As(33)	Total
Percentage :	40.13	4.63	36.02	2.49	16.5	0.23	100

(b) Irradiation energy and dose data.

SAMPLE	PROTON ENERGY (MeV)	PROTON DOSE
BA1	44.6±0.4	1.67×10^{16}
BA3	40.6±0.6	1.67×10^{16}
BA5	36.4±0.6	1.67×10^{16}
BA7	32.2±0.6	1.67×10^{16}
BA10	26.4±0.9	1.67×10^{16}
BA3-6	24.1±0.7	1.21×10^{16}
BA3-7	22.0±0.5	1.21×10^{16}
BA4-2	20.1±0.5	2.19×10^{16}
BA4-6	11.9±0.8	2.19×10^{16}

APPENDIX II

Elemental composition (10^{-2}g.g^{-1}) of gabbro and diorite spheres. The corresponding values for H and L chondrites are also given.

Element	gabbro	diorite	L-chondrite[1]	H-chondrite[1]
O	47.60	49.50	40.00	35.70
Na	1.87	2.37	0.66	0.57
Mg	4.45	2.05	15.20	14.20
Al	9.15	7.89	1.10	1.01
Si	24.60	27.70	18.70	17.10
K	0.19	1.10	0.09	0.08
Ca	5.89	4.50	1.28	1.19
Fe	5.30	4.83	21.80	27.60
A_{mean}	21.1	21.3	23.1	24.4
Z_{mean}	10.4	10.6	11.3	11.9

[1]taken from Mason(1971)

APPENDIX III

Details of the Irradiation Experiments at various high energies

Accelerator used	Nature of Experiment	Proton energy used(MeV)	Proton Flux $(cm^{-2}s^{-1})$	Time of Irradiation (s)	Proton dose	Equiv. GCR exp. age(Ma)
CERN[*] (SC 96/1)	Thick target (5cm diorite sphere)	600	$(1.64\pm0.01) \times 10^{11}$	29370	$(4.82\pm0.02) \times 10^{15}$	53
CERN[*] SC 96/2	Thick target (25cm gabbro sphere)	600	$(4.83\pm0.01) \times 10^{9}$	45000	$(2.174\pm0.005) \times 10^{14}$	2.4
Los Alamos[**]	Thin target	800	$(7.25\pm0.14) \times 10^{10}$	20400	$(1.48\pm0.03) \times 10^{14}$	
Saclay	Thin target	1200	$(8.67\pm0.10) \times 10^{10}$	39660	$(3.44\pm0.04) \times 10^{15}$	
Saclay	Thin target	2600	$(2.47\pm0.05) \times 10^{10}$	43080	$(1.06\pm0.02) \times 10^{15}$	

[*]   Dragovitsch (1987)

[**] Michel R., Personal Communication (1991)

[**] Assuming $J_{GCR} = 2.86$ $cm^{-2}.s^{-1}$

APPENDIX IV

Xenon component resolution in lunar rocks

Let

sol - denote the solar (SW + SF) component

tra - denote the trapped component

gcr - denote the gcr produced component

and scr - denote the scr produced component

For the R1 sample we can express the measured Xe concentrations as follows:

(R1) $^M Xe = {}^M Xe_{sol} + {}^M Xe_{tra} + {}^M Xe_{gcr}$ (M=124, 126, 128 and 130)(1)

The SCR contributions to the above isotopes can be neglected based on our cross-section measurements and from the Xenon production rates calculated on the lunar surface.

(R1) $^M Xe = {}^M Xe_{sol} + {}^M Xe_{tra} + {}^M Xe_{gcr}$ (M = 129, 131 and 132)   (2)

and

(R1) $^M Xe = {}^M Xe_{sol} + {}^M Xe_{tra} + {}^M Xe_{gcr}$ (M = 134 and 136)   (3)

The isotopes ^{134}Xe (and the isotope ^{136}Xe is not produced at all) is having negligible yields in high energy and low energy spallation reactions on Ba.

In case of R2 samples

(R2) $^M Xe = {}^M Xe_{tra} + {}^M Xe_{gcr}$ (M = 124, 126, 128 and 130)   (4)

(R2) $^M Xe = {}^M Xe_{tra} + {}^M Xe_{gcr} + {}^M Xe_{scr}$ (M = 129, 131 and 132) (5)

some amount of SCR produced Xe can be expected in this sample

(R2) $\quad {}^M Xe = {}^M Xe_{tra} + {}^M Xe_{fis}$ (M = 134 and 136) $\qquad$ (6)

and for R(3) sample

(R3) $\quad {}^M Xe = {}^M Xe_{tra} + {}^M Xe_{gcr}$ (M = 124, 126, 128 and 130) $\qquad$ (7)

(R3) $\quad {}^M Xe = {}^M Xe_{tra} + {}^M Xe_{gcr}$ (M = 129, 131 and 132) $\qquad$ (8)

(R3) $\quad {}^M Xe = {}^M Xe_{tra} + {}^M Xe_{fis}$ (M = 134 and 136) $\qquad$ (9)

Further, it is assumed that

(R1) ${}^M Xe_{tra}$ = (R2) ${}^M Xe_{tra}$ = (R3) ${}^M Xe_{tra}$

$\qquad$ as the trapped Xenon in incorporated at the time of formation of the rock. The samples R1, R2 and R3 from the same rock were formed in the same environment and have trapped gases having the same isotopic composition

and

(R1) ${}^M Xe_{gcr}$ = (R2) ${}^M Xe_{gcr}$ = (R3) ${}^M Xe_{gcr}$ $\qquad$ (10)

since production by gcr particles remain the same at small change in shielding depths

Substracting

(R1) ${}^M Xe$ - (R3) ${}^M Xe = {}^M Xe_{sol}$ (M = 124, 126, 128 and 130) $\qquad$ (11)

(R1) ${}^M Xe$ - (R3) ${}^M Xe = {}^M Xe_{sol} + {}^M Xe_{scr}$ (M = 129, 131 and 132) (12)

(R1) ${}^M Xe$ - (R3) ${}^M Xe = {}^M Xe_{sol}$ (M = 134 and 136) $\qquad$ (13)

The ${}^{134}Xe$ concentrations at (R1-R3) stage is used to determine the amounts of trapped solar (implanted SW + SF) Xe concentrations in R1 sample. The excesses in the case of isotopes ${}^{129}Xe$, ${}^{131}Xe$ and ${}^{132}Xe$, over and above the trapped solar concentrations are due to

177

production by SCR protons. The (R1-R2) fraction may be treated in a similar manner to check consistancy of results.

Few comments about xenon measurements in similar rocks

Based on their experiments on Apollo 16 samples Bernatowictz et al., (1978 and 1977) reported excesses at some xenon isotopes over and above the trapped xenon amounts in these samples. These excesses were concluded to be surface correlated as the excesses became larger when larger sized grains were analysed. Similar results were also reported earlier by Drozd et al.,(1976 and 1972), Reynolds et al.,(1974) and Graf et al.,(1973) with Apollo 14 samples. In all the experiments described above a large portion of solar wind xenon amounts are released at comparatively low temperatures of 400 to 600 °C. In the present experiments with lunar rocks a low temperature release fraction at 600°C was done. We observed that there is little xenon released at these low temperature. The released xenon amounts at this temperature was only ~1 to 1.5% of the xenon amounts released at 1600°C. Further it was also observed that xenon released at these temperatures have isotopic composition similar to that of terrestrial atmosphere. The major xenon isotopic ratios ,i.e. $^{129}Xe/^{130}Xe$, $^{131}Xe/^{130}Xe$ and $^{132}Xe/^{130}Xe$, were also found to be same as that of terrestrial atmosphere in this temperature fraction.

REFERENCES

Alexander E.C., Lewis R.S., Reynolds J.H. and Michel M., *Science* 172 (1971), p.837.

Amin B.S., Lal D., Lorin J.C., Pellas P., Rajan R.S., Tamhane A.S. and Venkatavaradan B.S., *Meteorite Research* [Edit. by Millman P.M.] (1968), p.316.

Amstrong T.W. and Alsmiller R.G., *Proc. Lunar Planet. Sci. Conf. 2nd* (1971), p.1729.

Anders E. and Ebihara M., *Geochim. Cosmochim. Acta* 46 (1982), p.2363.

Arakita Y., Hirayama H., Ignaki T. and Miyajima M., *Nucl. Instr. and Meth.* 164 (1979), p.255.

Aylmer D., Herzog G.F., Klein J. and Middleton R., *Geochim. Cosmochim. Acta* 52 (1988), p.1691.

Bar K. and Herr W., *Proc. Lunar Sci. Conf.5th* (1974), p.188.

Begemann F., Weber H.W., Vilesek E. and Hitenberger H., *Geochim. Cosmochim. Acta* 50 (1976), p.353.

Begemann F. and Wanke H., ^{39}K (n,p)-produced ^{39}Ar in chondrites : New data and their interpretation in terms of size, exposure age on orbital elements. In Meteorite Research (ed. P.M.Millman) D.Reidel Publ. Co. (1969a), p.363.

Begemann F. and Vilesek E., Chlorine-36 and Argon-39 production rates in the metal of stone and stony iron meteorites. In : Meteorite Research (ed. P.M.Millman) D.Reidel Publ. Co. (1969b), p.355.

Berman B.L. and Browne J.C., *Phy. Rev. C7* (1973).

Bernatowitz T.J., Drozd R.J., Hohenberg C.M., Lugmair G., Morgan C.J. and Podosek F.A., *Proc. Lunar Sci. Conf. 8th* (1977), p.2763.

Bernatowitz T.J., Hohenberg C.M., Hudson B., Kennedy B.M. and Podosek F.A., *Proc. Lunar Planet. Sci. Conf. 9th* (1978), p.1571.

Bhai N.B., Gopalan K., Goswami, J.N., Rao M.N. and Venkatesan T.R., *Proc. Lunar Planet. Sci. Conf. 9th* (1978), p.1629.

Bhandari N., Padia J.T., Rao M.N., Shukla P.N., Suthar K.M., Sarafin R. and Herpers U., *Meteoritics* 23 (1988), p.103.

Bhandari N., Bhattacharya S.K. and Padia J.T., *Proc. Lunar Sci. Conf. 6th* (1975), p.1913.

Bhandari N., Bhattacharya S.K. and Padia J.T., *Proc. Lunar. Sci. Conf. 7th* (1976), p.513.

Bhandari N., Lal D., Rajan R.S., Arnold J.R., Marti K. and Moore C.B., *Nucl. Tracks.* 4 # 4 (1980) p.213.

Bhandari N., Bhattacharya S.K. and Somayajulu B.L.K., *Earth Planet. Sci. Lett.* 33 (1978), p.275.

Bhandari N. and Potdar M.P., *Earth Planet Sci. Lett.* 58 (1982), p.116.

Bhattacharya S.K. and Bhandari N., *Proc. Lunar Sci. Conf. 6th* (1975), p.1901.

Blanchard D.P., Jacobs J.W. and Brannon J.C., *Proc. Lunar Sci. Conf. 8th* (1977), p.2507.

Blann M. and Bisplinghoff, *UCID-19614* (1982).

Blann M. and Vonach H.K., *Phys. Rev.* C28 (1983) p.1475.

Blann M., *ALICE LIVERMORE 87*, Private Communication to Michel (1987).

Bogard D.D., Funkhouser J.G., Burnett D.S. and Wasserburg G.J., *Geochim. Cosmochim. Acta.* 35 (1971), p.1231.

Brown H., *Phys. Rev.* 72 (1947), p.348.

Burnett D.S. and Woolum D.S., *Phys. Chem. Earth* 10 (1977), p.63.

Cameron A.G.W., *Icarus 1* (1962), p.13.

Cameron A.G.W., *Space Science Reviews*, 15 (1973) p.121.

Cameron A.G.W. and Truran J.W., *Icarus 30* (1977), p.447.

Cressy P.J., *Geochim. Cosmochim. Acta* 35 (1971), p.1283.

Cressy P.J. and Bognard D.D., *Geochim. Cosmochim. Acta.* (1976), p.749.

Dragovitsch P., *Thesis, Universitat zu Koln* (1987).

Drozd R.J., Hohenberg C.M. and Ragan D., *Earth Planet. Sci. Lett* 15 (1972), p.338.

Drozd R.J., Kennedy B.M., Morgan C.J., Podosek F.A. and Taylor G.J., *Proc. Lunar Sci. Conf. 7th*, (1976), p.599.

Eberhardt P., Eugster O. and Geiss J., *J. Geophys. Res.* 70 (1965), p.4427.

Eberhardt P., Geiss J., Graf H., Grogler N., Krahlenbühl U., Schwaller H., Schwarzmüller J. and Stettler A., *Earth Planet. Sci. Lett. 10* (1970), p.67.

Eberhardt P., Geiss J., Graf H., Grogler N., Mendia M.D., Morgeli M., Schwaller H., Stettler A., Krahlenbühl U. and Von Gunten H.R., *Proc. Lunar. Planet. Sci. Conf. 3rd* (1972), p.1821.

Eberhardt P., Geiss J., Garf H., Grogler N., Krahlenbühl U., Schwaller H. and Stettler A., *Geochim. Cosmochim. Acta* 38 (1974), p.97.

Englert P. and Herr W., *Earth Planet. Sci. Lett.* 47 (1980), p.361.

Englert P., Reedy R.C. and Arnold J.R., *Nucl. Instrum. Meth. A262* (1987), p.496.

Eugster O.,Tera F.,Burnett D.S. and Wasserburg G.J., *Earth Planet. Sci. Lett.* 8 (1970), p.20.

Eugster O., Eberhardt P., Geiss J., Grogler N., Jungck M., Meier F., Morgeli M. and Niederer· F., *Jour. of Geophy. Res.* 89 (1984), p.B498.

Eugster O. and Niedermann S., *Earth and Planet. Sci. Lett.* (1988), p.15.

Eugster O., *Geochim. Cosmochim. Acta.* 52 (1988), p.1649.

Evans J.C., Reeves J.H. and Reedy R.C., *Lunar and Plan. Sci. XVIII (Houston : Lunar and Planetary Institute)*, (1987), p.271.

Fields R.R., Friedman A.M., Milsted J., Lerner J., Stevens C.M., Metta D. and Sabine W.K., *Nature* 212 (1966), p.131.

Fireman E.L. and Zahringer J., *Phys. Rev.* 107 (1957), p.1695.

Fireman E.L., *Geochrim. Cosmochim. Acta* 31 (1967), p.1691.

Fisher D.E., *Earth Planet. Sci. Lett.* 16 (1972), p.391.

Funk H. and Rowe M.W., *Earth Planet. Sci. Lett.* 2 (1967), p.215.

Funk H., Podosek F. and Rowe M.W., *Earth Planet. Sci. Lett.* 3 (1967), p.193.

Ginneken A. Van and Turkevich A., *J. Geophys. Res.* 75 (1970), p.5121.

Goles G.G. and Anders E., *J. Geophys. Res.* 66 (1961), p.889.

Gopalan K., Rao M.N. and Agarwal J.K., *Technical Report,* TIFR (1973), p.1.

Goswami J.N., McGuire R.E., Reedy R.C., Lal D. and Jha R., *J. Geophys. Res.* 93 (1988), p.7195.

Graf Th., Shirck J., Son S. and Walker R.M., *Proc. 4th Lunar Sci. Conf., Geochim. Cosmochim. Acta, Suppl.* 4, Vol.2 (1973), p.2145.

Graf Th., Vogt S., Bonani G., Herpers U., Signer P., Suter M., Wieler R. and Woelfli W., *Nucl. Instru. Meth.* B29 (1987), p.262.

Graf Th, Signer P. and Wieler R., *Meteoritics* 23 (1988), p.271.

Herpers U. and Englert P., *Proc. Lunar Planet Sci. Conf. 14th, J. Geops. Res. Part 1* (1983), 88: B312.

Herzog G.F. and Cressy P.J., Jr., *Geochim. Cosmochim. Acta* 38 (1974), p.1827.

Hohenberg C.M., Podosek F.A. and Reynolds J.H., *Science* 156 (1967), p.233.

Hohenberg C.M., Davis P.K., Kaiser W.A., Lewis R.S. and Reynolds J.H., *Proc. of the Apollo 11 Lunar Sci. Conf. 2nd* (1970), p.1283.

Hohenberg C.M., Marti, K., Podosek F.A., Reedy R.C. and Shirck J.R., *Proc. Lunar Planet. Sci. Conf. 9th* (1978), p.2311.

Hohenberg C.M. and Kennedy B.M., *Geochim. Cosmochim. Acta* 45 (1981), p.489.

Honda M., *Meteoritics* 23 (1988), p.3.

Hörz F., Brownlee D.E. Fechtig H., Hartung J.B., Morrison D.A., Neukum G., Schneider E. and Vedder J.F., *Planet. Space Sci. Rev.* 23 (1975), p.151.

Hubbard N.J., Rhodes J.M., Weigmann H., Shih C.Y. and Bansal B.M., *Proc. Lunar Sci. Conf. 5th* (1974), p.1227.

Hyde E.K., The nuclear properties of Heavy Elements Vol.3, *Dover Publications Inc., New York* (1971).

Jeffery P.M. and Reynolds J.H., *J. Geophys. Res.* 66 (1961), p.3582.

Kaiser W.A. and Bermann B.L., *Earth Planet. Sci. Lett.* 15 (1972), p.320.

Kaiser W.A. and Rajan R.S., *Earth Planet. Sci. Lett.* 20 (1973), p.286.

Kaiser W.A., Damm G., Herpers U., Herr W., Kulus H., Michel R., Rosner K.P., Thiel K. and Weigel H., *Proc. Lunar Sci. Conf. 6th* (1975), p.1927.

Kaiser W.A., *Phil. Trans. Royal Soc., London* A 285 (1977), p.337.

Kirsten T.A. and Schaeffer O.A., High Energy Interactions in Space, In Elementary particles : Science, Technology and Society Academic Press, New York (1971).

Kohl C.P., Murrel M.T., Russ III G.P. and Arnold J.R., *Proc. Lunar Planet. Sci. Conf. 9th* (1978), p.2299.

Kohman T.P. and Bender M.L., in : *High Energy Nuclear Reactions in Astrophysics, ed., Shen B.S.P.* (Benjamin, New York, 1967), p.169.

Krummenacher D., Merrihue C.M., Pepin R.O. and Reynolds J.H., *Geochim. Cosmochim. Acta* 26 (1962) p.231.

Kuroda P.K., *Nature*, 187 (1960), p.36.

Lal D. and Venkatavardhan V.S., *Earth Planet. Sci. Lett.* 3 (1967), p.299.

Lal D., *Space Sci. Rev.* 14:3 (1972), p.102.

Lal D. and Marti K., *Nucl. Track. Detection* 1 # 2 (1977), p.127.

Langevin Y., Arnold J.R. and Nishiizumi K., *J. Geophys. Res.* 87 (1982), p.6681.

Lavielle B. and Marti K. *proc. Lunar Planet Sci. Conf. 18* (1988), p.565.

Lavrukhina A.K., Ustinova G.K., Malyshev V.V. and Saratoua L.M., *At. Energiya* 34 (1973), p.23.

Laul J.C., Hill D.W. and Schmitt R.A., *Proc. Lunar Planet. Sci. Conf. 5th* (1974), p.1047.

Lipschutz M.E., Signer P. and Anders E., *J. Geophys. Res.* 70 (1965), p.1473.

Lugmair G.W. and Marti K., *Earth Planet. Sci. Lett* 13 (1971), p.32.

Lugmair G.W. and Marti K., *Proc. 3rd Lunar Sci. Conf.* Suppl.3, 2 (1972), p.1891.

Laul J.C. and Schmitt R.A., *Proc. Lunar Sci. Conf. 4th* (1973), p.1349.

Marti K., Eberhardt P. and Geiss J., *Z. Naturforsch* 21a (1966), p.398.

Marti K., *Phys. Rev. Lett.* 18 (1967), p.264.

Marti K., Lugmair G.W. and Urey H.C., *Proc.* of the Apollo II Lunar Sci. Conf. 2nd (1970), p.1357.

Marti K. and Lugmair G.W., *Proc. Lunar Sci. Conf. 2nd* 2 (1971), p.1591.

Masarik J.P., Emrich P., Povinec P. and Tok'ar S., *Nucl. Instru. Meth. in Phys. Res.* B17 (1986), p.483.

Mason B., Ed., *Handbook of Elemental Abundances in Meteorites., Gorden and Breach, New York (1971).*

Mc Guire R.E. and Von Rosenvinge T.T., *Adv. Space Res.* 4 (1984), p.117.

Mc Guire R.E., Von Rosenvinge T.T. and Mc Donald F.B., *Astrophys. J.* 301 (1986), p.938.

Mc Gee, Bence A.E., Eichhorn G. and Schaeffer O.A., *Proc. Lunar Planet Sci. Conf. 9th* (1978), p.743.

Michel R., Weigel H., Kulus H. and Herr W., *Radiochimica Acta.* 21 (1974), p.169 and 179.

Michel R., Brinkmann G., Weigel H. and Herr W., *J. Inorg. Nucl. Chem.* 40 (1978a), p.1845.

Michel R., Weigel H. and Herr W., *Z. Physik* A286 (1978b), p.393.

Michel R., Brinkmann G., Weigel H. and Herr W., *Nucl. Phys.* A322 (1979), p.40.

Michel R. and Brinkmann G., *J. Radioanal. Chem.* 59 (1980), p.467.
Michel R. and Stück R., *Proc. Int. Nucl. Data for Science and Technology* (1982), p.952.

Michel R., Brinkmann G. and Stück R., *Earth. Planet. Sci. Lett.* 59 (1982), p.33 and 64 (1985) erratum p.174.

Michel R., Dragovitsch P., Englert P., Peiffer F., Stück R., Theis S., Begemann F., Weber H., Signer P., Wieler R., Filges D. and Cloth P., *Nuclear Inst. and Meth. in Phy. Res.* B16 (1986), p.61.

Michel R., Peiffer F., Theis S., Begemann F., Weber H., Signer P., Wieler R., Cloth P., Dragovitsch P., Filges D. and Englert P., *Nucl. Instr. and Meth.* B42 (1989), p.76.

Mathew K.J., Rao M.N. and Michel R., *Lunar and Planet. Sci.* 20 (1989a), p.624.

Mathew K.J., Rao M.N., Michel R. and Prescher K., *Abstracts of the 52nd Meeting of the Meteoritical Society, Meteoritics* 54 (1989b) p.300.

Nautiyal C.M., Padia J.T., Rao M.N. and Venkatesan T.R., *Proc. Lunar Sci. Conf. 12th* (1981), p.627.

Nautiyal C.M., *Ph.D. Thesis, Gujarat University* (1983).

Nier A., *Rev. Sci. Instr.* 18 (1947), p.398.

Nishiizumi K., Regnier S. and Marti K., *Earth Planet. Sci. Lett* 50 (1980), p.156.

Nishiizumi K., Klein J., Middleton R., Kubik P.W., Elmore D. and Arnold J.R., *Geochim. Cosmochim. Acta* 50 (1986), p.1017.

Nishiizumi K., Imamura M., Kohl C.P. Nagai H., Kobayashi K., Yoshida K., YYamashita H., Reedy R.C., Honda M. and Arnold J.R., *Proc. Lunar Planet. Sci. Conf. 18th* (1988), p.79.

Nishiizumi K., Arnold J.R., Kubik P.W. and Sharma P., *Proc. Lunar Planet. Sci. Conf. 21st* (1990).

Paneth F.A., Reasback P. and Mayne K.I., *Geochim. Cosmochim. Acta* 2 (1952), p.300.

Paneth F.A., Reasback P. and Mayne K.I., *Nature* 172 (1953), p.200.

Peiffer F., *Thesis, Universitat Koln* (1986).

Pepin R.O., Nyquist L.E., Phinney D. and Black D.C., *Proc. of the Apollo II Lunar Sci. Conf. 2nd* (1970), p.1435.

Podosek F.A., *Geochim. Cosmochim. Acta.* 34 (1970), p.341.

Prescher K., Brinkmann G. and Herr W., NEANDC (E)-212 Vol. V, INDC (Ger)-22/L + Special (1980), p.50.

Prescher K., Peiffer F., Stueck R., Michel R., Bodemann R., Rao M.N. and Mathew K.J., *Nucl. Instr. and Meth. in Phy. Res.* B53 (1991), p.105.

Rao M.N., Venkatesan T.R., Goswami J.N., Nautiyal C.M. and Padia J.T., *Proc. Lunar Planet. Sci. Conf. 10th* (1979), p.1547.

Reedy R.C., *Proc. Lunar Sci. Conf. 8th* (1971), p.1729.

Reedy R.C., and Arnold J.R., *J. Geophs. Res.* 77 (1972), p.537.

Reedy R.C., *Proc. Lunar Sci. Conf. 8th* (1977), p.365.

Reedy R.C., *Proc. Conf. Ancient Sun* (1980), p.365.

Reedy R.C., Arnold J.N. and Lal D., *Annu. Rev. Nucl. Part. Sci.* 33 (1983), p.505.

Reedy R.C., *Proc. of fourth Inter. Symp. on AMS* (1987).

Reedy R.C. and Marti K., *In Sun in Time, Univ. of Arizona Press* (1990).

Reynolds J.H., *Rev. Sci. Instr.* 27 (1956), p.928.

Reynolds J.H. and Lipson J.I., *Geochim. Cosmochim. Acta* 12 (1957), p.330.

Reynolds J.H., *Phys. Rev. Letters* 4 (1960a), p.351.

Reynolds J.H., *Phys. Rev. Letters* 4 (1960b), p.8.

Reynolds J.H., *J. Geophys. Res.* 68 (1963), p.2939.

Reynolds J.H., Alexander E.C. Jr., Davis P.K. and Srinivasan B., *Geochim. cosmochim. Acta* 38 (1974), p.401.

Rison W. and Zaikowski A., *Proc. Lunar Planet. Sci. Conf.* 11 (1980), p.977.

Rowe M.W. and Kuroda P.K., *J. Geophys. Res.* 70 (1965) p.709.

Rowe M.W., Bogard D.D., Brothers C.E. and Kuroda P.K., *Physical Review Lett.* 15 (1965), p.843.

Rowe M.W., Bogard D.D. and Kuroda P.K., *J. Geophys. Res.* 71 (1966), p.4679.

Schultz L. and Freundel M., *Centre Nationale d'Etudes Spatiales, Cepadues Editions, Toulouse, France* (1985), p.27.

Schultz L. and Signer P., *Earth. Planet. Sci. Lett* 30 (1976), p.191.

Shedlovsky J.P., Honda M., Reedy R.C., Evansjun J.C., Lal D., Lindstorm P.M., Delany A.C., Arnold J.R., Loosli H.H., Fruchter J.S. and Finkel R.C., *Proc. Apollo II Lunar Sci. Conf. 2nd* (1970), p.150.

Shukolyukov A. Yu and Gorin V.D., *Geokhimiya* 4 (1988), p.592.

Signer P. and Nier A.O., in : Researches in Meteorites, ed., Moore C.B. (Wiley, New York, 1962), p.7.

Signer P. and Nier A.O., *J. Geophys. Res.* 65 (1960), p.2947.

Simpson J.A., *Annu. Rev. Nucl. Part. Sci.* 33 (1983), p.323.

Srinivasan B., *Proc. Lunar Sci. Conf. 5th* (1974), p.2033.

Stettler A., Eberhardt P., Geiss J., Grogler N. and Maurer P., *Proc. Lunar Planet. Sci. Conf. 4th* (1973), p.1865.

Suess H.E., *Z. Phys.* 125 (1948), p.386.

Suess H.E., Wanke H. and Wlotzka F., *Geochim. Cosmochim. Acta.* 28 (1964), p.595.

Swindle T.D., Trapped Noble gases in Meteorites, In Meteorites and the Early Solar System, Ed. Kerridge J.F. and Mathews M.S., University of Arizona Press, Tucson (1988).

Trivedi B.M.P. and Goel P.S., *J. Geophys. Res.* 78 (1973), p.4885.

Thiel K., Damm G. and Herr G., *Proc. Lunar Sci. Conf. 5th* (1974), p.2609.

Venkatesan T.R., Nautiyal C.M., Padia J.T., Rao M.N., *Proc. Lunar Planet. Sci. Conf. 11th* (1980), p.1271.

Wasserberg G.J. and Hayden R., *Nature* 176 (1955), p.130.

Wasserburg G.J., Fowler W.A. and Hoyle F., *Phys. Rev. Lett.* 4 (1960), p.112.

Wasserburg G.J. Huneke J.C. and Bunett D.S., *J. Geophys. Res.* 74 (1969), p.4221.

Williamson C.F., Boyot J.P. and Picard J., *CEA-R3042* (1966).

Yaniv A. and Marti K., *The Astrophys. Jour.* 247 (1981), p.L143.

List of Publications

1.Bhandari N.,Bonino G., Callegari E., Cini Castagnoli, **Mathew K.J.**, Padia J.T. and Queirazza G., The TORINO, H6, Meteorite Shower, *Meteoritics,* 24(1)(1989),p1493.

2.Presher K., Peiffer F., Stueck R., Michel R., Bodemann R., Rao M.N. and **Mathew K.J.**, Thin-Target Cross-sections of proton-induced reactions on Barium and Solar Cosmic Ray Production rates of Xenon isotopes in the Lunar Surface Materials, Nucl. Instru. Meth. in Phys. Res.,(1991).

3.**Mathew K.J.**, Rao M.N. and Michel R., High Energy Spallation Xenon spectrum from Barium targets, In Lunar and Planet. Sci. Conf. (Abstracts) p624

4.**Mathew K.J.**, Rao M.N., Michel R. and Prescher K., Xe Isotope Production from Barium Targets by protons in the energy range of 12 to 45 MeV (student award paper), 52nd annual meeting of the Meteoritical Society, Vienna, Austria, *Meteoritics,* 24 (1989) p300.

5.Bhandari N., **Mathew K.J.** , Rao M.N., Herpers U., Vogt S., Woelfli W., Hoffmann, H.J., Michel R. and Bodemann R., Production rates of Cosmogenic Nuclides in Meteorites Determined by Accelerator and Conventional Mass Spectrometry., Fifth National Symposium on Mass Spectrometry, PRL, Ahmedabad, (1991), EPS3/1.